Co-published by
Institute of Fluid-Flow Machinery
Polish Academy of Sciences
Committee on Thermodynamics and Combustion
Polish Academy of Sciences

http://www.imp.gda.pl/archives-of-thermodynamics/

ARCHIVES OF THERMODYNAMICS

Effects of roughness geometry on heat transfer, fluid flow and thermo-hydraulic performance of solar air heaters: A comprehensive review

Dilbag Singh Mondloe[a], Harish Kumar Ghritlahre[b*], Gajendra Kumar Agrawal[c], Kamini Rathore[d], Hemant Naik[e], Onika Parmar[f]

[a]Department of Mechanical Engineering, Chhattisgarh Institute of Technology (CGIT), Jagdalpur, Chhattisgarh 494001, India
[b]Department of Energy and Environmental Engineering, Chhattisgarh Swami Vivekanand Technical University, Bhilai, Chhattisgarh 491107, India
[c]Department of Mechanical Engineering, Government Engineering College, Bilaspur, Chhattisgarh 495009, India
[d]Department of Civil Engineering, Rungta College of Engineering and Technology Bhilai, Chhattisgarh 490024, India
[e]Department of Mechanical Engineering, O. P. Jindal University Raigarh, Chhattisgarh 496109, India
[f]Department of ET&T, Rungta College of Engineering and Technology Bhilai, Chhattisgarh 490024, India
*Corresponding author email: harish.ghritlahre@gmail.com

Received: 05.07.2024; revised: 04.11.2025; accepted: 04.12.2025

Abstract

In the present review article, an effort has been made to review various experimental and numerical research, which include heat transfer rate and fluid flow characteristics of a modified solar air heater (SAH) using various artificial roughness. As it is clear that artificial roughness enhances the heat transfer and performance, in this review study, various types of roughened SAH performances have been examined. These various roughness patterns are V-shape, W-rib, arc shape, spherical ball and S-type, and their placement arrangements, like transverse, inclined and longitudinal, are discussed in this article. The comparative studies of thermo-hydraulic performance with heat transfer and fluid flow investigations of various roughened SAHs have been described to identify optimal performance parameters to select the optimum configuration that can be further used for various applications. In addition to this, various correlations of the Nusselt number and friction factor developed by various investigators have also been reported. The main aim of this study is to evaluate the SAH performance using various roughness patterns. It also provides several essential recommendations for effectively designing and implementing SAHs. This review encompasses a comprehensive analysis of 178 research articles published between 1988 and 2024, focusing on advancements in the field. The findings showcase the peak values for the Nusselt number as 7.61, the friction factor reaching 6.48 times that of a smooth duct for discrete multiple-arc ribs, and the maximum thermal-hydraulic performance reported at 4.73 for dimple or protrusion ribs.

Keywords: Solar air heaters; Roughness geometry; Heat transfer; Fluid flow; Thermo-hydraulic performance

Vol. 47(2026), No. 2, 5–57; doi: 10.24425/ather.2026.158685

Cite this manuscript as: Mondloe, D.S., Ghritlahre, H.K., Agrawal, G.K., Rathore, K., Naik, H., & Parmar, O. (2026). Effects of roughness geometry on heat transfer, fluid flow and thermo-hydraulic performance of solar air heaters: A comprehensive review. *Archives of Thermodynamics*, 47(2), 5–57.

1. Introduction

Various energy resources are utilised in industry, transport, the residential sector, etc. The energy sources widely used are natural gas, coal, fossil fuel, oil, renewable and other sources. It is a fact that sustainable energy sources are a global problem. Across the globe, treaties have been employed and implemented to check and restrain global warming, climate change and energy depletion quickly. These resources are fixed in quantity, but at the same time, their exploration and utilisation are hugely

Nomenclature

A_c – surface area of collector, m²
A_o – area of orifice meter, m²
B/S – relative roughness length
C_d – coefficient of discharge
C_{pf} – air specific heat, J/(kg K)
c/H – relative baffle height
d_b – ball diameter, m
d_p – perforated diameter, m
d/D – relative print diameter
d/w – relative gap position of additional gap in symmetrical rib
d/x – relative gap position
D_h – hydraulic diameter, m
D_j – jet diameter, m
e – height of roughness (rib height), mm
e/d_d – dimple depth to diameter ratio
e/D, e/D_h – relative roughness height
e/w – rib aspect ratio
e^+ – roughness Reynolds number
e'/e – rib chamfered aspect ratio
f – friction factor
g – width of gap, gap of discrete rib, m
g/e, g_w/H_r – relative gap width
g/P – relative groove position
g'/e – relative gap size of additional gap in symmetrical gap elements
$G(e^+)$ – heat transfer roughness function
G_d/L_v – relative gap distance
h – heat transfer coefficient, W/(m² K)
h/H – relative height ratio (for fins and ribs)
h/d_p – relative perforated ratio
H – height of the duct, m
H_j – jet height, m
H_r – rib height, m
k – thermal conductivity, W/(m K)
L – length of the test section in the duct, m
L/e – relative long way length
$\dot{m}_f$ – mass flow rate of air, kg/s
N_g – number of main gaps
Nu – Nusselt number
O – hole position from baffle base, m
p/P – relative staggered pitch
P – perimeter, roughness (rib) pitch, m
ΔP_o – pressure drop, Pa
P/e – relative roughness pitch
P/g – relative pitch to gap ratio
P/H – relative rib pitch
Pr – Prandtl number
q – solar irradiation, W/m²
$\dot{Q}_u$ – useful heat gained by air, W
r_d – depth of dimple cavity, m
r/e – depth of dimple cavity, m
r_d/D_h – relative dimple depth
$R(e^+)$ – friction roughness function
Re – Reynolds number
S/e – relative short way length
s/H – relative baffle pitch
St – Stanton number
T – temperature, K
Tu – turbulence intensity
V – air velocity in the duct, m/s
x/r_d – longitudinal pitch ratio
X/D_h – streamwise pitch ratio
y/r_d – transverse pitch ratio
Y/D_h – spanwise pitch ratio
w – rib width, m
w/e – relative rib width
W – duct width, m
W_{AC} – width of discrete multi-arc shaped rib, m
W/H – duct aspect ratio
W/w – width of duct to width of collector

Greek symbols

α – angle of arc, °
β – ratio of orifice meter to pipe diameter
β_0 – open area ratio
ρ – density, kg/m³
ϕ – wedge/chamfer angle, °

Subscripts and Superscripts

a – air
avg – average
B – baffle
f – fluid
fi – air inlet
fo – air outlet
m – mean
np – non-perforated
p – plate, perforated
s – smooth

Abbreviations and Acronyms

ANN – artificial neural network
CCD – central composite design
CFD – computational fluid dynamics
LCT – liquid crystal thermography
PCM – phase change material
SAH – solar air heater
SPR – sinusoidal protrusion rib
STC – solar thermal collector
THP – thermo-hydraulic performance

expedited to meet the energy demand of the growing populations and other development works. Therefore, the governments emphasise using renewable energy sources to meet the demand at the required rate. Solar energy is an abundantly available, clean, green, and never-ending energy source that can meet the energy demand. Many solar thermal systems are available, such as solar space heating, solar water heating, concentrated solar power, solar air conditioning, solar crop drying, solar cooking and solar ponds. These are solutions that utilise sunlight to convert it into thermal energy. There are several major types of solar thermal technologies in use. These are unglazed solar collectors, transpired solar air collectors, flat-plate solar collectors, evacuated tube solar collectors and concentrating solar systems. But due to high cost and sustainable use, the focus has always been on solar air heaters. Many types of air heaters are available, such as duct heaters, enclosure heaters, forced air heaters, heat torches, flame heaters, radiators, space heaters and room heaters, and tubular heaters. The utilisation of solar air heaters is encouraged due to their easy installation, relatively low cost and portability. However, these systems have certain drawbacks. One significant limitation is the low heat transport capacity of the absorber sheet, which hinders efficient heat transfer. Another factor is the low thermal conductivity of the absorber sheet, which results in a reduced heat transfer rate between the absorber sheet and the flowing air. Consequently, the overall effectiveness and utilisation of solar air heaters are diminished. To overcome these limitations, researchers have focused on creating turbulence inside solar air heaters. The objective is to disrupt the laminar sublayer formed near the absorber plate and enhance the heat transfer rate. However, passive methods used to generate turbulence have disadvantages, such as increased fluid friction and the need for higher pumping power.

Researchers continue to explore alternative approaches to address these challenges and improve the performance of solar air heaters. By developing innovative methods and designs, the goal is to enhance heat transfer efficiency without significantly increasing fluid friction or energy consumption. There are many techniques used by various researchers, such as evaluations of solar air heaters (SAH) in terms of thermo-hydraulic performance [1], thermal performance [2], single pass [3], double pass [4], parallel pass [5] and longitudinal fins [6]. Limited researchers investigated experimentally and numerically various types of artificial roughness, such as arc shaped [7], apex up-down arc shaped [8], concave dimple [9], wingets [10], multi-V shaped [11], S-shaped [12], V-corrugated [13], aluminium cans as fins [14], porous fins [15], packed bed [16], porous bed [17], wire mesh [18], corrugated fins [19], wavy fins [20], turbulators [21] and SAH made from plastic-metal waste [22], etc. for increasing the performance of SAHs. The utilisation of irregular surfaces is a widely employed and effective technique for enhancing heat transfer in solar air heaters. This passive approach involves applying artificial roughness on the underside of the absorber plate using various methods, such as ribs, grooves, dimples, winglets, baffles, twisted tapes, mesh wires, and more. These modifications create disturbances in the flow, promoting turbulence and improving heat transfer. In Fig. 1, a schematic diagram showcases different types of heat transfer augmentation techniques implemented in solar air heaters.

The artificial roughness is strategically placed on the underside of the blackened absorber plate to enhance heat transfer, while keeping an increase in pumping power to a minimum. This approach ensures that the disturbance or turbulence is created in close proximity to the heated surface, specifically targeting the laminar sublayer. By implementing these modifications, solar air heaters can achieve improved heat transfer performance without requiring significant additional pumping power. This technique allows for efficient utilisation of the available thermal energy and enhances the overall effectiveness of the solar air heating system.

The primary objective of this study is to review experimental and analytical work on the performance of solar air heaters using the concept of artificially roughened solar air heaters. This analysis provides researchers with an energy efficiency concept and a strategy for designing and operating industrial operations. In addition, this research work also involves an extensive examination of various roughness geometries employed in solar air heaters and their impact on the mechanisms of heat transfer and fluid flow. The study focused on understanding how different surface textures affect the exchange of heat and movement of fluids within SAH. Further, this paper identifies research gaps for future work and is beneficial for those working with artificially roughened solar air heaters.

From the literature review (Table 1), it has been observed that many review papers have been published on solar air heaters, particularly on roughened SAHs. But very few reviews have been conducted on the heat transfer and fluid flow of solar air heaters. In this area, there is a large opportunity in the near future for increasing the performance of SAHs with novel geometry

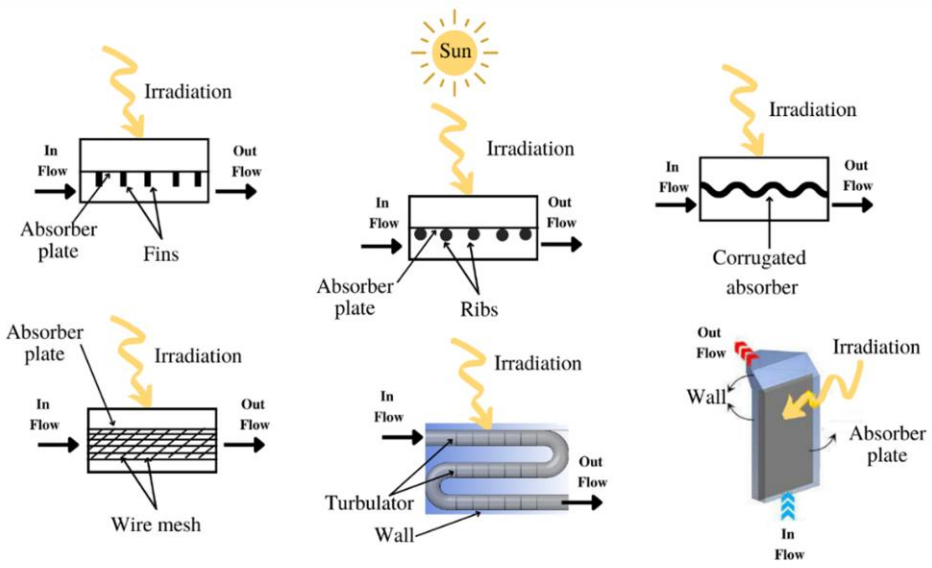

Fig. 1. Modifications implemented in solar air heaters.

Table 1. Review papers published from 2000 to 2022 on artificial roughness of solar air heaters.

Reference	Year	Studied issues
Varun et al. [23]	2007	Heat transfer (Nu) and friction (*f*) characteristics, correlations developed for Nu and *f*.
Gupta and Kaushik [24]	2009	Heat transfer, friction characteristics, energy and exergetic efficiency, effective efficiency.
Hans et al. [25]	2009	Heat transfer and friction characteristics, and correlations developed for Nu and *f*
Chamoli et al. [26]	2012	Heat transfer, friction characteristics and flow pattern.
Chamoli et al. [4]	2012	Fins, packed bed energy analysis, thermal efficiency, heat transfer enhancement.
El-Sebaii and Shalaby [27]	2012	Detailed description, fundamentals and previous work performed on solar dryers and solar air heaters.
Yadav and Bhagoria [28]	2013	CFD analysis, design parameters for improved performance include heat transfer, mass and momentum transfer, optimal design parameters and turbulence model.
Yadav and Thapak [29]	2014	Numerical analysis, developed codes in MATLAB-7, heat transfer, friction characteristics, and correlations developed for Nu and *f*.
Gawande et al. [30]	2014	Numerical and experimental study, thermal performance evaluation, heat transfer, friction characteristics, and correlations developed between Nu and *f*.
Kumar et al. [1]	2014	Exergetic efficiency, thermo-hydraulic performance (THP), thermal performance
Alam et al. [31]	2014	Numerical analysis, different turbulators used, heat transfer, friction characteristics and correlations developed for Nu and *f*.
Alam et al. [32]	2014	Experimental study, different turbulence generators, heat transfer, friction characteristics and correlations developed for Nu and *f*.
Mund et al. [33]	2014	Heat transfer, friction characteristics and correlations developed for Nu and *f*.
Anil Kumar Patil [34]	2015	Fluid turbulence and heat transfer mechanism, rib geometries, Reynolds number and temperature rise parameter, effective efficiency.
Sharma and Kalamkar [35]	2015	Different roughness geometrical elements, thermo-hydraulic performance, heat transfer and friction characteristics.
Kumar and Kim [36]	2015	Used different ribs, fins and baffles; heat transfer, friction characteristics, and correlations developed for Nu and *f*
Lanjewar et al. [37]	2015	Used different rib geometries; heat transfer, friction characteristics, and correlations developed for Nu and *f*
Sheikholeslami et al. [38]	2015	Different turbulators used on rib geometries; heat transfer, friction characteristics and heat transfer performance.
Singh et al. [39]	2015	Thermo-hydraulic performance comparison, heat transfer, friction factor, relative roughness pitch.
Saxena et al. [40]	2015	Optimising the dimensions, improving thermal performance.
Kumar et al. [41]	2016	Experimental and numerical analysis, triangular duct; heat transfer, friction characteristics and heat transfer performance.
Aravindh and Sreekumar [42]	2016	Used different modifications on rib geometries; heat transfer, friction characteristics and heat transfer performance.
Sharma and Kalamkar [43]	2016	CFD analysis, modelling, different meshing type, suitable turbulence model, thermo-hydraulic performance.
Kumar and Kim [44]	2016	Energy efficiency, heat transfer enhancement, turbulence models, thermo-hydraulic performance, RNG k-ε model.
Ravi and Saini [45]	2016	Experimental and theoretical investigations, performance enhancement techniques, a double pass system, thermal performance, and correlations developed.
Gawande et al. [46]	2016	CFD analysis, modelling, different meshing type, operating and system parameters, suitable turbulence model, thermo-hydraulic performance.
Yadav and Thapak [47]	2016	Experimental and CFD approaches on different roughness elements for heat transfer, friction characteristics and thermo-hydraulic performance.
Kabeel et al. [48]	2017	Experimental and theoretical study, different modifications on the absorber plate, recycling process for heat transfer, friction characteristics and thermo-hydraulic performance.
Alam and Kim [49]	2017	Experimental study on different roughness elements; heat transfer, friction characteristics and thermo-hydraulic performance.
Singh and Singh [50]	2018	Experimental and theoretical study, different modifications on the absorber plate, flow visualisation to asses heat transfer, friction characteristics and thermo-hydraulic performance.
Singh et al. [51]	2018	Experimental study on different roughness elements for heat transfer, friction characteristics thermo-hydraulic performance, thermal efficiency, effective efficiency and energy – exergy performance.
Kumar et al. [52]	2018	Energy efficiency, blockage height, blockage arrangement, thermal hydraulic performance, air passage.
Chauhan et al. [53]	2018	Jet impingement, heat transfer, friction factor, multi criteria decision making, thermodynamic behaviour, control factors on heat transfer and friction characteristics.

Table 1. Review papers published from 2000 to 2022 on artificial roughness of solar air heaters (*continued*).

Reference	Year	Studied issues
Elsheikh et al. [54]	2019	Artificial neural network (ANN) method for optimising and predicting the performance of different solar energy devices.
Hu and Zhang [55]	2019	Correlation development on performance improvement method, reorganisation of flow of air stream.
Prakash and Saini [2]	2019	Experimental study, different modifications on absorber plate, flow visualisation for heat transfer, friction characteristics and thermo-hydraulic performance.
Chhaparwal et al. [56]	2019	Experimental, different modifications on absorber plate, physics involved in flow visualisation for heat transfer, friction characteristics and thermo-hydraulic performance.
Ghritlahre and Sahu [57]	2020	Experimental study on different roughness elements for heat transfer, friction characteristics, thermo-hydraulic performance, thermal performance, effective efficiency and energy – exergy performance.
Vengadesan and Senthil [58]	2020	Experimental study on different modification on SAH for heat transfer, friction characteristics, thermo-hydraulic performance, thermal performance.
Yadav and Prasad [59]	2020	Mathematical model, codes in MATLAB, thermal efficiency, thermo-hydraulic efficiency.
Arunkumar et al. [60]	2020	Thermal performance, design considerations, geometries used, flow conditions and their influence on turbulence; heat transfer, friction characteristics and thermo-hydraulic performance.
Nidhul et al. [61]	2021	Thermo-hydraulic performance, correlations for heat transfer and friction factor, effective efficiency and energy – exergy performance.
Chamarthi and Singh [62]	2021	Energy and exergy efficiencies, performance enhancement, solar air heater, testing standards.
Ghritlahre et al. [63]	2021	Solar air heaters, porous bed, artificial roughness, artificial neural network, learning algorithm (LA), multi-layer perceptron (MLP).
Ghritlahre et al. [64]	2022	Solar air heater, energy analysis, exergy analysis, thermal performance.

and various parameters. Thus, the present systematic review work on the heat transfer, fluid flow characteristics and thermo-hydraulic performance of roughened solar air heaters is necessary to identify existing research gaps, while also incorporating the latest published studies.

In the present paper, a comprehensive review on heat transfer, fluid flow characteristics and thermo-hydraulic performance of roughened solar air heaters has been reported. Various geometries of roughness, which were used by many researchers, have been discussed. The main objectives of the present review are as follows:

1. To study the heat transfer and fluid flow characteristics of various roughness geometries.
2. To find out the optimal thermo-hydraulic performances in various roughness geometries.
3. To report the developed Nusselt number and friction factor correlations of various roughened solar air heaters.
4. To find out the research gaps for future work.

2. History of development of a solar air heater

Since ancient times, the sun's energy has been used for many purposes, such as crop drying, vegetable drying, cloth drying and making salts, etc. In 1877, Daniels and Duffie [65] were the first to report that solar energy can be stored in iron. The air passed through the iron and got heated, and then it was used for heating the room.

In 1881, an American researcher E. Morse, structured and developed an accredited SAH. This SAH was designed with a wooden-framed cabinet with a metallic absorber sheet, which was covered with a transparent glass cover. This SAH works on the concept of convection; the solar radiation is absorbed by the steel sheet absorber plate, and air flows through the cabinet, where it absorbs heat from the absorber sheet and transfers it to the blowing air.

This system came into light, but still progress is needed on various modification options in SAH [66]. During this time, several solar-heated homes have been developed and operated in various places around the world. Between 1946 and 1949 in Massachusetts, SAH was modified using a chemical compound, which inherently has the ability to absorb heat and emit heat energy to the air. This technology is known as phase change material (PCM), which has wide applications in various industries and households. At that time, up until 1978, new and novel designs of houses were developed at the Massachusetts Institute of Technology (MIT). It is also observed that many stakeholders, i.e. industries, manufacturing, etc., are designing new solar air heaters for applications such as air heating, crop heating and vegetable heating. In the past few years, after detailed studies, many researchers have developed this solar system for many applications. These studies are summarised in Table 2.

3. Basic construction of a solar air heater

3.1. Basic design of a solar air heater

The basic design of a solar air heater is described in Table 3. SAH is mainly designed with a frame, absorber or collector plate, glass cover, insulation, black interior surfaces, and the inlet and outlet sections. Solar radiation falls upon the absorber plate, as shown in Fig. 2. The thermal energy of the solar radiation is absorbed by the plate, which is then conveyed to the following air through the duct.

Table 2. The developments in the past few years.

Researchers/ Inventors)	Year	City/Place/ Country	Novelty of the invention
Cabot [67]	1938	Boston	Groundwork for research on fully functional solar air heating took place at the Massachusetts Institute of Technology (MIT). The developed solar thermal system was designed to meet almost one-third of the total heating requirement in Boston.
Telkes and Raymond [68]	1949	Dover	Firstly, solar homes were defined at Dover (MIT). The solar homes worked on the principle of solar thermal energy storage by using fusion of $NaSH_3$. The primary objective was to meet the heating load for consecutive 5 days.
Bliss [69]	1955	Arizona desert	A fully functional solar-heated house has been designed and developed in the desert of Arizona. The system comprises air stream flow through combined heater and thermal energy storage (TES) system.
Lof [70]	1959	Denver	Solar air heaters have been developed by using overlapped transparent glass as an absorber plate in a solar collector. They have also utilised pebble bed as solar thermal energy storage, while developing a dwelling in Denver. During 1963, 1964, 1976 and 1978, the researchers have examined the SAHs with all variations and reported the evidence.
Doherty [71]	2007	USA	The system utilised two novel features to increase the mean temperature of the system. They have given a solution to prior problems with mixing of cold fluid stream with hot air. They reported an increase in the system efficiency.
Vachon [72]	2010	USA	They achieved higher thermal efficiency by using the principle of heating and heat recovery in a solar heat collector. This system comprises glazing in contact with air. The spacing used in glazing over the back surface was the reason for higher performance of the system.
MacKay et al. [73]	2011	USA	Air heating was effective using a modular method. The modular system contained different sizes and angles to get maximum absorption of incoming thermal energy. The applications vary from industries, households and agriculture, etc.
Ryan [74]	2011	USA	The boundary of the heating system was defined at the verge between the absorber plate and the plenum. This system was employed to support the surface, a mechanism for flowing air stream and other parts of SAHs.
Hao [75]	2013	China	This novel SAH comprises a frame, a sheet of glass, supports and two ducts with a roof at the top, and there is a greenhouse at the bottom. The advantage of the design was that it achieved high thermal efficiency.

Table 3. The basic design of a solar air heater.

Component	General specification/ dimensions/materials	Purpose
Collector or absorber plate	An absorber plate is made of GI or aluminum and painted black to maximise radiation absorption.	This collects solar energy and transmits it to moving air.
Insulation	Generally, material used as glass wool or mineral wool up to 50 to 80 mm thickness.	It is provided to prevent heat losses from the bottom and sides of the ducts.
Matte black interior	It is matte black paint/ sticky powder.	The interior surfaces of test sections are painted with black matte paint to maximise solar absorption.
Glass cover	Glass covers with a thickness of 3 to 4 mm are commonly utilised.	The use of a glass cover over the top of the absorber plate reduces convection and re-radiation losses from the absorber surfaces to the environment.
Glazing	Glaze sheet is made of carbonate, acrylic and tempered glass materials.	Glazing is provided on the top surface of the glass cover to give adequate solar radiation absorption.
Inlet/outlet section	Bell mounted wooden inlet section and trapezoidal wooden outlet section.	The inlet and outlet sections are designed to make air intake and discharge easier.
Frame	Generally, the frame is made of woods or metal.	To provide support for the SAH body components.

3.2. Classification of SAHs

Solar air heaters are classified into various categories, such as flow patterns, applications, hybriding, collector (absorber) materials, glass covers, flow types and collector (absorber) surface type. The classification of SAHs is described in Table 4.

3.3. Applications of SAHs

Solar air heaters are mainly used for heating air for various purposes. Some important applications of SAHs are shown in Fig. 3.

Table 4. Classifications of SAHs.

Main classification	Subclassification			
	A	B	C	D
The collector cover (glass)	Bare plate	Single	Double	–
The absorber material	Metallic	Non-metallic	Matrix	–
The shape of absorbing surface	With slate	With porous media	With fins	–
Type of absorber flow pattern	Over	Under	On both side	–
Type of flow	Single pass	Double pass	Double flow	Triple pass
Hybrid collectors	Air	Water	Water-air	–
Applications	Drying	Space heating	Preheating	Cooling

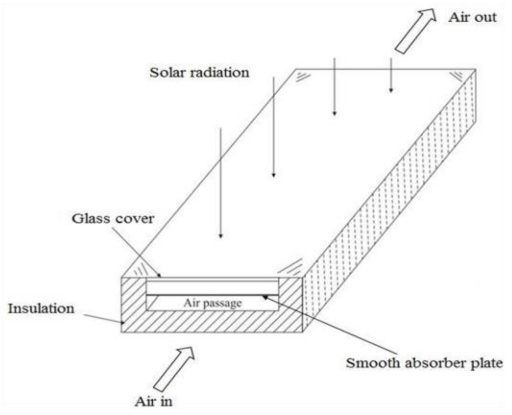

Fig. 2. Convectional solar air heater (drawn after [58]).

Fig. 3. Different applications of SAHs.

4. Performance evaluation of solar air heaters

Solar air heaters can be evaluated by both experimental and analytical approaches. The parameters under evaluation include the plate temperature of an absorber sheet, the air stream temperature, the rate of mass flow, and the thermal and thermo-hydraulic performance. These parameters are explained below in brief.

4.1. Mass flow rate

Mass flow rate is the function of the associated pressure drop through the SAH. The formula utilised for the mass flow rate of fluid is:

$$\dot{m}_f = C_d A_o \left[\frac{2\rho_a (\Delta P_o)_a}{1-\beta^4}\right]^{0.5}, \tag{1}$$

where: C_d – coefficient of discharge, A_o – area of an orifice meter, ΔP_o – pressure drop across an orifice meter, β – ratio of the orifice diameter to the pipe diameter.

4.2. Hydraulic diameter

$$D_h = \frac{4A_D}{P} = \frac{4(WH)}{2(W+H)}, \tag{2}$$

where: W – width of the duct, H – height of the duct, A_D – cross-sectional area of the duct, P – perimeter of the duct.

4.3. Velocity of air

$$V = \frac{\dot{m}_f}{\rho_a A_D}, \tag{3}$$

where $\rho = \rho_a$ denotes the density of air.

4.4. Reynolds number

$$\text{Re}= \frac{\rho V D_h}{\mu}, \tag{4}$$

where μ is the kinematic viscosity.

4.5. Heat transfer coefficient

The heat transfer coefficient (h) is a key factor in evaluating the performance of SAH. This coefficient is influenced by the nature and condition of the absorber surface and the flowing fluid. The heat transfer coefficient can be calculated using the following formula:

$$h = \frac{\dot{Q}_u}{A_c(T_{pm}-T_{fm})}, \tag{5}$$

where A_c represents the surface of a collector, and T_{pm} and T_{fm} are the mean temperatures of the plate and air, respectively.

The evaluation of useful heat gained ($\dot{Q}_u$) by the air is calculated using the formula:

$$\dot{Q}_u = \dot{m}_f C_{pf} \Delta T = \dot{m}_f C_{pf}(T_{fo} - T_{fi}), \tag{6}$$

where: C_{pf} – specific heat at constant pressure of fluid used, T_{fo} – outlet temperature of the fluid, T_{fi} – inlet temperature of the fluid.

4.6. Heat transfer

The ratio of convective heat transfer to conductive heat transfer is evaluated using the Nusselt number for a roughened duct. This dimensionless parameter can be calculated from:

$$\mathrm{Nu} = \frac{hD_h}{k}, \tag{7}$$

where k represents the thermal conductivity of the fluid.

Furthermore, the Dittus-Boelter equation can be used to calculate the Nusselt number for a smooth duct of SAH:

$$\mathrm{Nu_s} = 0.023\mathrm{Re}^{0.8}\mathrm{Pr}^{0.4}, \tag{8}$$

where Pr stands for the Prandtl number.

4.7. Fluid flow characteristics

The frictional characteristics in SAH is calculated using the pressure drop (ΔP). The Darcy equation formula can be used to evaluate friction factor for the roughened duct:

$$f = \frac{2\Delta P D_h}{4\rho_a L_t V^2}, \tag{9}$$

where L_t is the length of a test section. For a smooth duct, the friction factor can be calculated using the modified Blasius equation:

$$f_s = 0.085\,\mathrm{Re}^{-0.25}. \tag{10}$$

4.8. Thermo-hydraulic performance

The thermo-hydraulic performance in SAH can be calculated using the given formula:

$$\mathrm{THP} = \frac{\frac{\mathrm{Nu}}{\mathrm{Nu_s}}}{\left(\frac{f}{f_s}\right)^{\frac{1}{3}}}. \tag{11}$$

5. Roughness concept

Artificial roughness is a technique used to enhance fluid flow and heat transfer by introducing specially designed roughness elements on surfaces. The artificial roughness influences fluid flow patterns and improves heat transfer rates as compared to natural surface roughness, which has a minimal impact on convective heat transfer. The artificial roughness over the absorber plate or sheet has different shapes and sizes, such as ribs, dimples, grit, baffles, wings, protrusions, spherical balls, V-shapes, W-shapes and many others. These various roughness elements have different impacts on the flow behaviour and heat transfer characteristics in the SAH. Different researchers used different methodologies, such as experimental, analytical, and codes in advanced platforms like MATLAB, OpenFOAM, etc., to evaluate the performance of the SAH.

Much research has concluded that the reattachment of a fluid flow after the fluid passes the roughness element has a huge impact on the heat transfer coefficient. Sparrow et al. [76] demonstrated this relationship through experimental and numerical investigations. Additionally, Okamoto et al. [77] found that the maximum heat transfer rate occurred at the reattachment point.

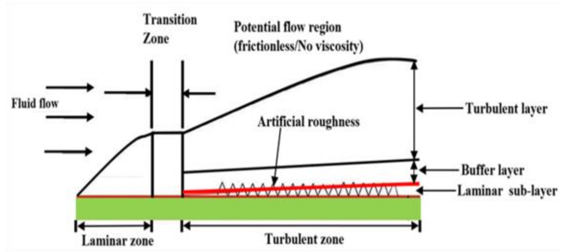

Fig. 4. Concept of roughness over a typical flat plate.

Researchers have also conducted analyses to develop correlations between different dimensionless geometrical governing parameters and operating parameters and heat transfer coefficients (Stanton number), friction factor and Nusselt number, based on their experimental studies. These correlations have been used as performance forecasting tools to evaluate roughened SAH performance, such as thermal and hydraulic performance.

The impact of artificial roughness elements on frictional characteristics, velocity profile and turbulence generation has been studied by various researchers. Nikuradse [78] examined the effect of roughness on friction by using grains of sand for fluid flow through a pipe, while Nunner [79] proposed a fluid flow model that highlights the influence of roughness elements on reducing the thermal resistance in the turbulent near-wall region. Dipprey and Sabersky [80] developed a correlation for heat transfer in a tube roughened by sand grains, and Lewis [81] used smooth, as well as roughened surfaces, to calculate thermal and hydraulic performance by firstly introducing the thermal efficiency. Also, experiment was conducted by Han et al. [82] on a roughened surface to evaluate heat transfer (Nu) and fluid flow characteristics (f), taking into account geometrical variables such as different attack angle, type of ribs and pitch to height ratio. Artificial roughness is a highly effective technique for inducing turbulence and enhancing forced convection heat transfer rates. By strategically placing roughness elements inside ducts and using fans or blowers to create turbulence, it is possible to increase heat transfer without excessive friction losses. The size and configuration of the roughness elements play a crucial role in achieving this balance.

In general, the relative roughness height (e/D), as well as the relative roughness pitch (P/e), are two highly influencial parameters, which increase the rate of heat transfer for a roughened SAH. Various shapes, such as ribs, grooves, fins, and chamfers, can be utilised as roughness elements to enhance the heat transfer performance of conventional SAH.

In solar air heaters, improving the roughness of the absorber plate is essential for enhancing thermal efficiency. Artificial roughness techniques are particularly effective in generating turbulence on the absorber plate, resulting in improved heat transfer. While simple roughness methods like grinding tools are less effective, artificial roughness offers superior performance.

In summary, artificial roughness has a significant impact on fluid flow and heat transfer. By using specially designed roughness elements, it is possible to manipulate flow patterns, promote turbulence and enhance heat transfer rates. This technique finds application in various fields, including solar air heaters, where improving roughness can lead to improved thermal efficiency, as shown in Fig. 4.

6. Impact of various roughness parameters

The solar air heaters can be modified using different roughness parameters. These roughness parameters include operating and control parameters such as height, pitch, angle of inclination, cross-sectional area, Reynold number, mass flow rate and other metrological parameters. These parameters have a significant influence on the thermal performance and thermo-hydraulic performance of SAH. Understanding how these factors affect the system can help optimise its efficiency.

Many researchers evaluated the performance of SAH and developed correlations for heat transfer (Nu) and friction factor (f) using various operating and geometrical parameters, such as Reynolds number, mass flow rate, etc. In a nutshell, heat transfer can be broadly expressed as a function of Reynolds number, relative roughness pitch, relative roughness height, angle of attack (α), different rib shapes and various duct shapes, the number of

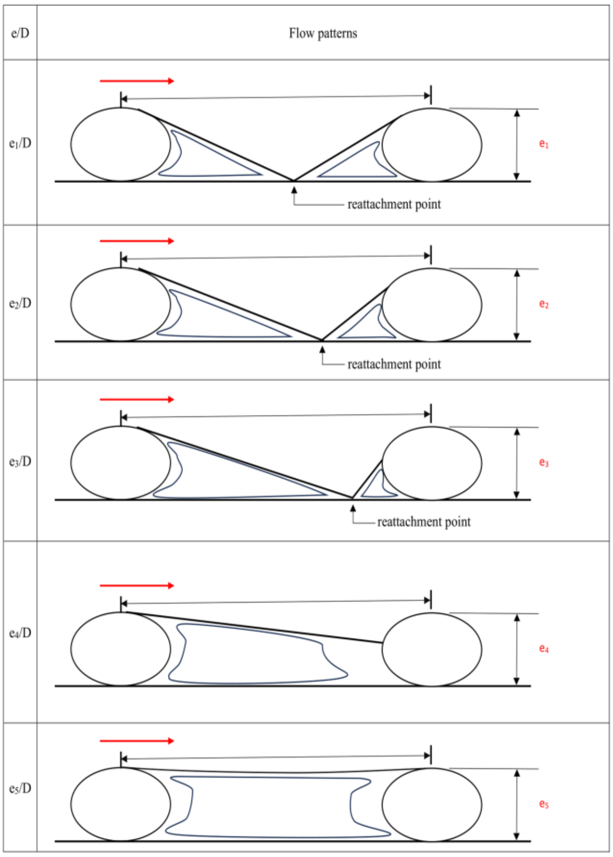

Fig. 5. Effect of relative roughness height on the flow patterns downstream (drawn after [84]).

roughened walls, etc. Furthermore, the same parameters also affect the friction factor.

Understanding and optimising these geometrical factors is essential for achieving enhanced thermal and thermo-hydraulic performance in SAH ducts. By carefully adjusting rib height, rib

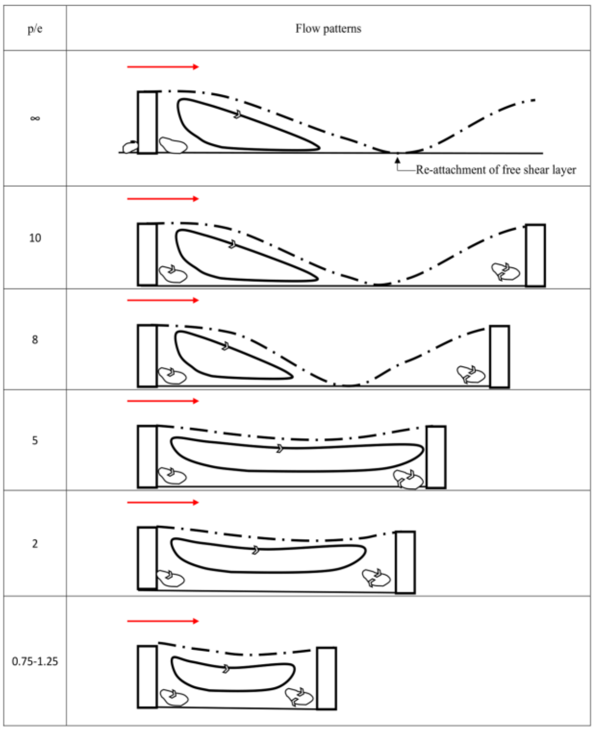

Fig. 6. Effect of relative roughness pitch (P/e) on the flow patterns downstream (drawn after [84]).

pitch, inclination, rib cross-section, and considering the appropriate Reynolds number, it is possible to achieve improved heat transfer efficiency while minimising pressure drop and pumping power requirements.

The geometrical parameters of artificial roughness elements play a crucial role in the performance of solar air heaters. These parameters include the relative roughness height, relative roughness pitch, angle of attack, shape, and arrangement of the roughness elements, etc.

6.1. Impact of relative roughness pitch and relative roughness height

Prasad and Saini [83] modified conventional SAH with circular wire ribs as artificial roughness elements. They used relative roughness height and relative roughness pitch firstly in the field of SAH as geometrical variable. They observed that increasing the relative roughness height leads to an increment in heat transfer and friction factor. For the relative roughness pitch values below 8, the flow reattachment did not occur, which led to a decrease in the rate of heat transfer. However, as the roughness pitch reduced, the friction factor kept increasing. Figure 5 illustrates the flow patterns in the downstream region of circular wire ribs, associated with the changes in relative roughness height and relative roughness pitch. The effect of relative roughness pitch, flow regimes and the development of flow vortices downstream are shown in Fig. 6.

6.2 Impact of angle of attack

Many researchers found the angle of inclination (α) to be the crucial parameter in the SAH performance. In general, when rib

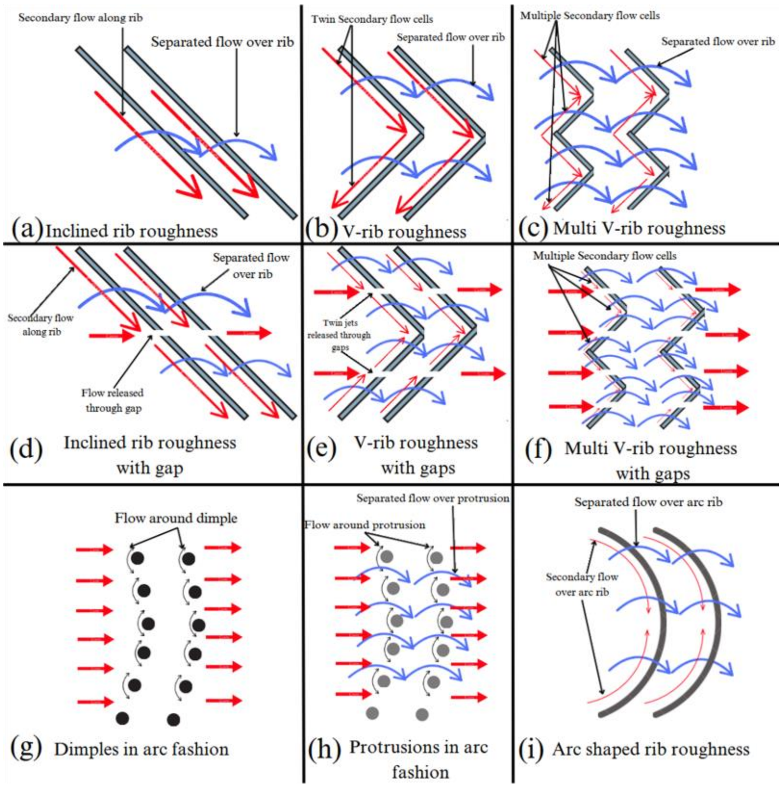

Fig. 7. Flow regime developed by introducing different roughness elements (drawn after [51]).

is inclined, it geometrically divides the main fluid flow into two parts, namely, the primary and the secondary stream flow. This segregation of the flow regime enhances the heat transfer and fluid flow characteristics. Taslim et al. [17] utilised inclined ribs as roughness elements to modify SAH. They observed that when fluid enters the leading edge of the rib and passes through the trailing edge, the whole flow regime acts as a high heat transfer zone. Secondary flow accelerates heat transfer and increases fluid friction.

6.3. Impact of V-shaped rib

Modifying conventional SAH by V-shaped rib roughness leads to creating spanwise counter-rotating flows. The general observation was that V-shaped ribs enhance heat transfer by inducing spanwise counter-rotating flows, which promote vigorous fluid mixing, suppress laminar flow and decrease the thermal resistance (flow obstruction) in the boundary layer, as shown in Fig. 7b.

6.4. Impact of multiple V-shaped rib roughness

Various researchers observed that numerous secondary flow cells are introduced by using multiple V-shaped ribs that interconnect with the main flow. Multiple V-shaped ribs enhance heat transfer by introducing chaotic fluid mixing, which leads to higher heat transfer rates, but also to increased frictional losses, as seen in Fig. 7.

6.5. Impact of gap in inclined, V- and multiple V-shaped rib roughness

V-shaped ribs with gaps enhance heat transfer rate by releasing secondary flow. The secondary flow accelerates flow inside the boundary layer, which promotes better fluid mixing. The main reason behind the improvement in the heat transfer rate is a twin secondary flow that passes along the ribs. The release of jets through small gaps arranged along the longitudinal axis are shown in Fig. 7.

6.6. Impact of dimples and protrusions

Arc-shaped dimples and protrusions on the absorber plate enhance heat transfer by inducing flow impingement, flow separation and vortex formation. Sethi et al. [85] observed that flow vortices generated on both sides of the protrusion element over the absorber plate and the main flow impingement on the upstream side of the protrusion result in an enhancement of heat transfer in the modified SAH.

7. Various geometries used for solar air heaters performance improvements

The solar air heater (SAH) has been studied in order to improve its performance. The primary goal of these studies was to collect data on improvements in Nusselt number, friction factor, thermo-hydraulic performance and correlation developments. Researchers conducted research using a variety of methods, including not only experimental but also numerical and machine learning approaches. They used various roughness geometries and geometrical configurations of SAH to achieve the aforementioned goal, as summarised in Table 5.

7.1. Transverse ribs

Prasad and Saini [86] conducted an experimental study of SAHs to determine the effect of a protrusion wire (small diameter) over the flat plate (absorber sheet). The objective was to evaluate heat transfer enhancement between the flowing air stream and the heated absorber sheet, as shown in Fig. 8. They considered the design parameters, such as a *P*/*e* ratio ranging from 10 to 20, an *e*/*D* ratio ranging from 0.020 to 0.033, and Re ranging from 5000 to 50 000. Following the completion of the experimental investigation, they obtained an increase of 2.38 in Nu and an increase of 4.25 in *f* for a *P*/*e* ratio of 10. The researchers reported an increasing effect of the *P*/*e* ratio in increasing Nu and *f*. Additionally, when increasing *f*, a decrease in Nu was observed while increasing the relative roughness pitch.

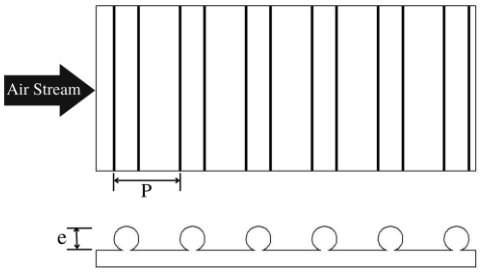

Fig. 8. Transverse wire rib (drawn after [86]).

Gupta [87] conducted an experimental study on a conventional-cum-modified solar air heater with a rectangular duct to investigate the heat transfer mechanism and flow behaviour over the absorber plate. He employed transverse wire ribs as artificial roughness to find the effect of rib roughness on the thermal performance of the modified SAH in the transitional rough region, as depicted in Fig. 9. He used design and flow parameters, such as the aspect ratios of 6.7 to 11.5, *P*/*e* ratio of 10, *e*/*D* ratio ranging from 0.018 to 0.052, and Re within 3000−18 000. As a result, he reported that a correlation between heat and momentum transfer roughness functions $R(e^+)$ and $G(e^+)$ for a varying range of roughness Reynolds numbers of 5 to 70. He concluded that the correlation between $R(e^+)$ and $G(e^+)$ can be used to design a SAH. He also found a strong correlation between Nu and *f*, based on theoretical and experimental values.

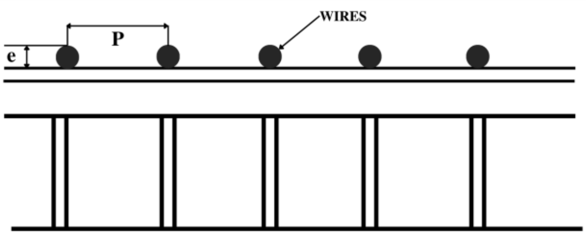

Fig. 9. Transverse wire rib (drawn after [87]).

Karwa [88] performed an experimental study on the rectangular duct in view of the performance improvement of SAH using different types of repeated ribs, as seen in Fig. 10. These ribs

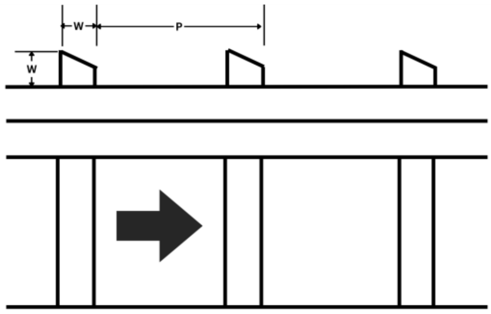

Fig. 10. Transverse wire rib (drawn after [88]).

are transverse, V-discrete, V-continuous, and inclined types of patterns were tested. The parameters involved in the study were a *P*/*e* ratio of 10 (fixed), an *e*/*D* ratio ranging from 0.0467 to 0.050, an angle of inclination fixed at 60°, and the working parameters such as Re varying between 2800 and 15 000. The author reported that the V-down discrete pattern of augmented absorber plate-based SAH provided the maximum increment in heat transfer under unique conditions. In addition, the author reported significant correlations for Nu and *f* in the performance evaluation of SAH.

Layek et al. [89] experimentally investigated the repeated transverse chamfered rib-grooved roughened SAH (Fig. 11) to understand heat flow and entropy generation inside the duct. The physical parameters taken included the chamfer angle from 5° to 30°, a relative roughness height of 0.03 (fixed), the relative groove position (*g*/*P*), a relative roughness pitch of 10 (fixed) and Reynolds number varying between 3000 and 21 000. The authors found that the Nusselt number and friction factor for the roughened SAH increased 2.6 and 3.35 times, respectively, compared to the smooth SAH at an optimised chamfer angle of 18°. Also, they reported that the maximum thermo-hydraulic performance achieved was 1.76.

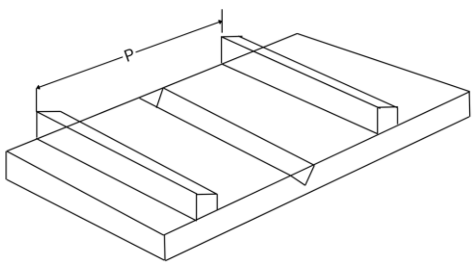

Fig. 11. Transverse wire rib (drawn after [89]).

Saini and Saini [90] conducted an experimental study to see the effect of expanded metal mesh wire based artificially roughened SAH on the heat transfer phenomena, as seen in Fig. 12. They utilised the system parameters such as the relative long-way length of a mesh (*L*/*e*) of 25 to 71.87, the relative short-way length of a mesh (*S*/*e*) of 15.62 to 46.87 and the relative height of a mesh (*e*/*D*) of 0.012 to 0.039, and the Reynolds number ranging from 1900 to 13 000. In the case of the modified SAH with the mesh wire based rib roughness, they obtained a maxi-

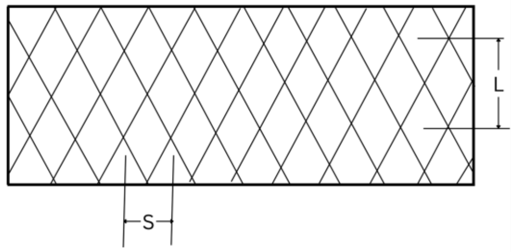

Fig. 12. Expanded metal mesh wire (drawn after [90]).

mum increase in Nu and *f* of 4 and 5, respectively, compared to a smooth SAH. They also reported a strong correlation between Nu and *f* for the accurate prediction of fluid flow behaviour.

Verma and Prasad [91] performed an experiment to evaluate the impact of transverse wire artificial roughness on the fluid flow characteristics and the rate of heat transfer along with the flow behaviour – the flow mechanism inside the SAH is shown in Fig. 13. They employed the design parameters and working parameters, such as a *P*/*e* ratio of 10–40, an *e*/D ratio ranging from 0.01 to 0.03, and Re ranging from 5000 to 20 000. They also considered the roughness Reynolds number (e+) for the study. For a roughened duct, they obtained an enhancement in Nu ranging from 1.25 to 2.08 compared to a smooth duct-based SAH, and also reported an optimum thermo-hydraulic performance (THP) of 1.71.

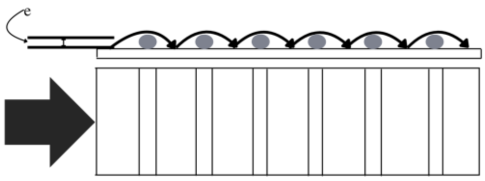

Fig. 13. Transverse wire roughness (drawn after [91]).

Singh et al. [92] performed experimental and numerical studies of multiple transverse broken and square wave-shaped ribs as roughness elements, depicted in Fig. 14, for evaluation of the performance characteristics of SAH. They utilised design parameters such as *e*/*D* = 0.043 (fixed), *W*/*w* = 7 (fixed), *P*/*e* = 10 (fixed), and the Reynolds number as the working parameter, varied from 3000–18 000 (six levels). They concluded that SAH with multiple broken ribs performed better, achieving 2.38 times higher THP under identical conditions compared to the solar air heater with broken transverse ribs. Furthermore, they found that at Re of 15 000, THP for multiple broken transverse ribs was 2.10 times higher, and for square wave-shaped ribs, 1.62 times higher, compared to smooth duct SAH. Also, they obtained increased values of Nu and *f* – 2.50 times and 3.92 times, respectively, for multiple transverse broken ribs, and 3.24 times and 3.85 times, respectively, for square wave-shaped ribs.

Singh et al. [93] studied the impact of artificially roughened SAH using square-wave shaped and non-uniform ribs (shown in Fig. 15) to evaluate an enhancement in the thermal performance.

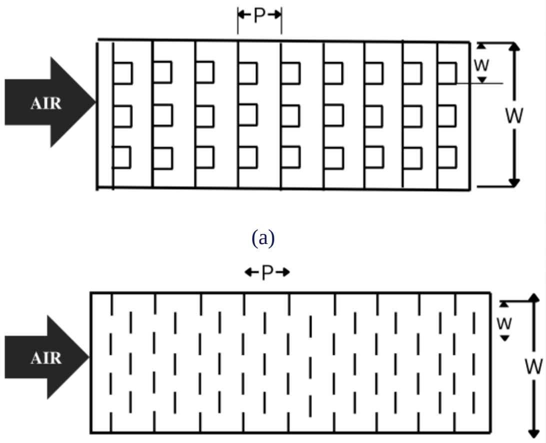

Fig. 14. Roughness elements: (a) square wave-shaped ribs, (b) multiple transverse broken ribs (drawn after [92]).

They employed a CFD (computational fluid dynamics) technique to save resources and periodic gaps to minimise eddies just after the ribs. They also used the following design and working parameters: a relative roughness width of 10–310; a relative roughness pitch of 10 (fixed); a relative roughness height of 0.043 (fixed); the Reynolds number ranging from 3000 to 15 000. The authors quoted a maximum augmentation of the Nusselt number of 2.22 and a maximum augmentation of the friction factor of 3.44. They also reported a maximum thermo-hydraulic performance value of 1.49. Finally, they concluded that non-uniform rib-based SAH gives better performance compared to uniform rib-based SAH.

Sharma et al. [94] analysed SAH by employing six distinct roughness geometries, such as transverse ribs with and without an inclination angle, dimples with and without an inclination angle, arc-based rib and sine-wave type rib, using a CFD approach to improve heat transfer and fluid flow characteristics. The design parameters used were *P*/*e* = 10 (fixed) and e/D_h = 0.271 (fixed), and the working parameter was the Reynolds number varying from 3000 to 18 000 to capture the behaviour of SAH exactly. The authors reported maximum enhancement in Nu of 3.60 at the optimum Re of 15 000 and maximum augmentation in *f* of 15.5 at Re = 3000 for sine wave-shaped baffles compared

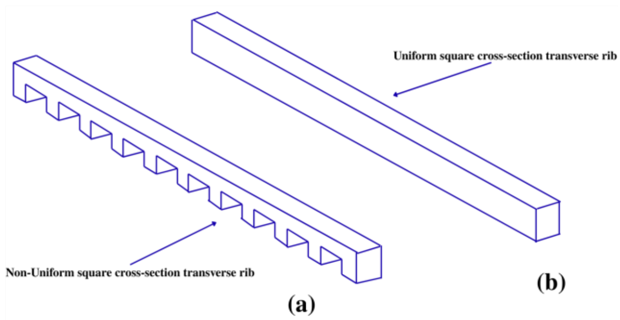

Fig. 15. Roughness elements: (a) non-uniform ribs, (b) uniform ribs (drawn after [93]).

to the smooth case. They also found the maximum THP value for the sine wave-shaped baffles based SAH amounting to 2.05 at the optimal Re of 15 000.

Mahanand and Senapati [95] performed a CFD analysis of a SAH for the prediction of heat transfer and fluid flow characteristics using transverse inverted-T shaped ribs shown in Fig. 16 as roughness elements. As control parameters, they used an e/D ratio of 0.042 (fixed), a P/e ratio varying from 7.14 to 17.86, and Re varied from 3800 to 18 000 over a two-dimensional (2D) fluid flow SAH domain. Additionally, boundary conditions were implemented utilising an aluminium absorber plate along with the RNG (renormalization group theory) k–ε model with an enhanced wall treatment for capturing a real-time view inside SAH. The authors obtained a maximum augmentation of Nu for SAH with an absorber plate roughened with the inverted-T ribs by a factor of 2.747 compared to a smooth plate SAH. The optimum design parameters for improved Nu were P/e = 7.14 and Re = 15 000. Also, for P/e of 7.14 and Re of 3800, the maximum f achieved was 3.404 times that of a smooth duct. They also reported a THP of 1.87 for an inverted T-shaped ribbed SAH, under the following operating conditions: P/e ratio of 7.14 and e/D_h ratio of 0.042 at Re = 15 000. They also found sound correlations between Nu and f.

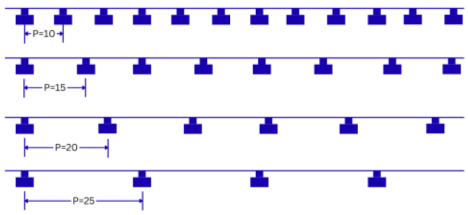

Fig. 16. Roughness elements in the form of transverse inverted-T shaped ribs (drawn after [95]).

Gawande et al. [96] studied two novel roughness geometries, such as combined square and equilateral triangular ribs over a flat absorber plate (Fig. 17) for thermal and thermo-hydraulic performance enhancement, using both experimental and CFD techniques. The design and flow parameters utilised were: a P/e ratio varying from 7.14 to 17.86, an e/D ratio of 0.042 (fixed) and Re varying from 3800 to 18 000. In this study, a constant heat flux of 1000 W/m^2 and the RNG k–ε turbulence model were employed to minimise the deviation between the experimental and CFD results. The highest increments in Nu and f reported were 2.877 and 3.849 for a P/e ratio of 7.14, an e/D ratio of 0.042 and Re of 18 000. Also, a THP of 1.86 was obtained at the optimum operating parameters, such as P/e = 7.14, e/D = 0.042 and Re = 18 000. It was observed that combined ribs give better SAH performance compared to individual ribs.

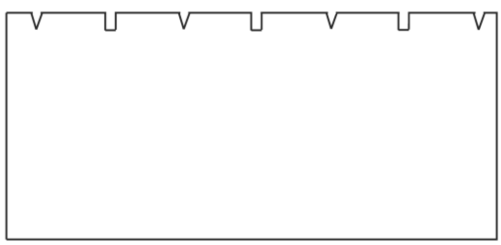

Fig. 17. Roughness geometry of combined square and equilateral triangular ribs (drawn after [96]).

Kumar et al. [97] studied experimentally the double-pass SAH consisting of a flat plate kind absorber to enhance thermal performance compared to conventional SAH, as depicted in Fig. 18. They employed asymmetric semi-circular and symmetric circular shapes as roughness over the absorber plate. They found that asymmetric semi-circular based roughness performed better in SAH compared to a symmetrical shape based SAH. Moreover, novel correlations were developed for Nu and f as a function of Reynolds number and relative roughness height. This correlation showed strong prediction capability.

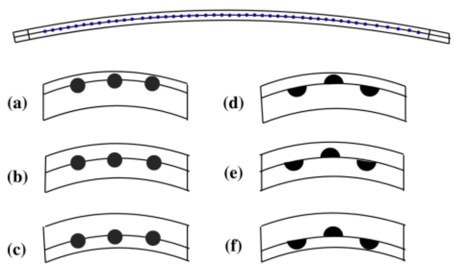

Fig. 18. Symmetric circular (a – c) and asymmetric semi-circular (d – f) shapes as roughness (drawn after [97]).

Kumar and Layek [98] combined two techniques to emphasise the rate of heat transfer and fluid flow characteristics of a modified SAH with roughness geometry of circular ribs over an absorber plate, using liquid crystal thermography (LCT) and CFD technique. The roughness geometry is represented in Fig. 19. The design parameters involved were: a P/e ratio taken as 10 and 20, a constant e/D_h ratio and Re varying from 8551 to 11149. Liquid crystal thermography produced graphical results of Nu and f. The maximum enhancement in the Nusselt number obtained through the combined approach was 1.97 compared to the smooth duct.

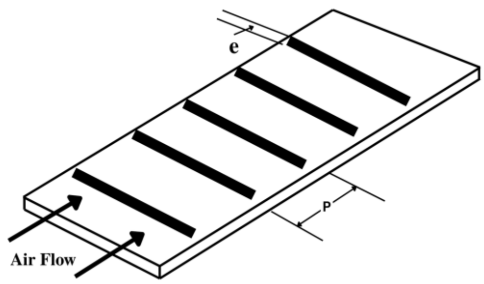

Fig. 19. Roughness geometry of circular ribs (drawn after [98]).

Kumar et al. [99] modified SAH with square ribs and also modified the cross section of the duct to capture an impact on thermal and thermo-hydraulic performance of the SAH compared to a conventional SAH, as illustrated in Fig. 20. Two sets

Fig. 20. Roughness geometry of square ribs(drawn after [99]).

of design parameters were tested by the CFD technique, i.e. the *P*/*e* ratio ranging from 5 to 13 and the *e*/*D* ratio ranging from 0.013 to 0.05. The authors also mentioned Re varying from 3900 to 17 900. They found that the *k*–*ε* based turbulent model performed significantly better than other methods tested. The enhancement in performance evaluated after modification showed that Nu increased by 1.97 times and *f* increased by 2.53 times compared to the smooth duct. The highest THP calculated was 1.44 at the optimum parameters of *P*/*e* = 10 and *e*/*D* = 0.05 at Re of 17 900. Their study revealed a strong correlation for Nu and *f*, with a maximum deviation of about 15%.

Kumar et al. [100] studied the mechanism of heat transfer and fluid flow phenomena of SAH using rectangular ribs over the absorber plate, as depicted in Fig. 21. The duct was triangular in cross-section, created for CFD evaluations. The physical design parameters employed for the study were the aspect ratio (*e*/*w*) in the range of 0.25 to 4.0, *e*/*D* ratio in the range of 0.02 to 0.04, *P*/*e* ratio in the range of 5 to 15; Re varied between 4000 and 18 000. The authors reported a maximum THP of 1.89 at optimum parameters: a *P*/*e* ratio of 10, an *e*/*w* ratio of 4.0, an *e*/*D* ratio of 0.04 and Re of 15 000.

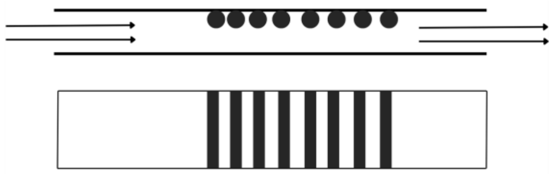

Fig. 21. Roughness geometry of rectangular ribs (drawn after [100]).

Kumar et al. [101] evaluated the performance of SAH with three novel models of SAH and roughness over the absorber plate. The roughness geometry is shown in Fig. 22. The design parameters used were the apex angle of 60, number of rounded corners 0 to 1, a curvature radius of 0 to 0.393 *H* (where *H* is the duct height) and operating parameter Re varied from 4000 to 18 000. The minimum enhancement in the performance of SAH

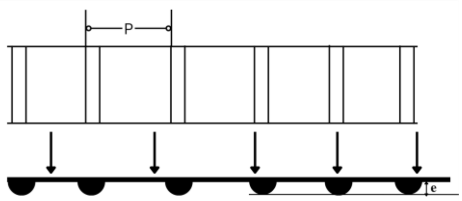

Fig. 22. Roughness geometry of semi-circular ribs (drawn after [101]).

reported was 1.87 times that of the conventional model with no roughness element over the absorber plate.

7.2. Arc-shaped rib roughness

Saini and Saini [102] performed an experimental investigation on modified SAH for performance enhancement. The modification of SAH was carried out using an arc-shape parallel wire as the roughness element (Fig. 23). The design and operating parameters considered in the study were *P*/*e* ratio of 10 (fixed), a relative roughness height (*e*/*D*) ranging from 0.0213 to 0.0422, a relative angle of attack (*α*/90°) varying between 0.3333 and 0.6666, and Re ranging from 2000 to 17 000. It was found that, compared to the smooth duct of SAH, Nu increased by 3.80 times and *f* increased by 1.75 times. Based on the experimental datasheet of Nu and *f*, strong correlations were developed with good accuracy.

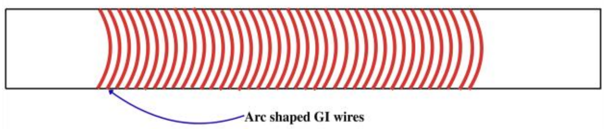

Fig. 23. Roughness geometry of arc-shaped parallel wires (drawn after [102]).

Singh et al. [103] used multiple arc-shaped ribs as roughness elements for the modification of SAH (Fig. 24) to improve its thermal performance. The parameters of practical and operating conditions, such as Re ranging from 2200 to 22 000, *e*/*D* ratio ranging from 0.018 to 0.045, *W*/*w* ratio ranging from 1 to 7, *P*/*e* ratio varied between 4 and 16, and arc angle (*α*) within the range of 30° to 75°. They reported the maximum increase in Nu and *f* of 5.07 and 3.71, respectively, compared to the smooth duct. The optimum parameters they obtained were: Re of 22 300, *W*/*w* ratio of 5, *e*/*D* ratio of 0.045, *P*/*e* ratio of 8 and *α* of 60°. The maximum THP reported at optimum parameters was 3.4.

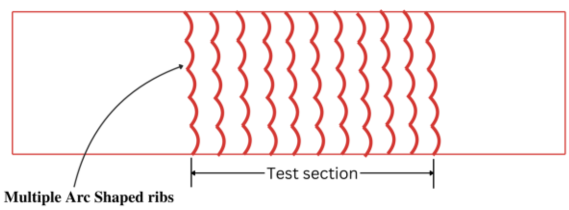

Fig. 24. Roughness geometry of multiple arc-shaped ribs (drawn after [103]).

Sahu and Prasad [104] investigated a modified SAH for exergetic performance enhancement using roughness geometry in the form of arc-shaped wire ribs (Fig. 25), using an analytical approach. The mathematical model was developed to validate the results. The maximum exergetic performance improvement compared to a smooth duct was found to be 56%.

Kumar et al. [105] modified the SAH with a novel roughness geometry consisting of discrete multi arc-shaped ribs combined

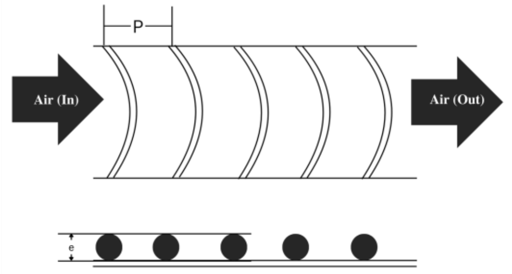

Fig. 25. Roughness geometry as arc-shaped wire ribs (drawn after [104]).

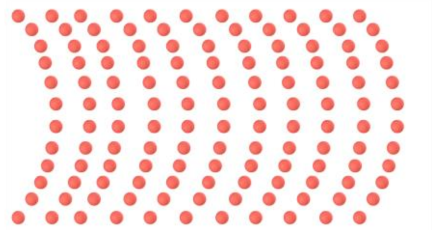

Fig. 27. Circular protrusions in angular arc-shaped arrangement (drawn after [106]).

with jet impingement for an enhancement in heat transfer and fluid flow characteristics, as seen in Fig. 26. The design and operating parameters utilised were: the relative discrete distance of 0.27−0.86, the relative discrete width of 0.32−1.72 (varying), the relative rib height of 0.025−0.047 (varying), the relative rib pitch of 0.58−3.1 (varying), the arc angle of 35°−65° (varying), the stream wise pitch ratio of 0.47−1.72 (varying), the spanwise pitch ratio of 0.46−0.82 (varying) and the Reynolds number varying from 3000 to 19 000. They reported an increment in Nu and *f* for a modified SAH of 7.61 and 6.48, respectively, as compared to the smooth SAH. In addition, the THP for optimised design parameters was 4.1. Correlations were developed for Nu and *f* to predict thermal and fluid characteristics inside the SAH.

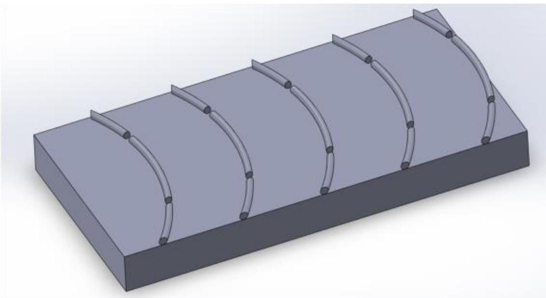

Fig. 26. Discrete multi arc-shaped ribs combined with jet impingement (drawn after [105]).

Yadav et al. [106] studied experimentally the effect of heat transfer and fluid flow mechanism of a modified SAH, incorporating circular protrusions in angular arc-shaped arrangement as roughness elements, as seen in Fig. 27. The physical and operating variables used included: a *P*/*e* ratio varying from 12 to 24, an *e*/*D* ratio varying from 0.015 to 0.03, the arc angle of protrusions arrangement varying from 45° to 75° and Re ranged from 3600 to 18 100. The maximum augmentation of Nu and *f* was 2.89 and 2.93 times, respectively, in comparison to a smooth SAH. The authors also developed correlations for Nu and *f*.

Ghritlahre [107] performed an experimental study for augmentation of heat transfer and fluid flow characteristics by modifying conventional SAH with a novel arc-shaped artificial roughness in two major configurations, such as apex up and apex down, as shown in Fig. 28. They employed the design parameters as a *P*/*e* ratio of 10 (fixed), an *e*/*D* ratio of 0.0395 (fixed), a rib roughness of 2.5, and an arc angle of 60°. The operating

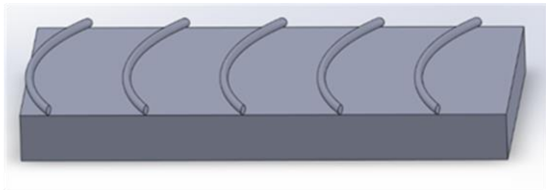

(a)

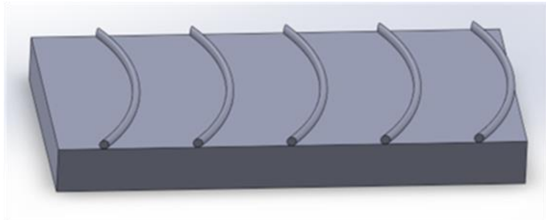

(b)

Fig. 28. Arc-shaped ribs in two major models, such as apex up and apex down (drawn after [107]).

parameter they used was the mass flow rate, ranging from 0.007 to 0.022 kg/s. They observed the maximum enhancement of 1.42 in heat transfer compared to smooth SAH in the apex upstream flow.

Srivastava et al. [108] performed CFD analysis of modified SAH, using artificial roughness in the form of dissimilar repeated ribs. These ribs were arc-shaped with a gap and V-shaped with a gap (Fig. 29) for the enhancement of thermal and thermo-hydraulic performance of the SAH. The boundary conditions were set as: a *g*/*e* ratio of 1, an *e*/*D* ratio of 0.04, a *P*/*e* ratio of 10, a *p*/*P* ratio of 0.65, a relative gap distance (*d*/*W*) of 0.69, a number of gaps – 1, an arc angle of 60°, a constant heat flux of 1000 W/m^2, and Re ranging from 3000 to 15 000. The Nu and *f* for arc-shaped ribs with gaps were increased by 2.4 and

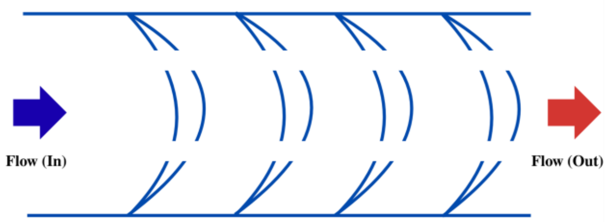

Fig. 29. Arc-shaped ribs with gaps as roughness elements (drawn after [108]).

3.94 times, respectively, at Re = 3000. The maximum THP values reported were 2.21 and 1.5 for V-shaped ribs and arc-shaped ribs, respectively.

Gill et al. [109] conducted experimental studies on modified SAH using broken arc ribs combined with staggered rib for enhancement of thermal and thermo-hydraulic performance of the SAH, as seen in Fig. 30. They utilised the following design parameters: a fixed relative staggered rib position of 0.4, an e/D ratio of 0.043, a relative gap size of 0.65, an arc angle of 60°, and a P/e ratio of 10 (fixed). They used Re ranging from 2000 to 16 000 as the operating variable. The maximum augmentation of Nu and f was 3.06 and 2.50, respectively, compared to the smooth duct. They also reported the highest THP of 2.27 in the whole study.

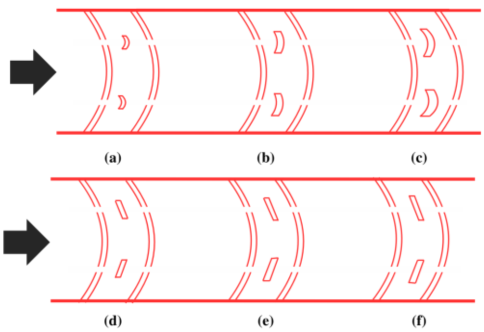

Fig. 30. Roughness in the form of the broken arc ribs combined with staggered rib (drawn after [109]).

Bhuvad et al. [110] performed an experimental study on the enhancement of heat transfer and fluid flow characteristics of modified SAH using roughness elements as novel apex-up discrete arc rib, as depicted in Fig. 31. They modified SAH by augmenting parameters, such as the angle of attack (α) in three-step (30°, 40°, 60°), the g/e ratio of 4 (fixed), the e/D ratio of 0.045 (fixed), P/e set to 10, and the number of gaps set to 3. They used Re ranging from 3000 to 14 000 as the operating parameter. The authors obtained the maximum increase in Nu and f of 2.92 and 3.04 times, respectively, compared to smooth SAH. The maximum THP found was 2.01 across all cases of studied SAH. The correlations for Nu and f were developed for the prediction of similar cases in SAH.

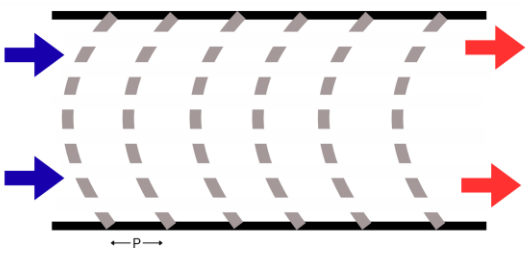

Fig. 31. Apex-up discrete arc rib as a roughness element (drawn after [110]).

Korpale et al. [111] developed a modified SAH using rectangular section ribs, shown in Fig. 32, to enhance the heat transfer capability of SAH. They employed the following design parameters: a P/e ratio range of 5−60, an e/D ratio in the range of 0.065−0.252, a w/W ratio in the range of 0.5−10 and Re varying from 4000−20 000. The maximum THP found for modified SAH was 2.77. They also validated the experimental results with CFD results for optimisation.

Fig. 32. Roughness element as the rectangular section ribs (drawn after [111]).

Kumar et al. [112] developed SAH with a novel geometry consisting of multiple-arc shaped ribs with gaps (Fig. 33), designed for better heat transfer and fluid flow under the absorber plate of a new modified SAH. The parameters they used for the study were: a number of gaps of 3, a relative gap width of 0.5−1.5, a relative gap position of 0.3−0.9, and varying Reynolds number of 4000−20 000. They reported an enhancement of the Nusselt number and an increase in friction factor, with deviation of ± 6.15% and ± 5.74%, respectively, compared to the smooth- duct-based SAH. Additionally, the maximum THP obtained for the modified SAH was 2.77 at optimum parameters. These were: a relative pitch of 17.22, a relative rib height of 0.044, a relative gap width 0.5 and the Reynolds number of 20 000.

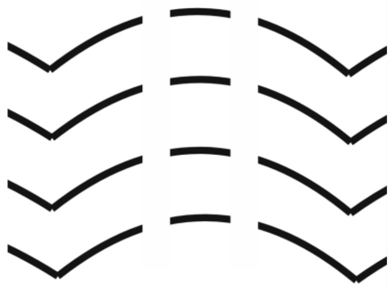

Fig. 33. Multiple-arc shaped ribs with gaps as roughness elements (drawn after [112]).

7.3. V-shaped ribs

Singh et al. [113] experimentally investigated SAH with discrete V-shaped ribs as artificial roughness, with the view to heat trans-

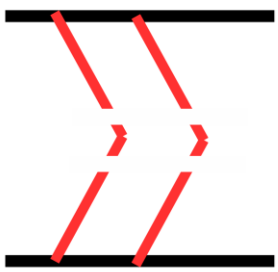

Fig. 34. Roughness elements in the form of discrete V-shaped ribs (drawn after [113]).

fer and fluid flow enhancement (Fig. 34). They used various design parameters, such as a P/e ratio ranging from 4 to 12, an e/D ratio ranging from 0.015 to 0.043, α of 30° to 75°, a g/e ratio varying between 0.5 and 2.0, and a relative gap position (d/w) ranging from 0.20 to 0.80. They also used Re varying from 3000 to 15 000 as an operating parameter. The authors found the maximum augmentation in Nu and f of 3.04 and 3.11, respectively, as compared to the smooth duct. They also reported the optimal parameters to achieve the highest Nu and f using the discrete V-shaped rib roughness, which were: a d/w ratio of 0.65, a g/e ratio of 1.0, a P/e of 8.0, α of 60° and an e/D ratio of 0.043. They also developed the correlations for Nu and f in terms of Re and other rib variables.

Momin et al. [114] reported an experimental analysis of a SAH modified with V-shaped rib roughness (Fig. 35) for evaluating an enhancement of heat transfer and fluid flow behaviour. The design and operating parameters used by the authors were: an e/D ratio of 0.02 to 0.034, α of 30° to 90° (fixed), a P/e ratio of 10, and varying Re ranging from 2500 to 18 000. The reported maximum increments across all configurations of modified SAH were: an enhancement in Nu by 2.30 times and an increase in f by 2.83 times compared to the smooth SAH. They also developed correlations for Nu and f, with the conclusion that Re has more impact on the performance than α.

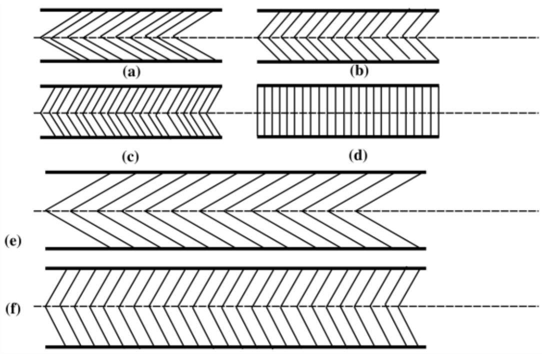

Fig. 35. Roughness element formed by the V-shaped rib (drawn after [114]).

Hans et al. [25] performed an experimental investigation on a SAH, modifying it with an artificial roughness in the form of different types of multiple V-shaped ribs for amelioration in heat transfer and fluid flow behaviour in the SAH. They utilised the design parameters, such as an e/D ratio varying from 0.019 to 0.043, a P/e ratio varying from 6 to 12, α varying from 30° to 75°, a W/w ratio varying from 1 to 10 and Re ranging from 2000 to 20 000 as operating parameter. By modification, they obtained the highest increase in Nu and f – of 6 and 5 times, respectively – compared to a smooth duct. They also developed a statistically based correlation for Nu and f for predicting the SAH performance.

Deo et al. [115] conducted an experimental study on modification of SAH by using artificial roughness in the form of multi-gap V-down ribs combined with staggered ribs for performance enhancement of conventional SAH, as portrayed in Fig. 36. The variables they used for design and operation were: a P/e ratio of 4−14, an e/D ratio of 0.026−0.057, α of 40°−80°, a g/e ratio of 1 (gap width to rib height as fixed), a w/e ratio of 4.5 (staggered rib length to rib height ratio as fixed), a p/P ratio of 0.65 (relative staggered rib pitch as fixed), a N_p of 2 (number of gaps), and Re in the range of 4000 to 12 000. The obtained maximum augmentation in Nu was 3.34 and the maximum THP found was 2.45.

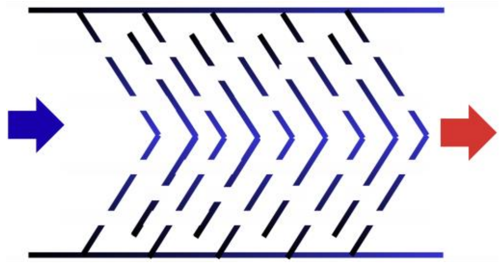

Fig. 36. Roughness elements in the form of multi-gap V-down ribs combined with staggered ribs (drawn after [115]).

Singh et al. [116] developed an experimental setup of modified SAH with V-down ribs with a gap as roughness elements to examine an enhancement of thermal and thermo-hydraulic performance of conventional SAH, as shown in Fig. 37. They utilised design parameters and operating parameters, including an angle of attack of 60° (fixed), a relative roughness height of 0.043 (fixed), a duct aspect ratio of 12, a relative roughness pitch of 4−12 (five step) and the Reynold number varying from 3000 to 12 000. For the modified SAH, they reported the maximum augmentation in the Nusselt number and friction factor of 2.70 and 2.86, respectively. They also found that the highest THP for the modified SAH was 1.93.

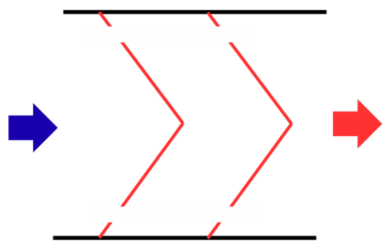

Fig. 37. V-down ribs with a gap as roughness elements (drawn after [116]).

Kumar et al. [117] accomplished an experimental study on the modified SAH, using artificial roughness in the form of multiple V-shaped ribs with gaps to improve heat transfer and fluid flow behaviour of a SAH. They used the design and run parameters, such as a P/e ratio of 10 (fixed), an e/D ratio of 0.043 (fixed), a W/w ratio of 6 (fixed), a relative gap distance (G_d/L_v) within a range of 0.24 to 0.80, a g/e ratio ranging from 0.5 to 1.5, an α of 60°(fixed), and Re varying between 2000 to 20 000. They observed the maximum increase in Nu and f of 6.32 and 6.12, respectively, for modified SAH as compared to a smooth duct. They also observed an improvement in THP of 3.6 for the modified duct compared to conventional smooth SAH.

Patel and Lanjewar [118] developed the modified SAH using artificial roughness as a V-geometry with symmetrical gap and staggered elements, as depicted in Fig. 38. To achieve the objec-

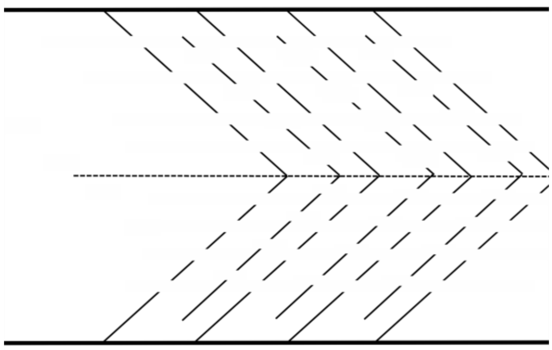

Fig. 38. Roughness formed by a V-geometry with symmetrical gap and staggered elements (drawn after [118]).

tive they employed the governing design parameters, such as a duct aspect ratio (W/H) of 12 (fixed), a P/e ratio of 10, an e/D_h ratio of 0.043, an α of 60°, a ratio of staggered rib position to pitch (P'/P) of 0.4 (fixed), a ratio of gap width to rib height (g/e) of 4, a number of main gaps (N_g) equal to 4, a ratio of staggered size to rib height (r/e) of 4, a relative gap size of additional gap in the symmetrical rib elements (g'/e) in the range of 0.5 to 2, the relative gap position of additional gap in the symmetrical rib elements (d/w) in the range of 0.25 to 0.85, and Re varying between 4000 to 15 000. The maximum obtained enhancement in Nu and f for modified SAH was 2.51 and 2.70, respectively, compared to the smooth SAH. The maximum THP found was 1.82 for the optimum variables, such as Re of 12 524, a g'/e ratio of 1 and a d/w ratio of 0.65.

Srivastava et al. [108] performed a CFD analysis of the SAH modified using dissimilar repeated ribs as artificial roughness to enhance the SAH's thermal and thermo-hydraulic performance. The ribs were of V-shape with a gap, as illustrated in Fig. 39. The boundary conditions used were: a g/e ratio of 1, an e/D ratio of 0.04, a P/e ratio of 10, a p/P ratio of 0.65, a d/W ratio of 0.69, a number of gaps of 1, arc angle of 60°, constant heat flux of 1000 W/m^2, and Re ranging from 3000 to 15 000. The maximum enhancement in Nu and f they obtained for V-shaped ribs was 2.4 and 3.4, respectively, at Re = 15 000. The maximum THP values reported were 2.21 and 1.5 for V-shaped ribs and arc-shaped ribs, respectively.

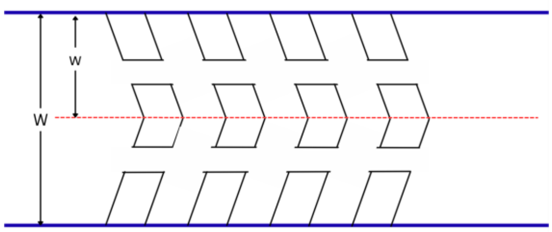

Fig. 39. Roughness element in the form of a V-shaped rib with a gap (drawn after [108]).

7.4. Dimple or protrusion ribs

Kumar and Prasad [119] extensively conducted an experimental study on a modified SAH roughened with concave dimples for better performance of conventional SAH. They compared a 3-sided roughened SAH with a 1-sided conventional SAH. They utilised various design and operating parameters, such as a P/e ratio in the range of 8 to 15, an e/D ratio in the range of 0.018 to 0.045, an e/d ratio in the range of 1 to 2, and Re varied from 2500 to 13 500. They reported that Nu and f were affected by roughness parameters. The maximum increase in Nu and f across all cases investigated was 3.94 and 2.79.

Saini and Verma [120], aimed at improving the performance of SAH, performed an experimental investigation artificially roughened SAH with dimple shape roughness elements, as shown in Fig. 40. The employed design and operating parameters were: a relative roughness height (e/D) in the range of 0.018−0.037, a relative pitch (p/e) in the range of 8−12, and the Reynolds number ranging within 2000−12 000. They observed that, under all studied cases, the maximum Nu and f were 7.58 and 4.68, respectively, compared to a smooth duct. They also developed correlations for Nu and f for the performance prediction of SAH.

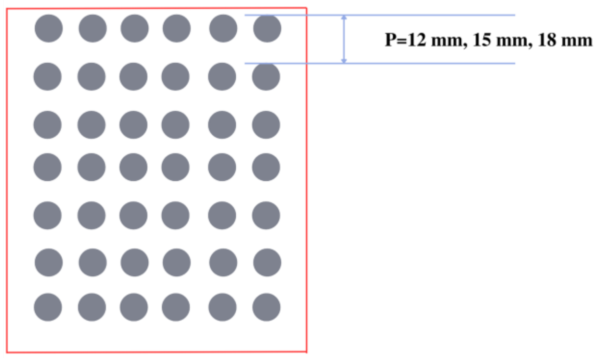

Fig. 40. Dimple-shaped roughness elements (drawn after [120]).

Kumar and Verma [121] performed extensive experimental, as well as numerical investigation, on sinusoidal-based SAH for performance enhancement. They employed the design and operating parameters, such as a hydraulic diameter (D_h) of 33.33 mm, a roughness pitch (P) of 10−18 mm (in three steps), a roughness height (e) of 1 mm, an aspect ratio (W/H) of 5, and the Reynolds number varied from 4000 to 15 000. Compared to a smooth duct, they obtained maximum augmentation in Nu and f of 2.48 and 1.76, respectively. The highest calculated THP was 2.05 at the optimum parameters of P = 10 mm and Re = 4000. The authors also concluded that THP obtained from experimental analysis deviated by 6.77% compared to the CFD results.

Bhusan and Singh [122] developed a modified SAH with protrusion roughness for an enhancement of SAH performance, as illustrated in Fig. 41. The employed various design and operating parameters included: a relative short way length (S/e) in the range of 18.75 to 37.50, a relative long way length (L/e) in the range of 25.00 to 37.50, a relative print diameter (d/D) ranging from 0.147 to 0.367, a relative roughness height (e/D) of

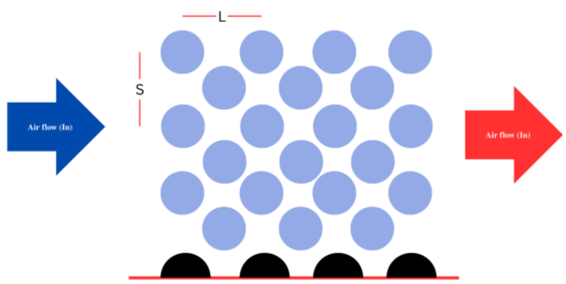

Fig. 41. Protrusions as roughness elements (drawn after [122]).

0.03 (fixed), and the Reynolds number ranging between 4000 and 20 000 during experimentation. The maximum Nu and f obtained were 3.8 and 2.2, respectively, compared to a smooth duct. The maximum performance was evaluated at the optimum parameters, as the S/e ratio of 31.25, L/e ratio of 31.25 and d/D ratio of 0.294. They also developed correlations for Nu and f.

Hassan et al. [123] performed an experimental investigation on modified SAH by using artificial roughness as dimple roughened in multiple arc pattern in the view of performance enhancement as seen in Fig. 42. The employed design and operating parameters included a relative roughness pitch (p/e) in the range of 4 to 16, a relative roughness height (e/D_h) in the range of 0.018 to 0.045, a relative roughness width (W/w) in range of 1 to 5, an angle of attack in the range of 30° to 75°, and the Reynolds number of 2000 – 18 000 as governing parameters for the modified SAH. The maximum increase in the Nusselt number and friction factor was found to be 5.61 and 2.27 times, respectively, compared to a smooth duct. The optimum parameters in that case were: Re of 17 984, a W/w ratio of 4, an e/D_h ratio of 0.036, a P/e ratio of 12 and α of 60°.

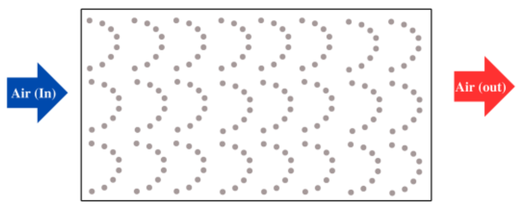

Fig. 42. Roughness elements in the form of dimples in multiple arc pattern (drawn after [123]).

Kumar [9] performed an experimental study on 1- and 3-sided concave dimple-roughened modified SAH (Fig. 43) aimed at improvement of thermal and thermo-hydraulic performance. The author employed the roughness design and run parameters, such as a relative dimple pitch in the range of 8 to 15, a relative dimple height of 0.018 – 0.045, a relative dimple depth in the range of 1 to 2, and a Reynolds number in the range of 2000 to 13 500. The maximum Nu and f were found to be 3.94 times and 2.79 times that of a smooth duct. Additionally, statistical correlations were developed for Nusselt number and friction factor. The percentage deviation between experimental and data collected through correlations was within the range of 5−6%.

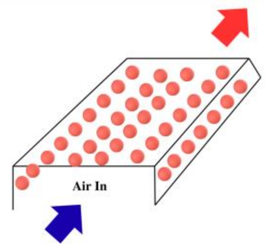

Fig. 43. Concave dimples as roughness elements (drawn after [9]).

Alam and Kim [124] fabricated a modified SAH using conical protrusion ribs as roughness elements for gaining higher thermal and thermo-hydraulic performance, as seen in Fig. 44. The design parameters employed were: a relative rib pitch (P/e) ranging between 6 and 12, a relative rib height (e/D) ranging from 0.200 to 0.044, and a Reynolds number of 4000 to 16 000. The authors developed correlations for Nu and f. They found maximum augmentation in Nu and f of 2.49 and 7.29, respectively, compared to a smooth SAH.

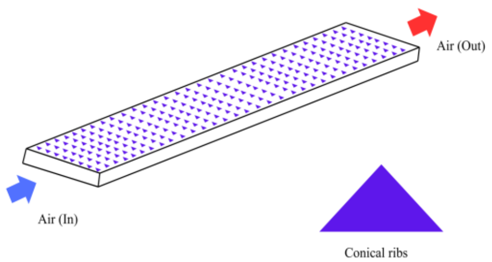

Fig. 44. Conical protrusion rib as a roughness element (drawn after [124]).

7.5. W-shaped ribs

Lanjewar et al. [125] developed modified SAH using W-shaped ribs with inclination as artificial roughness to optimise the performance of a conventional SAH. There were two major models tested with respect to flow as downstream W-down and upstream W-up, as shown in Fig. 45. They utilised various design parameters to evaluate proposed performance enhancement, such as a duct aspect ratio (W/H) of 8, a P/e ratio of 10 (fixed), an e/D of 0.03375 (fixed), α of 30° to 75°, and used Reynolds number varying from 2300 to 14 000 as a run parameter. The

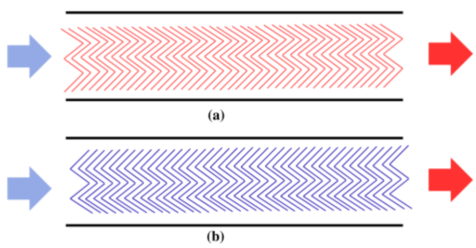

Fig. 45. Downstream W-down (a) and upstream W-up (b) roughness elements (drawn after [125]).

maximum increase in Nu and f obtained in the study was 2.36 and 2.01, respectively, for W-down ribs at the optimum parameters. These parameters were α = 60°, e/D = 0.03375 and Re = 14 000. They also developed correlations for Nu and f, which were acceptable within the range of 5 to 10% in any case.

Kumar et al. [126] conducted an experimental analysis on modified SAH using discrete W-shaped elements as artificial roughness for performance enhancement of conventional SAH, as illustrated in Fig. 46. They employed various design parameters, such as the duct aspect ratio of 8, Reynolds number varied from 3000 to 15 000, relative roughness height of 0.0168 to 0.0338, relative roughness pitch of 10 and the angle of attack (α) varied from 30° to 75°. They found that the modified SAH has the maximum increase of the Nusselt number and friction factor of 2.16 and 2.75 times, respectively, for α = 60°. They also developed correlations for Nu and f for SAH performance prediction.

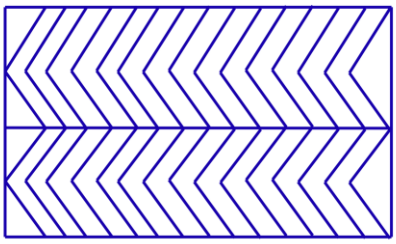

Fig. 46. Discrete W-shaped ribs as roughness elements (drawn after [126]).

Thakur and Thakur [127,128] developed modified SAH using multi-staggered rib parameters of the W-rib roughness as novel roughness geometry for the performance enhancement of conventional SAH, as illustrated in Fig. 47. The employed design and operating parameters included: a duct aspect ratio (W/H) of 10 (fixed value), an approach angle (α) 60° (as fixed value), a Reynolds number (Re) in range of 4000−14 000, a relative roughness height (e/D_h) 0.0423 (as fixed value), relative roughness pitch (P/e) in the range of 10 to 14, number of gaps (N_g) of 1 to 2, relative gap width (g/e) in the range of 0.5 to 2.0, relative staggered rib length (w/e) in the range of 1.5 to 6.0 and the relative staggered pitch (p/P) in the range of 0.45 to 0.75. They obtained the maximum Nu and f of 4.10 and 2.4, respectively, at the optimum parameters, which were: g/e = 1, N_g = 2, Re = 12 000, p/P = 0.65, P/e = 12 and w/e = 4.5. The calculated THP for the studied case was 3.24.

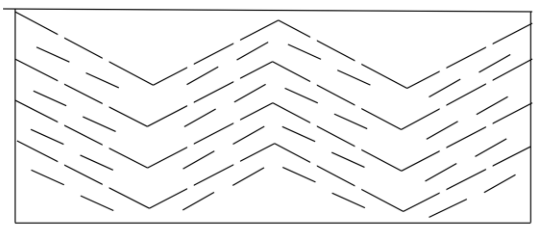

Fig. 47. Roughness in the form of W-shaped ribs with symmetrical gaps with staggered ribs patterns (drawn after [127,128]).

7.6. Spherical ball roughness

Murmu et al. [129] experimentally investigated the effects of artificial roughness on heat transfer and fluid flow characteristics of modified SAH using the spherical ball as roughness elements. The operating and design parameters they employed were: a relative roughness pitch (P/e) varied from 9 to 18, a relative roughness height (e/D_h) ranging from 0.024 to 0.040, a ball's height-diameter ratio (e/d_b) varied from 0.5 to 2, an angle of attack (α) ranging from 35° to 75° and a Reynolds number varied from 2500 to 18 500. In their study, the maximum increase in Nu and f were 3.56 and 2.67, respectively, compared with the smooth duct-based SAH. They also developed a correlation to predict the performance of SAH in terms of Nu and f.

7.7. Non-uniform ribs

Kumar et al. [100] performed a numerical study on a ribbed solar air heater to enhance heat transfer and thermo-hydraulic performance. Forward chamfered rib was in centre of their investigation, as shown in Fig. 48. They performed the analysis using Ansys CFD for the geometrical configuration and variables, such as a relative roughness height (e/D) of 0.018−0.043, a rib chamfered height ratio (e'/e) of 0 to 1, a rib aspect ratio (e/w) of 0.24 to 1.5 and Reynolds number ranging from 4000 to 17 000. The maximum increment in Nu and f reported in this research was 2.88 and 3.52 times, respectively. They also developed correlations for predicting the SAH performance.

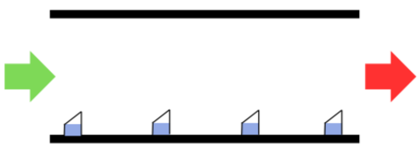

Fig. 48. Forward chamfered ribs as roughness elements (drawn after [100]).

Bhagoria et al. [130] conducted an experimental investigation to improve heat transfer in an SAH modified using wedge-shaped integral transverse ribs (Fig. 49), and developed correlations for heat transfer and friction factor. The utilised variables and physical parameters were: a Reynolds number varying from 3000 to 18 000, a relative roughness height varied between 0.015 and 0.033 and a rib wedge angle of 8°, 10°, 12° and 15°.

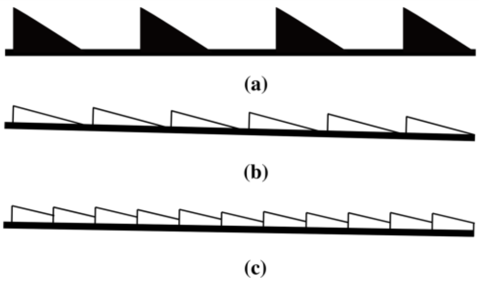

Fig. 49. Wedge-shaped ribs as roughness elements (drawn after [130]).

The authors reported a modified SAH to yield a Nusselt number up to 2.4 times higher and friction factor 5.3 times higher compared to a smooth duct. They also developed correlations for the Nusselt number and friction factor within an error band of ±15%, using functional parameters such as rib spacing, rib height, rib wedge angle and Reynolds number.

Barik et al. [131] modified SAH using six different types of ribs: T-shaped rib, left arm inclined T-shaped rib, right arm inclined T-shaped rib, Y-shaped rib, and concave and convex T-shaped ribs, to enhance the performance of SAH, as shown in Fig. 50. They analysed a modified SAH through experimentation and numerically. They developed a physical model using various parameters, such as the pitch from 20 mm to 90 mm, stem height from 3 mm to 11 mm, an inclination angle of the rib from 0° to 60° and a Reynolds number varying from 5000 to 18 000. They obtained the highest increment of Nu and f for a T-shaped rib. They also reported the highest THP of 1.7 for a T-shaped rib.

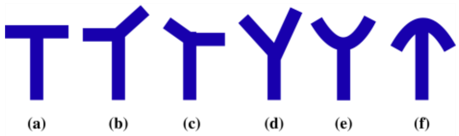

Fig. 50. Roughness element in the form of: T-shaped rib (a), right arm inclined T-shaped rib (b), left arm inclined T-shaped rib (c), Y-shaped rib (d), concave (e) and convex (f) T-shaped ribs (drawn after [131]).

Kumar and Goel [132] numerically investigated SAH considering various shapes of roughness elements, such as semi-circular, circular, triangular, square and rectangular, as depicted in Fig. 51, to enhance heat transfer through the absorber plate. The triangular passage was used with different parameters, such as Reynolds number varying from 3700 to 18 700, a relative rib-height of 0.0433, a relative rib pitch of 11, a rib aspect ratio (e/w) of 0.67 and 2.0, and a relative chamfered height of 0.75. They reported the highest THP value of 2.75 for a forward-chamfered rectangular rib at the optimum parameters of Re = 18 700 and e/w = 2.0.

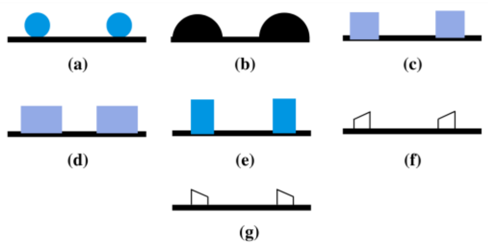

Fig. 51. Semi-circular, circular, triangular, square and rectangular shapes as roughness elements (drawn after [132]).

Zina et al. [133] analysed conventional SAH, modifying an absorber plate with triangular and semi-circular nooks with variable height of a three-rib set (Fig. 52) for performance enhancement. They performed a numerical analysis under changing pitch from 10 to 20, rib height from 0.7 to 2.2 and Reynolds number varying between 3800 and 18 000. The maximum enhancement in Nu and f found under that study were 2.55 and 0.22, respectively. They also reported an optimum THP of 1.93 for Re = 5000.

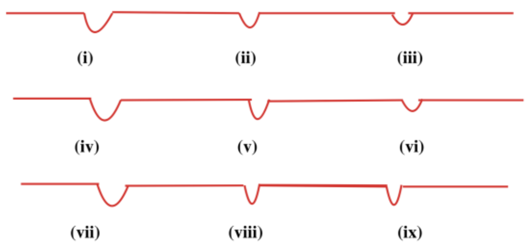

Fig. 52. Roughness element in the form of triangular and semi-circular nooks with variable height of three ribs (drawn after [133]).

Gawande et al. [134] investigated SAH numerically, as well as experimentally, using various ribs such as 20° chamfered rib, right-angle triangular and reverse L-shaped ribs, shown in Fig. 53, in terms of increasing Nu and f. They employed operating and control parameters, such as a rib height (e) of 0.7 to 1.4, a relative roughness pitch (P/e) of 7.14 to 35.71, a relative roughness height (e/D) of 0.021 to 0.042 and a Reynolds number ranging from 3800 to 18 000. They reported a maximum augmentation in heat transfer and fluid flow characteristics of 3.218 and 4.047, respectively, for 20° chamfered ribs based modified SAH. The calculated THP values were 2.047, 2.035 and 1.903, for 20° chamfered rib, right-angle triangular and reverse L-shaped ribs, respectively.

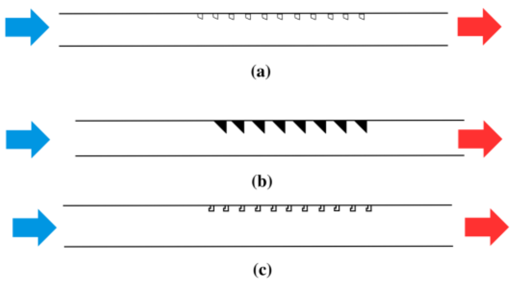

Fig. 53. Roughness elements in the form of 20° chamfered rib, right-angle triangular and reverse L-shaped ribs (drawn after [134]).

7.8. Inclined baffles

Aharwal et al. [135] performed an experimental investigation of a solar air heater modified with roughness of repeated square cross-section split-rib with gap for evaluation of heat transfer and friction behaviour of the fluid, as depicted in Fig. 54. They employed various process control parameters, including a relative roughness pitch of 10 (fixed), a relative roughness height of 0.0377, an angle of attack of 90° (fixed), a relative gap width ranging from 0.5 to 2.0, a relative gap position varying from 0.1667 to 0.667 and a Reynolds number varying from 3000 to 18 000. They obtained a maximum increment in Nu and f of 2.59 and 2.87, respectively.

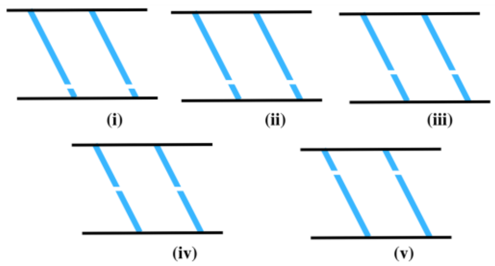

Fig. 54. Repeated square cross-section split-rib with gap as roughness elements (drawn after [135]).

Aharwal et al. [136] performed experimental investigation on modified SAH using integral repeated discrete square ribs as roughness element, as shown in Fig. 55. The used operating and physical parameters were: a relative roughness pitch of 4 to 10 (varying), a relative roughness height of 0.018 to 0.0377, an angle of attack of 30° to 90° (varying), a relative gap width ranging from 0.5 to 2.0, a relative gap position varying from 0.16 to 0.5 and a Reynolds number varying from 3000 to 18 000. In the study, the maximum obtained increase in Nu and *f* was 2.83 and 3.63 times, respectively, compared to a smooth SAH. The optimum parameters were: a relative gap position of 0.25 for a relative gap width of 1.0, a relative roughness pitch of 8.0, an angle of attack of 60° and a relative roughness height of 0.037.

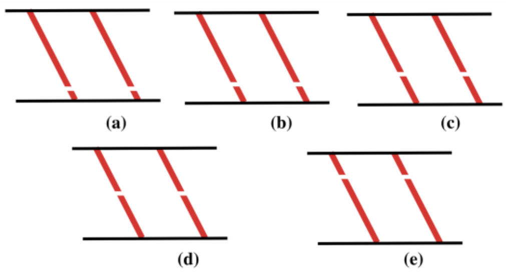

Fig. 55. Roughness element as integral repeated discrete square ribs (drawn after [136]).

Kumar et al. [137] modified SAH by using angled perforated baffles (Fig. 56) for improvement in heat transfer and fluid flow characteristics. They employed various parameters for evaluations, such as a relative baffle height of 0.5, a relative baffle pitch of 10, a relative hole position of 0.266, an open area ratio (β_0) of 12% and a Reynolds number varying from 5000 to 17 000. In the case under study, they obtained an enhancement in Nu and *f* of 3.82 and 7.14 times, respectively. The maximum determined value of THP for modified SAH was 1.94.

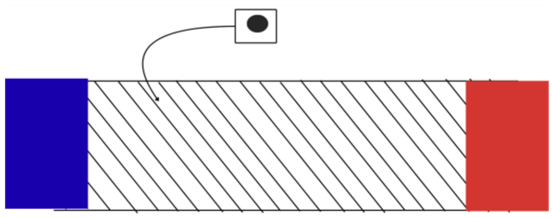

Fig. 56. Angled perforated baffles as roughness elements (drawn after [137]).

Kumar and Layek [138] experimentally analysed modified SAH using winglet type rib for enhancement in heat transfer and frictional flow behaviour (Fig. 57). They used operating parameters, such as a relative roughness pitch varying from 5 to 12, an attack angle changing from 30° to 75°, a relative roughness width varying from 3 to 7, a Reynolds number varying between 3000 to 22 000. They obtained an improvement in Nu and an increase in *f* of 2.83 and 3.63 times, respectively.

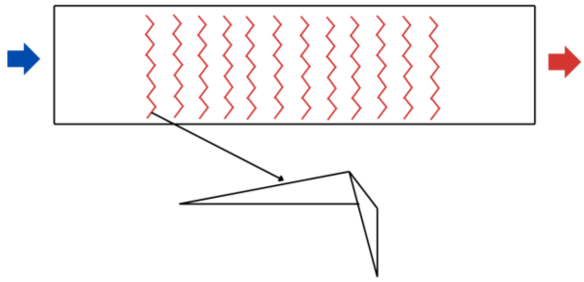

Fig. 57. Winglet type rib as a roughness element (drawn after [138]).

Kottayat et al. [139] performed experimental and numerical analysis of a modified SAH using discrete multiple inclined baffles, as shown in Fig. 58. They employed various parameters, including a relative baffle height of 0.1 (fixed), a relative baffle pitch varying from 0.6 to 1 and a Reynolds number varying from 6000 to 14 000. The obtained increments in Nu and *f* were 2.47 and 3.07 times, respectively, compared to a smooth SAH.

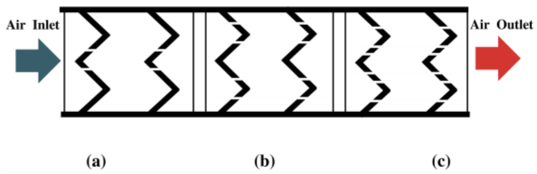

Fig. 58. Roughness elements in the form of multiple discrete inclined baffles (drawn after [139]).

Parsa et al. [140] conducted a numerical study of a modified SAH configuration using novel staggered cuboid baffles (shown in Fig. 59) to enhance heat transfer and fluid flow characteristics. The operating parameters employed were: relative length ranging from 1 to 3, relative width from 0.2 to 1.0, relative height from 0.1 to 0.9, relative pitch from 1.5 to 3.5, attack angle ranging from 0° to 90°, and Reynolds number varying from 5080 to 10 160. The highest obtained THP value was 3.43.

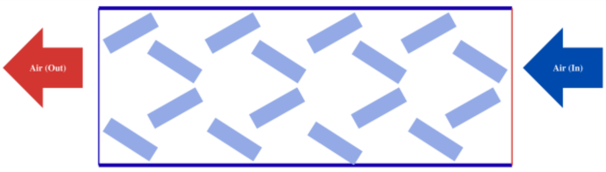

Fig. 59. Roughness element in the form of novel staggered cuboid baffles (drawn after [140]).

7.9. S-shaped ribs

Kumar et al. [12] carried out an experimental analysis of heat transfer and friction factor in a solar air heater duct with the S-shaped wire rib roughness, as shown in Fig. 60. They used parameters such as the relative roughness pitch (P/e) between 4 and 16, the relative roughness height (e/D_h) from 0.022 to 0.054, arc angles (α) ranging from 30° to 75°, and relative roughness width (W/w) between 1 and 4. Tests were conducted across a Reynolds number range of 2400 to 20 000. The findings reveal that the roughened duct exhibits superior performance compared to the smooth duct under the examined conditions. The optimal values of Nu and f were recorded at W/w = 3, P/e = 8, α = 60°, and e/D_h = 0.043. Additionally, predictive correlations for Nu and f were developed using the experimental results, accounting for the effects of both roughness and operating parameters.

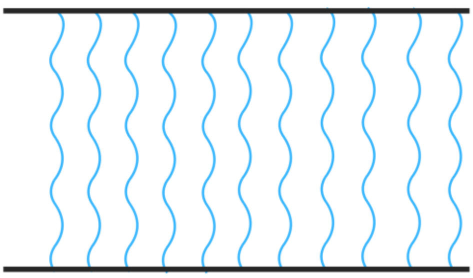

Fig. 60. S-shaped wire ribs as roughness elements (drawn after [12]).

7.10. Other roughness geometries

Jaurker et al. [141] experimentally investigated a modified SAH using rib-grooved artificial roughness, as displayed in Fig. 61. They employed operating parameters, such as Reynolds number ranging from 3000 to 21 000, relative roughness height varying from 0.0181 to 0.0363, relative roughness pitch range of 4.5 to 10, and groove position to pitch ratio of 0.3 to 0.7. They obtained a maximum performance of a modified SAH, such as a Nusselt number up to 2.7 times higher, while the friction factor rising up to 3.6 times compared to a smooth SAH. They also developed predictive correlations for estimating the Nusselt number and friction factor.

Karmare and Tikekar [142,143] experimentally studied SAH using metal grit ribs for enhancement of heat transfer and friction factor, as shown in Fig. 62 and Fig. 63. The parameters they

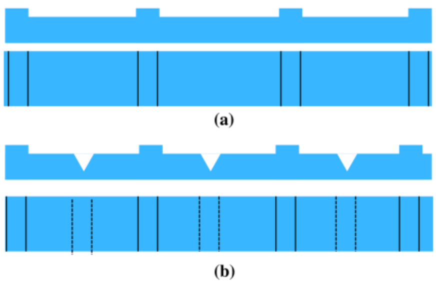

Fig. 61. Roughness element as rib-grooved [141].

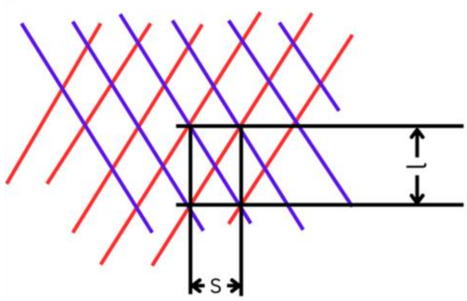

Fig. 62. Schematic of inclined roughness elements showing the spacing details of the ribs used.

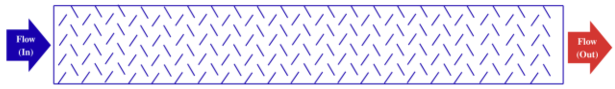

Fig. 63. Roughness element in the form of metal grit ribs (drawn after [143]).

employed for the study were: a relative roughness height of grit between 0.035 and 0.044, a relative roughness pitch of grit between 12.5 and 36, a relative length of grit of 12.5 to 36, and Reynolds number varied from 4000 to 17 000. They found that the Nusselt number and friction factor increased by a maximum of 1.87 and 2.13 times, respectively, compared to a smooth SAH. They also made an effort to determine the predictive correlations for Nu and f.

Bopche and Tandale [144] experimentally investigated SAH using artificial roughness as an inverted U-shaped rib for better heat transfer and friction factor, as illustrated in Fig. 64. They employed various parameters for this investigation, such as e/D varied from 0.0186 to 0.03986, P/e changing from 6.667 to 57.14, α fixed at 90°, and Re varied from 3800 to 18 000. They obtained a maximum increase in Nu and f of 2.82 and 3.72, respectively.

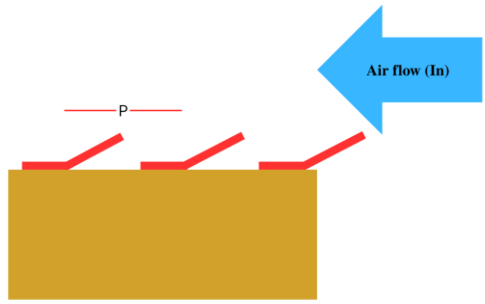

Fig. 64. Inverted U-shaped rib as a roughness element (drawn after [144]).

Kumar and Verma [145] numerically investigated modified SAH using artificial roughness as a sinusoidal protrusion rib with the view of higher Nusselt number and friction factor. They used various operating and control parameters, such as e of 1 mm, P varied from 10 to 18 mm and Re in the range of

4000 to 15 000. They obtained a maximum THP of 2.02 under optimum operating condition of P = 10 mm and Re = 4000.

Saravanan et al. [146] conducted an experimental investigation to study the thermo-hydraulic performance of a solar air heater with staggered multiple C-shaped perforated and non-perforated finned absorber plate, as depicted in Fig. 65. The experiments were carried out for a relevant range of flow parameters, i.e. Reynolds number ranging from 3000 to 27 000, and geometric parameters, such as the relative pitch to gap ratio from 3.4 to 3.8, the relative height ratio from 0.3 to 0.7 and the relative perforated ratio from 1.5 to 3, with a focus on their effects on the maximum heat transfer enhancement. They reported a maximum THP of 1.64. They also developed correlations to predict and match the experimentally obtained Nu and f for non-perforated and perforated fins.

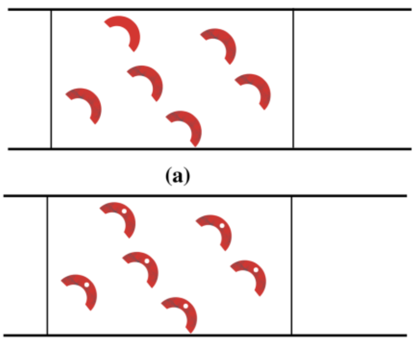

Fig. 65. Roughness element in the form of (a) staggered multiple C-shaped perforated, and (b) non-perforated finned absorber plate (drawn after [146]).

Bezbaruah et al. [147] analysed SAH numerically using altered conical vortex generators in a staggered arrangement (Fig. 66). The operating parameters used included a relative pitch ratio ranging from 2.67 to 15, a relative height ratio changing from 0.17 to 0.34 and a Reynolds number varied from 3500 to 16 000. The highest THP they obtained under these investigations was 2.04.

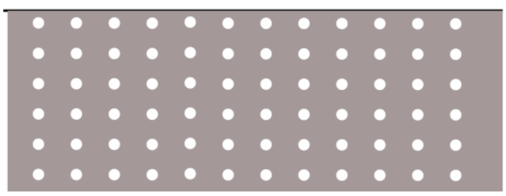

Fig. 66. Roughness elements in the form of altered conical vortex generators in a staggered arrangement (drawn after [147]).

Goel et al. [148] conducted a comprehensive parametric investigation on SAH using hemispherical cavities as artificial roughness elements, displayed in Fig. 67, for an enhancement in heat transfer and fluid flow characteristics. They obtained maximum enhancement in the Nusselt number by a factor of 5.33 compared to a smooth SAH under the optimum operating condition of a transverse-pitch ratio, a longitudinal-pitch ratio and

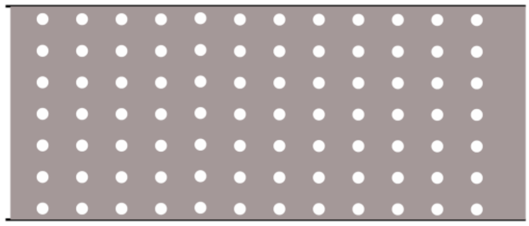

Fig. 67. Hemispherical cavities as roughness elements (drawn after [148]).

a relative dimple depth of 11, 11 and 0.039, respectively, and a Reynolds number of 2160.

Yadav and Saini [149] performed a numerical study on a modified SAH using jet impingement technique for increasing the heat transfer, as shown in Fig. 68. They used a jet diameter ratio ranging from 0.065 to 0.195, a jet height ratio ranging from 0 to 0.433 and the Reynold number from 3500 to 17 500. They reported maximum increases in Nu and f of 7.58 and 9.01 times, respectively, compared to a smooth SAH under optimum conditions, such as a jet diameter ratio of 0.0650 and a jet height ratio of 0.216 at a Reynolds number of 17 500. They also quoted a maximum THP of 3.66 at a jet height ratio of 0.216 (fixed), jet diameter ratio of 0.065 (fixed) and a Reynolds number of 15 500 (fixed).

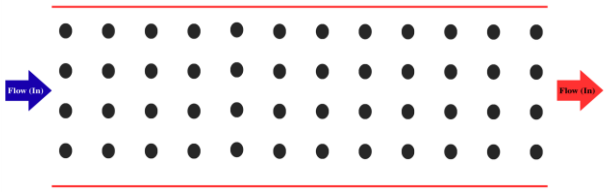

Fig. 68. Absorber plate with jet impingement (drawn after [149]).

Wang et al. [150] investigated SAH modified with S-shaped ribs with gap to improve heat transfer (Fig. 69). They employed various parameters for investigations, such as a gap width (g = 2 to 6 mm), a rib width (w = 30 to 50 mm), a rib spacing (p = 40 to 60 mm), a rib height (e = 4 mm), a rib thickness (s = 2 mm), P/e = 20 to 30, W/w = 3 to 5, e/D = 0.023 to 0.036, g/e = 1 to 2, and Re varied from 2000 to 20 000. The reported maximum augmentation achieved for Nu and f was 5.42 and 5.87, respectively, at Re = 19 258, W/w = 4, P/e = 20 and g/e = 1.5.

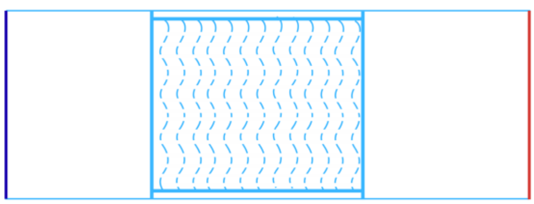

Fig. 69. S-shaped ribs with gap as roughness elements (drawn after [150]).

Table 5. Summary report.

Author(s) Ref.	Year	Roughness geometry	Reynolds number	Type of study	Main findings
			Tranverse ribs		
Prasad and Saini [84]	1988	Transverse rib	5000–50 000	Experimental	Nu/Nu_s=2.38 and f/f_s=4.25
Gupta et al. [151]	1993	Transverse rib with small diameter	3000–18 000	Experimental	Studied the effects of *e*/*D* on heat transfer and friction factor at fixed *P*/*e*=10
Karwa [88]	2003	Transverse rib Inclined rib V continuous rib V discrete rib	2800–15 000	Experimental	Stanton number enhancement for: Continuous rib: V-up = 102–137%, V-down = 110–147% Discrete rib: V-up = 93–134%, V-down = 102–142%
Verma and Prasad [91]	2000	Rectangular duct with thin wires	5000–20 000	Experimental	Thermo-hydraulic optimisation of the roughness and other parameters for the maximum heat transfer and minimum pressure drop was made.
Layek et al. [89]	2009	Repeated transverse chamfered rib-groove roughness	3000–21 000	Experimental and analytical	Maximum Nu and *f* found were 2.6 and 3.5 times the smooth SAH. Also, the maximum THP reported was 1.76.
Saini and Saini [142]	1996	Expanded metal mesh	2000–13 500	Experimental	Correlations for the Nusselt number and friction factor in terms of these parameters were developed that can correlate the experimental data reasonably well.
Singh et al. [92]	2019	Multiple broken transverse ribs and square-wave shaped rib	3000–15 000	Experimental and CFD analysis	The maximum increment in Nu was 2.22, and the consequent value for *f* increment of 3.44 was obtained. The highest THP value of 1.49 was obtained, while the maximum thermal efficiency of 68.6% was achieved.
Singh et al. [93]	2021	Uniform/non-uniform square-wave profile transverse roughness rib	3000–15 000	CFD analysis	The non-uniform ribs were found to yield better heat transfer enhancement as compared to uniform ribs.
Sharma et al. [94]	2021	Transverse, inclined transverse, dimple, inclined dimple, arc and sine wave	3000–18 000	Experimental and numerical	The results revealed that the positioning and shape of baffle unswervingly affect THP of the solar air heater.
Mahanand and Senapati [95]	2020	Transverse inverted T-shaped rib	3800–18 000	Numerical	A thermal enhancement factor of 1.87 was obtained as a result of enhancement in heat transfer for the SAH with an inverted T-shaped rib roughened absorber plate.
Gawande et al. [96]	2018	Combined square and equilateral triangular ribs	3800–18 000	Numerical and experimental	A value of 1.86 was recorded as an optimum value of THP for the range of parameters investigated.
Kumar et al. [152]	2017	Circular and semicircular rib	4000–24 000	Numerical and experimental	Two new correlations were developed for the Nusselt number and friction factor as a function of Reynolds number and relative roughness height. The values obtained from the developed correlations agree well with data from the model.
Kumar and Layek [98]	2019	Circular rib	8551–11 149	LCT technique and CFD technique	The maximum values of heat transfer rate were obtained at a roughness pitch ratio of 10, with a minimum penalty of frictional losses.
Kumar et al. [99]	2019	Square rib	3900–17 900	Numerical	Correlations were developed for both friction factor and Nusselt number based on observed results.
Kumar et al. [153]	2017	Rectangular rib roughened	4000–18 000	Numerical	The maximum value of thermo-hydraulic performance parameter (THP), 1.89, was found in the case of relative roughness pitch (*P*/*e*), rib aspect ratio (*e*/*w*) and relative roughness height (*e*/*D*) of 10, 4.0 and 0.04, respectively, at the Reynolds number of 15 000.
Kumar et al. [97]	2017	Transverse semicircular rib	5000–10 000	Numerical	The maximum thermo-hydraulic performance was observed for a higher relative roughness height value (*e*/*D*=0.067) and a lower relative roughness pitch (*P*/*e*=7.5) in a semi-circular rib roughened equilateral triangular duct is of the order of 1.7.
			Arc-shaped roughness		
Saini and Saini [102]	2008	Arc-shaped wire ribs	2000–17 000	Experimental	An enhancement of 3.80 times in heat transfer and 1.80 times in friction factor was observed at the optimum parameters compared to a smooth duct.
Singh et al. [103]	2014	Multiple arc-shaped ribs	2200–22 000	Experimental	Developed Nu and *f* correlations; observed effects of roughness on Nu and *f*

Table 5. Summary report (*continued*).

Author(s) Ref.	Year	Roughness geometry	Reynolds number	Type of study	Main findings
Sahu and Prasad [104]	2016	Arc-shaped ribs	2000–40 000	Analytical	Investigated the exergetic and effective efficiency
Gill et al. [109]	2017	Staggered piece and broken arc rib	2000–16 000	Experimental and CFD analyses	Examined the heat transfer and friction factor
Sahu and Prasad [154]	2017	Arc-shaped ribs	2900–35 000	Analytical	Examined the thermo-hydraulic performance.
Saravanakumar et al. [155]	2019	Arc shaped ribs Integrated with fins and baffles	2900–17 000	Analytical	The maximum exergy was obtained for 8 fins, a baffle length of 0.2 m, a baffle width of 0.015 m and a mass flow rate of 0.012 kg/s.
Bhuvad et al. [110]	2022	Apex-up discrete arc ribs	3000–14 000	Experimental	The results showed that the new apex-up discrete arc rib absorber plates had superior thermal performance to the existing best apex-down rib geometries. Maximum augmentation in Nu, achieved for an attack angle of 30°, was 2.92 times that of a smooth plate.
Kumar et al. [105]	2022	Discrete multiple-arc ribs	3000–19 000	Experimental	The Nusselt number and friction factor for a roughened solar thermal collector were found to be 7.61 and 6.48 times higher than those of a smooth channel.
Ghritlahre [107]	2021	Arc-shaped wire rib	No data*	Experimental	The above result reveals that apex upstream flow is more efficient than the apex downstream flow.
Korpale et al. [111]	2020	Rectangular section ribs	4000–20 000	Experimental and numerical	The maximum THP obtained was 2.77 at Reynolds number 20 000, relative rib pitch of 17.22, relative rib height of 0.044 and relative rib height of 0.5.
Kumar et al. [112]	2019	Discrete multiple arc-shaped ribs	11000–19 000	Experimental and numerical	A remarkable improvement in the thermal performance of the solar air heater was observed by varying roughness parameters, but it led to an increase in the pumping power of the solar air heater.
				V-shaped ribs	
Momin et al. [114]	2002	V-shaped ribs	2500–18 000	Experimental	Found an optimal thermo-hydraulic performance at an angle of attack = 60°.
Patel and Lanjewar [118]	2021	V-geometry roughened	4000–15 000	Experimental	The maximum augmentation in Nu and *f* was found to be 2.51 and 2.70 times that of a smooth plate, respectively, for g'/e=1 and d/w=0.65. Maximum value of η_{THP} was found to be 1.82 for g'/e=1 and d/w= 0.65.
Srivastava et al. [108]	2020	Arc-shaped with gap and V-shaped with gap	3000–15 000	Numerical	The maximum THP values for the V-shaped ribs and arc-shaped ribs were 2.21 and 1.5, respectively, at Re = 3000.
				Dimple or protrusion ribs	
Kumar and Prasad [119]	2019	Concave dimple	2000–13 500	Experimental	The maximum enhancement in Nusselt number for varying relative dimple pitch, relative dimple height and relative dimple depth was, respectively, of the order of 2.6–3.55, 1.91 to 3.42, 3.09 to 3.94 times, and that of the friction factor was of the order of 1.62–2.79, 1.52 to 2.34 and 2.21 to 2.56 times over those of the 1-side roughened ones.
Sethi et al. [85]	2012	Dimple roughness in arc-shaped arranged	3600–18 000	Experimental	Studied the roughness effect on Nu and *f*.
Kumar and Verma [145]	2022	Sinusoidal protrusion rib (SPR)	5000–10 000	CFD analysis	The thermal efficiency of the SPR model was found to be 69% at Re = 15000 in the range of Re investigated.
				W-shaped ribs	
Lanjewar et al. [125]	2011	W-shaped ribs	2300–14 000	Experimental	Found optimal thermo-hydraulic performance at an attack angle of 60° for the W-down rib.
				Spherical ball roughness	
Murmu et al. [156]	2019	Inclined spherical ball	2500–18 500	Experimental	Developed Nu and *f* correlations.
Kumar and Murmu [157]	2021	Inclined spherical ball	2500–18 500	Experimental	Maximum thermal efficiency for roughened ducts was found to be 81% compared to 38% for a smooth duct under the parameters: relative roughness pitch = 12, relative roughness height = 0.036, height-diameter ratio = 1 and angle of attack = 55° at a mass flow rate of 0.0319 kg/s.

Table 5. Summary report (*continued*).

Author(s) Ref.	Year	Roughness geometry	Reynolds number	Type of study	Main findings
Non-uniform ribs					
Karwa et al. [158]	1999	Chamfer rib	3000–20 000	Experimental	Developed correlations for heat transfer and friction factor; additionally observed the effects of chamfer angle
Bhagoria et al. [130]	2002	Wedge-shaped ribs	3000–18 000	Experimental	Obtained Nu_s=1.38, and developed correlations for Nu and *f*
Karmare and Tikekar [143]	2007	Wire ribs-grid shape	4000–17 000	Experimental	Developed correlations for Nu and *f*
Barik et al. [131]	2021	T-rib, left arm inclined T-rib, right arm inclined T-rib, Y-rib, concave and convex T-ribs	5000–18 000	Numerical	Among all the considered ribs, the T-rib was found to be the best heat transfer enhancer, keeping the friction factor at a low value.
Kumar and Goel [132]	2021	Semi-circular, circular, triangular, square, rectangular	3700–18 700	Numerical	The performance of SAH was strongly influenced by both shapes of the roughness element and the cross-sectional area of flow-passage through which air flows.
Inclined baffles					
Kumar et al. [137]	2022	Angled perforated baffles	5000–17 000	Experimental, CCD, ANN technique	The STC with roughened angled perforated baffles enhanced Nu and *f* by 3.82 and 7.14 times, respectively, as compared to the STC without baffles. The angled perforated baffles at *α* of 55º provided the highest THP at Re of 9000. A THP value of 1.94 was obtained for the array of designed parameters.
Kottayat et al. [139]	2022	Discrete multiple inclined baffle	6000–14 000	CFD and experimental	A maximum thermo-hydraulic performance of 2.69 was obtained for the gap at the trailing apex. The proposed design yielded a higher collector efficiency, 55–70%, compared to the ribbed rectangular SAH design exhibiting 30–55%. With lower exergy losses, the proposed SAH design had higher exergetic efficiency (1.5–2.2%) than the ribbed rectangular SAH (0.9–1.7%) for the range of Re studied.
Parsa et al. [140]	2021	Staggered cuboid baffles	5080, 7620, 10 160	Numerical	It is indicated that the relative baffle height (*c*/*H*) and relative baffle pitch (*s*/*H*) are the most influential parameters on the efficiency and thermo-hydraulic performance factor.
Kumar and Layek [138]	2020	Winglet shaped ribs	No data**	Experimental	By comparing with the smooth surface, the studied roughened surface could significantly improve the thermal efficiency of a solar air heater system. The highest value of thermal efficiency of the collector surface was 69% at the maximum mass flow rate.
Other roughness geometries					
Jaurker et al. [141]	2006	Rib-grooved roughness	3000–21 000	Experimental	Developed the correlations for Nu and *f*.
Patel et al. [159]	2021	Discrete reverse NACA profile ribs	6000–18 000	Experimental	Maximum Nu and THP were found to be 102.08 and 2.578, respectively.
Saravanan at al. [146]	2021	Staggered C-shape finned	3000–27 000	Experimental	The thermal performance and friction factor the for C-shape finned absorber plate without a perforated hole for a relative pitch-to-gap ratio of 3.8 and a relative height ratio of 0.6 were 2.61 and 5.93 times more than for the smooth plate absorber plate, respectively. The perforated fin with the same relative ratios gave thermal performance and friction factor 2.67 and 5.34 times higher than the smooth absorber plate solar air heater, respectively.
Bezbaruah et al. [147]	2021	Staggered conical vortex generators	3500–16 000	Experimental and numerical	The highest thermo-hydraulic performance parameter of 2.04 was achieved.
Goel et al. [148]	2021	Hemispherical dimple cavities	2100–18 500	Experimental and numerical analysis	The best augmentation in Nusselt number obtained was of the order of 5.33 which was observed for a transverse pitch ratio, a longitudinal-pitch ratio and a relative dimple depth values of 11, 11 and 0.039, respectively, at a Reynolds number of 2160.
Arunkumar et al. [160]	2021	Rectangular perforated duct inserts	3000–18 000	Experimental	It was found based on the experiments that thermal efficiency was maximum for the height ratio (*h*/*H*) of 0.66 when compared to height ratios of 0.50 and 0.83.
Yadav and Saini [149]	2020	Impinging jet	3500–17 500	Numerical	The maximum obtained thermo-hydraulic performance parameter value of 3.66 corresponded to a jet height ratio of 0.216 and a jet diameter ratio of 0.065 for the Reynolds number of 15 500.

Table 5. Summary report (*continued*).

Authors	Year	Roughness geometry	Reynolds number	Type of study	Main findings
Other roughness geometries					
Wang et al. [150]	2020	"S"-shaped ribs with gap	2000–20 000	Experimental	Compared with a smooth plate, the thermal efficiency of a solar air heater with artificial roughness was improved by 13% to 48% under different conditions. However, the work section pressure drop of this new solar air heater was within the range of 15.8–30 Pa.
Kumar and Verma [121]	2020	Sinusoidal rib	4000–15 000	Numerical	The results are also compared with the triangular and square rib and found that the optimal THP of the proposed rib was 20.06% and 33.31% higher.
Gawande et al. [134]	2020	Chamfered rib	3800–18 000	Experimental and numerical	The chamfered square rib with a 20° chamfer angle was found to provide the best thermo-hydraulic performance and, hence, was selected for further thermal analysis.
Zina et al. [133]	2020	Triangular ribs with semi-circular nooks	3800–18 000	Numerical	The optimum THP value of 1.93 could be obtained fo case C1 and Re of 5000.
Kumar et al. [100]	2018	Forward facing chamfered rectangular ribs	4000–17 000	Numerical	A remarkable change in f and Nu values was observed by varying both Re and roughness parameters.
Kumar et al. [161]	2020	Forward and backward facing arced ribs	2300–23 000	Experimental	Thermo-hydraulic performance improved by 3.61 times compared to the smooth flat plate solar air heater, for a curved-ribbed SAH for W/w=3, P/e=8, g/e=1, e/D=0.045, and d/x=0.65 at Re = 23 000.

*Mass flow rate $\dot{m}$ = 0.007–0.022 kg/s.

**Mass flow rate $\dot{m}$ = 0.00531–0.04041 kg/s.

8. Correlations for Nusselt number and friction factor

In the field of solar air heaters, the development of correlations is pioneering in performance prediction and optimisation, design improvement, scaling and adaptation, generalisation of results, energy efficiency and sustainability, cost reduction and customisable solutions. The first correlation, reported in 1991, involved transverse ribs to develop correlations for the Nusselt number and friction factor in a modified solar air heater. Various geometries have been explored since then, including arc-shaped ribs, V-shaped wire ribs, wire rib grid shapes, wedge-shaped ribs, chamfered rectangular ribs, angled perforated baffles, dimpled and protruded surface geometries and spherical ball-shaped ribs. The parameters used in these studies include e/D_h, P/e, Re, e/D, α, B/S, W/H, g/P, ϕ, $e+$, y, d/H, p/H, y/H, P, e/w, d/w, g/e, $\alpha/90^o$, N_g, D/L, g/H, P/H, X/D, Y/D, d/x, W/w, w/e, G/L, l/s, L/e, S/e, e'/e, O/H, β, and V. The error range associated with the correlations developed in these studies typically falls between 5% and 30%, depending on the complexity of the geometry and the experimental conditions. Table 6 presents the numerous correlations obtained by various investigators with the ranges of parameters selected for their studies.

9. Nusselt number and friction factor enhancement

In the field of renewable energy conservation systems, the performance of the system plays a vital role. In the flat plate solar air heater, the performance evaluation has been reported by many researchers. The conventional SAH has been modified using artificial roughness. The size, orientation, shape, material used, flow rate of fluid, gaps, and many other factors affect the values of Nu and f.

The comparison of various geometrical configurations used has been discussed in Table 7. As the enhancement of heat transfer and fluid friction in comparison with a smooth duct are subjected to various operating and control parameters, the maximum values can be obtained at the optimum parameters in the examined range of Reynolds number (mass flow rate), as listed in Table 7 as Nu/Nu_s and f/f_s, respectively. In this review study, the effort has been put on major geometries, such as transverse ribs, arc-shaped ribs, dimple or protrusion ribs, W-shaped ribs, V-shaped ribs, spherical ball roughness, non-uniform ribs, inclined baffles, and other roughness geometries.

Table 6. Details of correlations developed.

Author(s)	Novel geometry	Parameters	Correlation developed
		Transverse ribs	
Hong and Hsieh [162]	Transverse ribs	$P/e = 5.31$ $e/D_h = 0.19$	$\mathrm{Nu} = 0.056\mathrm{Re}_h^{0.74}$ for $\mathrm{Tu} = 0.04$ $\mathrm{Nu} = 0.03\mathrm{Re}_h^{0.79}$ for $\mathrm{Tu} = 0.07$ $\mathrm{Nu} = 0.019\mathrm{Re}_h^{0.83}$ for $\mathrm{Tu} = 0.07$
Prasad and Saini [84]	Small diameter protrusion wire	$P/e = 10 - 20$ $e/D_h = 0.020 - 0.033$ $\mathrm{Re} = 500 - 50000$	$\bar{\mathrm{St}} = \bar{f}/2\left[1 + \sqrt{f/2}(4.5(e^+)^{0.28}\mathrm{Pr}^{0.57} - 0.95(P/e)^{0.53})\right]$ $f = 2/[0.95(P/e)^{0.53} + 2.5\ln(D_h/2e) - 3.75]^2$
Gupta et al. [163]	Small diameter transverse ribs	$e/D = 0.018 - 0.52$ $\mathrm{Re} = 3000 - 18\,000$	$\mathrm{Nu} = 0.000824(e/D)^{-0.178}(W/H)^{0.284}\mathrm{Re}^{1.062}$, for $e^+ < 35$ $\mathrm{Nu} = 0.000307(e/D)^{-0.469}(W/H)^{0.245}\mathrm{Re}^{1.062}$, for $e^+ \geq 35$ $f = 0.06412(e/D)^{0.019}(W/H)^{0.237}\mathrm{Re}^{-0.185}$
Karwa [88]	Inclined, discrete and continuous wire rib	$e/D_h = 0.467 - 0.05$ $P/e = 10$ $\alpha = 60°, 90°$ $B/S = 3$ $W/H = 7.19 - 7.75$ $\mathrm{Re} = 2500 - 18\,000$	$G = 32.2e^{-0.006}(W/H)^{0.5}(P/e)^{2.56}\exp[0.7343\ln(P/e)^2](e^+)^{0.08}$ $f = 1.66e^{-0.0078}(W/H)^{-0.4}(P/e)^{0.2695}\exp[-0.719\ln(P/e)^2(e^+)^{-0.075}]$ for $7 \leq e^+ \leq 20R$ $f = 1.325e^{-0.0078}(W/H)^{-0.4}(P/e)^{0.2695}\exp[-0.719\ln(P/e)^2(e^+)^{-0.075}]$ for $20 \leq e^+ \leq 60R$
Layek et al. [164]	Transverse chamfered rib groove combination	$P/e = 4.5 - 10$ $\Phi = 5 - 300$ $e/D = 0.022 - 0.04$ $\mathrm{Re} = 3000 - 18\,000$ $g/p = 0.3 - 0.6$	$\mathrm{Nu} = 0.00206\mathrm{Re}^{0.936}(e/D)^{0.349}(P/e)^{30318}$ $\times \exp[-0.868(\ln(P/e))^2](g/p)^{1.108}$ $\times \exp[2.486\{\ln(g/p)\}^2 + 1.406\{\ln(g/p)\}^3]$ $f = 0.001227\mathrm{Re}^{-0.199}(e/D)^{0.585}(P/e)^{7.19}$ $\times \exp[-1.854\{\ln(P/e)\}^2](g/p)^{0.645}$ $\times \exp[1.513\{\ln(g/p)\}^2 + 0.8662\{\ln(g/p)\}^3]$
Verma and Prasad [91]	Small diameter transverse protrusion wire	$e/D = 0.01 - 0.03$ $P/e = 10 - 40$ $e^+ = 8 - 42$ $\mathrm{Re} = 5000 - 20\,000$	$\mathrm{Nu} = 0.08596(P/e)^{-0.54}(e/D)^{0.072}\mathrm{Re}^{0.723}$, for $e^+ \leq 24$ $\mathrm{Nu} = 0.0245(P/e)^{-0.016}(e/D)^{0.021}\mathrm{Re}^{0.802}$, for $e^+ > 24$ $f = 0.0245(P/e)^{-0.0206}(e/D)^{0.021}\mathrm{Re}^{-1.25}$
Mahanand and Senapati [95]	Transverse inverted-T shaped rib	$e/D_h = 0.042$ $P/e = 7.14 - 17.86$ $\mathrm{Re} = 3800 - 18\,000$	$\overline{\mathrm{Nu}} = 0.052927\mathrm{Re}^{0.8379}(P/e)^{-0.1357}$ $\bar{f} = 0.329536\mathrm{Re}^{-0.2325}(P/e)^{-0.1305}$
Gawande et al. [134]	Chamfered rib, right angle triangular and reverse L-shaped ribs, invented from square ribs	$q = 1000\ \mathrm{W/m^2}$ $\mathrm{Re} = 3800 - 18\,000$ $P/e = 7.14 - 35.71$ $e/D = 0.021 - 0.042$ $\alpha = 0° - 40°$	For 20° chamfered rib $\mathrm{Nu} = 0.0943\mathrm{Re}^{0.8248}(P/e)^{-0.3022}$ For right-angle triangular rib $\mathrm{Nu} = 133.36\mathrm{Re}^{0.8183}(e/D)^{3.6305}\exp[0.4480\ln(e/D)^2](P/e)^{-0.4807}$ $\times \exp[0.055\ln(P/e)^2]$ For reverse L-shaped rib $\mathrm{Nu} = 0.032\mathrm{Re}^{0.8332}(P/e)^{0.3479}\exp[-0.1004\ln(P/e)^2]$ For 20° chamfered rib $f = 0.653\mathrm{Re}^{-0.2883}(P/e)^{-0.2087}$ For right-angle triangular rib $f = 42.979\mathrm{Re}^{-0.2778}(e/D)^{1.1517}\exp[0.1105\ln(e/D)^2](P/e)^{-1.7453}$ $\times [0.3133\ln(P/e)^2]$ For reverse L-shaped rib $f = 0.2805\mathrm{Re}^{-0.2617}(P/e)^{0.0815}\exp[-0.0319\ln(P/e)^2]$
Kumar et al. [152]	Circular and semicircular rib	$L = 1600$ mm $H = 40$ mm $D = 77$ mm $d = 4, 6, 8, 10$ mm $P = 30$ mm $y = 10, 20, 30$ mm $d/H = 0.1, 0.15, 0.20, 0.25$ $P/H = 0.75$ $y/H = 0.25, 0.5, 0.75$ $q = 800\ \mathrm{W/m^2}$ $\mathrm{Pr} = 0.72$ $\mathrm{Re} = 5000 - 10\,000$ (6 values) $\alpha = 25°$	$\mathrm{Nu} = 0.44D_h^{0.69}(d/H)^{0.05}\exp\{-0.0165[\ln(d/H)]^2\}$ $f = 16.4D_h^{-0.406}(d/H)^{2.5}\exp\{0.44[\ln(d/H)]^2\}$
Kumar et al. [99]	Square rib	$P/e = 10$ $e/D = 0.013 - 0.05$ $\mathrm{Re} = 4000 - 18000$	$\mathrm{Nu} = 0.00415\mathrm{Re}^{0.95}(P/e)^{1.217}(e/D)^{0.243}\exp\{-0.265[\ln(P/e)]^2\}$ $f = 6.436\mathrm{Re}^{-0.4}(P/e)^{-1.033}(e/D)^{0.278}\exp\{-0.224[\ln(P/e)]^2\}$
Kumar et al. [153]	Rectangular rib roughened	$P/e = 5 - 15$ $e/D = 0.02 - 0.4$ $e/w = 0.25 - 4.0$ $\mathrm{Re} = 4000 - 18\,000$	$\mathrm{Nu_{avg}} = 0.365\{\mathrm{Re}^{0.83}(P/e)^{-1.322}(e/w)^{0.122}(e/D)^{0.216}$ $\times \exp[0.265(\ln(P/e))^2]\}$ $f_{avg} = 3.394 \times 10^2\{\mathrm{Re}^{-0.56}(P/e)^{-2.294}(e/w)^{0.130}(e/D)^{0.378}$ $\times \exp[0.408(\ln(P/e))^2]\}$

Table 6. Details of correlations developed (*continued*).

Author(s)	Novel geometry	Parameters	Correlation developed
Aharwal et el. [136]	Inclined and transverse ribs	$e/D_h = 0.0377$ $P/e = 10$ $\alpha = 60°$ $d/W = 0.167 - 0.5$ $W/H = 5.87$ $\mathrm{Re} = 3000 - 18\,000$	$\mathrm{Nu} = 0.0102\mathrm{Re}\ e^{1.148}(e/D)^{0.51}\{1 - [0.25 - (d/W)]^2(0.01[1 - (g/e)]^2$ $f = 0.5(e/D)^{0.72}\mathrm{Re}^{-0.0836}$
Varun et al. [165]	Inclined and transverse wire ribs	$P/e = 10$ $e/D_h = 0.030$ $\mathrm{Re} = 2000 - 20\,000$	$\mathrm{Nu} = 0.0006(P/e)^{0.0104}\mathrm{Re}^{1.213}$ $f = 1.0858(P/\bar{e})^{0.0114}\mathrm{Re}^{-0.3685}$
Arc-shaped ribs			
Saini and Saini [102]	Arc-shaped wire ribs	$g/e = 0.5 - 2$ $P/e = 10$ $\alpha/90 = 0.333 - 0.666$ $d/w = 0.167 - 0.5$ $W/H = 5.87$ $\mathrm{Re} = 2000 - 17\,000$	$\mathrm{Nu} = 0.001047(e/D)^{0.3772}(\alpha/90)^{-0.1198}\mathrm{Re}^{1.123}$ $f = 0.14408(e/D)^{-0.1765}(\alpha/90)^{0.1185}\mathrm{Re}^{-0.17103}$
Bhuvad, Azad and Lanjewar [110]	Apex-up discrete arc ribs	$W = 200$ mm $W/H = 8.0$ $\alpha = 30°, 45°, 60°$ $e/D_h = 0.045$ $P/e = 10$ $N_g = 3$ $g/e = 3$	$R = \sqrt{(2/)} + 2.5\ln(2e/D_h) + 3.75$ $e^+ = \sqrt{(f/2)}\,\mathrm{Re}(e/D_h)$ $G = (f/2\mathrm{St}) - 1\sqrt{(2/f)} + R$
Kumar et al. [105]	Discrete multi-arc ribs	$D_d/L_v = 0.27 - 0.86$ $g_w/H_r = 0.32 - 1.72$ $H_r/H = 0.025 - 0.047$ $P_r/H = 0.58 - 3.1$ $\alpha = 35° - 65°$ $X/D_h = 0.47 - 1.72$ $Y/D_h = 0.46 - 0.82$ $D_j/D_h = 0.065$ $W/W_{AC} = 5.0$ $\mathrm{Re} = 3000 - 19\,000$	$\mathrm{Nu} = 4.03 \times 10^{-18}\mathrm{Re}^{0.4674}(D_d/L_v)^{-0.3183}$ $\times \exp\{-0.1854[\ln(D_d/L_v)]^2\}(g_w/H_r)^{-0.0566}$ $\times \exp\{-0.0172[\ln(g_w/H_r)]^2\}(H_r/H)^{-2.7231}$ $\times \exp\{-0.4179[\ln(H_r/H)]^2\}(P_r/H)^{-0.0137}$ $\times \exp\{-0.1373[\ln(P_r/H)]^2\}\alpha_a^{9.0055}$ $\times \exp\{-1.1569[\ln(\alpha_a)]^2\}(X/D_h)^{-0.0254}$ $\times \exp\{-0.0888[\ln(X/D_h)]^2\}(Y/D_h)^{-0.4181}$ $\times \exp\{-0.4506[\ln(Y/D_h)]^2\}$ $f = 4.03 \times 10^{-18}\mathrm{Re}^{-0.338}\exp\{0.0239\{\ln(\mathrm{Re})\}^2\}(D_d/L_v)^{-0.9527}$ $\times \exp\{-0.6782[\ln(D_d/L_v)]^2\}(g_w/H_r)^{-0.167}$ $\times \exp\{-0.01021[\ln(g_w/H_r)]^2\}(H_r/H)^{-6.5696}$ $\times \exp\{-1.0137[\ln(H_r/H)]^2\}(P_r/H)^{-0.00067}$ $\times \exp\{-0.1612[\ln(P_r/H)]^2\}\alpha_a^{15.909}$ $\times \exp\{-2.0566[\ln(\alpha_a)]^2\}(X/D_h)^{-0.0409}$ $\times \exp\{-0.2004[\ln(X/D_h)]^2\}(Y/D_h)^{-0.4866}$ $\times \exp\{-0.6556[\ln(Y/D_h)]^2\}$
Kumar et al. [112]	Discrete multiple arc-shaped ribs	$g/e = 0.5 - 1.5$ $N_g = 1 - 3$ $d/x = 0.3 - 0.9$ $\mathrm{Re} = 11000 - 19000$	$\mathrm{Nu} = -619.14 + 161.14(g/e) + 632.75(d/x) +$ $+0.054\mathrm{Re} + 5.45N_g + 8.37 \times 10^{-5}(g/e)\mathrm{Re} +$ $-2.79 \times 10^{-4}(d/x)\mathrm{Re} + 0.72(d/x)N_g +$ $+5.39 \times 10^{-4}\mathrm{Re}N_g - 77.01(g/e)^2 +$ $-495.62(d/x)^2 - 1.28 \times 10^{-6}\mathrm{Re}^2 - 1.66N_g^2$ $f = -5.06 \times 10^{-3} + 0.014(g/e) + 0.0775(d/x) +$ $+1.51 \times 10^{-6}\mathrm{Re} + 4.69 \times 10^{-4}N_g +$ $+7.83 \times 10^{-4}(g/e)(d/x) + 3.65 \times 10^{-4}(g/e)N_g +$ $-2.25 \times 10^{-7}(d/x)\mathrm{Re} - 1.79 \times 10^{-7}\mathrm{Re}N_g +$ $-7.05 \times 10^{-3}(g/e)^2 - 0.059(d/x)^2 +$ $-1.023 \times 10^{-10}\mathrm{Re}^2 + 9.53 \times 10^{-4}N_g^2$
Kumar et al. [161]	Innovatively arranged arc (combination of alternatively arranged forward and backward facing arced ribs)	$\mathrm{Re} = 2300 - 23000$ $W/H = 11$ $e/D = 0.018 - 0.045$ $\alpha = 30° - 75°$ $g/e = 0.5 - 2.0$ $W/w = 1 - 4$ $d/x = 0.25 - 0.85$ $P/e = 4 - 16$	$\mathrm{Nu}_{avg} = 2 \times 10^{-7}\mathrm{Re}^{1.4079}(g/e)^{-0.1264}(d/x)^{-0.1596}$ $\times \alpha^{3.5008}(W/w)^{0.5932}(P/e)^{0.2322}(e/D)^{0.2958}$ $\times \exp\{-0.2429[\ln(g/e)]^2\}\exp\{-0.2484[\ln(d/x)]^2\}$ $\times \exp\{-0.4123(\ln\alpha)^2\}\exp\{-0.2534[\ln(W/w)]^2\}$ $\times \exp\{-0.0479[\ln(P/e)]^2\}$ $f = 0.004\,\mathrm{Re}^{-0.217}(g/e)^{-0.1152}(d/x)^{-0.2848}$ $\times \alpha^{1.8628}(W/w)^{0.3868}(P/e)^{0.6392}(e/D)^{0.1914}$ $\times \exp\{-0.1877[\ln(g/e)]^2\}\exp\{-0.2182[\ln(d/x)]^2\}$ $\times \exp\{-0.2304[\ln\alpha]^2\}\exp\{-0.1814[\ln(W/w)]^2\}$ $\times \exp\{-0.1668[\ln(P/e)]^2\}$

Table 6. Details of correlations developed (*continued*).

Author(s)	Novel geometry	Parameters	Correlation developed
Korpale et al. [111]	Rectangular section ribs	$Re = 4000 - 20\,000$ $P/e = 1 - 60$ $e/D = 0.017 - 0.252$ $w/e = 0.5 - 10$	$Nu = 0.024Re^{0.8032}(P/e)^{1.4013}(e/D)^{0.6762}(w/e)^{-0.5388}e^{A}$ $A = -0.1728\log(P/e)\log(e/D) + 0.1986\log(P/e)\log(w/e) + 0.0658\log(e/D)\log(w/e) - 0.3235[\log(P/e)]^2$ $f = 24.167Re^{-0.1953}(P/e)^{0.1906}(e/D)^{2.5305}(w/e)^{-0.3140}e^{B}$ $B = -0.2073\log(P/e)\log(e/D) + 0.1293\log(P/e)\log(w/e) + 0.0497\log(e/D)\log(w/e) - 0.1880[\log(P/e)]^2 + 0.2287[\log(e/D)]^2$
V-shaped ribs			
Gupta et al. [151]	V-shaped wire ribs and V-shaped inclined wire ribs	$e/D = 0.02 - 0.053$ $P/e = 7.5 - 10$ $\alpha = 30° - 90°$ $Re = 5000 - 20\,000$	$Nu = 0.00824(e/D)^{-0.178}(W/H)^{0.288}Re^{1.062}$, for $e^{+} < 35$ $Nu = 0.00307(e/D)^{-0.469}(W/H)^{0.245}Re^{0.812}$, for $e^{+} \geq 35$ $f = 0.06412(e/D)^{0.019}(W/H)^{0.0237}Re^{-0.185}$
Mulu-work et al. [166]	V-shaped staggered discrete wire ribs	$e/D = 0.02$ $B/S = 3 - 9$ $\alpha = 60°$ $Re = 2000 - 15500$	$Nu = 0.00534(B/S)^{1.3496}Re^{1.2991}$ $f = 0.7117(B/S)^{0.0636}Re^{-2.991}$
Momin et al. [114]	V-shaped continuous wire rib	$e/D_h = 0.02 - 0.034$ $P/e = 10$ $\alpha = 30° - 90°$ $Re = 2500 - 18\,000$	$Nu = 0.067Re^{0.888}(e/D_h)^{0.424}(\alpha/60°)^{-0.077}\exp[-0.782(\ln \alpha/60°)^2]$ $f = 6.266Re^{-0.425}(e/D_h)^{0.565}(\alpha/60°)^{-0.093}\exp[-0.719(\ln \alpha/60°)^2]$
Hans et el. [167]	Multiple V-shaped ribs	$P/e = 6 - 12$ $c/D = 0.0213 - 0.0422$ $\alpha = 30° - 75°$ $W/w = 1 - 10$ $Re = 2000 - 20\,000$	$Nu = 3.35 \times 10^{-5}Re^{0.92}(e/D)^{0.77}(W/w)^{0.43}(\alpha/90°)^{-0.49} \times \exp[-0.1177(\ln(W/W))^2] \times \exp\{-0.61[\ln(\alpha/90°)]^2\}(P/e)^{8.54}\exp\{-2.040[\ln(P/e)]^2\}$ $f = 4.47 \times 10^{-4}Re^{-0.3188}(e/D)^{0.73}(W/w)^{0.22}(\alpha/90°)^{-0.39} \times \exp\{-0.52[\ln(\alpha/90°)]^2\}(P/e)^{8.9}\exp\{-2.133[\ln(P/e)]^2\}$
Singh et al. [113]	Discrete V-shaped	$P/e = 4 - 12$ $g/e = 0.5 - 2$ $\alpha = 30° - 75°$ $d/w = 0.2 - 0.8$ $e/D_h = 0.015 - 0.043$ $Re = 3000 - 15\,000$	$Nu = 2.36 \times 10^{-5}Re^{0.90}(P/e)^{3.5}(\alpha/60°)^{-0.023}(g/e)^{-0.014}(e/D_h)^{0.47} \times \exp\{-0.84[\ln(p/e)]^2\}\exp\{-0.72[\ln(\alpha/60°)]^2\} \times \exp\{-0.05[\ln(d/w)]^2\}\exp\{-0.15[\ln(g/e)]^2\}$ $f = 44.13 \times 10^{-2}Re^{-0.126}(P/e)^{2.74}(\alpha/60°)^{-0.034} \times (d/w)^{-0.058}(g/e)^{-0.031}(e/D_h)^{0.70} \times \exp\{-0.685[\ln(P/e)]^2\}\exp\{-0.93[\ln(\alpha/60°)]^2\} \times \exp\{-0.058[\ln(d/w)]^2\}\exp\{-0.21[\ln(g/e)]^2\}$
Kumar et al. [117]	Multiple V-shaped ribs with gap	$P/e = 6 - 12$ $g/e = 0.5 - 1.5$ $e/D = 0.022 - 0.043$ $W/w = 1 - 10$ $G_d/L_v = 0.24 - 0.80$ $\alpha = 30° - 75°$ $Re = 2000 - 20\,000$	$Nu = 8.534 \times 10^{-3}Re^{-0.932}(e/D)^{0.175}(W/w)^{0.506} \times \exp\{-0.753[\ln(W/w)]^2\}(G_d/L_v)^{-0.0348} \times \exp\{-0.0653[\ln(G_d/L_v)]^2\}(g/e)^{-0.0708} \times \exp\{-0.223[\ln(g/e)]^2\}(\alpha/60°)^{-0.0239} \times \exp\{0.1153[\ln(\alpha/60°)]^2\}(P/e)^{1.196} \times \exp\{-0.2805[\ln(P/e)]^2\}$ $f = 3.1934Re^{-03.51}(e/D)^{0.268}(W/w)^{0.1132} \times \exp\{-0.974[\ln(W/w)]^2\}(G_d/L_v)^{0.0610} \times \exp\{-1.065[\ln(G_d/L_v)^2]^2\}(g/e)^{-0.1769} \times \exp\{-0.6349[\ln(g/e)]^2\}(\alpha/60°)^{0.1553} \times \exp\{-0.1527[\ln(\alpha/60°)]^2\}(P/e)^{-0.7941} \times \exp\{0.1486[\ln(P/e)]^2\}$
Spherical ball roughness			
Murmu et al. [156]	Inclined spherical ball	$P/e = 15$ $e/D_h = 0.036$ $e/d_b = 1$ $\alpha = 55°$	$Nu = 5.8 \times 10^{-7}Re^{1.0459}(e/D_h)^{2.8326}(p/e)^{1.56}(e/d_b)^{-0.231}(\alpha/55)^{-1.089} \times \exp(-0.87)[\ln(e/D_h)]^2\exp(-4.86)[\ln(P/e)]^2 \times \exp(-0.1817)[\ln(e/d_b)]^2\exp(-2.6542)[\ln(\alpha/55)]^2$ $f = 2.38 \times Re^{-0.05629}(e/D_h)^{0.017}(P/e)^{1.89}(e/d_b)^{-1.101}(\alpha/55)^{-0.1127} \times \exp(0.0664)[\ln(e/D_h)]^2\exp(-0.0429)[\ln(P/e)]^2 \times \exp(-0.526)[\ln(e/d_b)]^2\exp(-2.352)[\ln(\alpha/55)]^2$
Non uniform rib roughness			
Karmare and Tikekar [143]	Wire ribs-grid shape	$e/D_h = 0.035 - 0.044$ $P/e = 12.5 - 36$ $l/s = 1.72 - 1$ $Re = 4000 - 17000$	$Nu = 2.4(e/D_h)^{0.42}(l/s)^{-0.146}Re^{1/3}(P/e)^{-0.27}$ $f = 15.55(e/D_h)^{0.91}(l/s)^{-0.27}Re^{-0.26}(P/e)^{-0.51}$
Saini and Saini [142]	Expanded metal mesh	$l/e = 25 - 71.87$ $s/e = 15.62 - 46.87$ $e/D_h = 0.012 - 0.0390$ $Re = 1900 - 13\,000$	$Nu = 4.0 \times 10^{-4}Re^{1.22}(e/D)^{0.625}(s/10e)^{2.22} \times \exp\{1.25[\ln(s/10e)]^2\}(l/10e)^{2.66}\exp\{0.824[\ln(l/10e)]^2\}$ $f = 0.815Re^{0.316}(l/e)^{0.266}(s/10e)^{0.19}Re^{-026}(10e/d)^{0.591}$

Table 6. Details of correlations developed (*continued*).

Author(s)	Novel geometry	Parameters	Correlation developed
Karwa et al. [158]	Machined ribs	$P/e = 4.5 - 8.5$ $e/D_h = 0.014 - 0.0320$ $d/w = 0.167 - 0.5$ $W/H = 5.87$ $\mathrm{Re} = 3000 - 20\,000$	For $7 \le e^+ < 20$ $G = 103.77e^{-0.006}(W/H)^{0.5}(P/e)^{2.56}\exp[0.7343\ln(P/e)^2](e^+)^{-0.31}$ For $20 \le e^+ \le 60$ $G = 32.26e^{-0.006}(W/H)^{0.5}(+/e)^{2.56}\exp[0.7343\ln(P/e)^2](e^+)^{0.8}$ For $7 \le e^+ < 20R$ $f = 1.66e^{-0.0078}(W/H)^{-0.4}(P/e)^{0.2695}\exp[-0.762\ln(P/e)^2(e^+)^{-0.075}]$ For $20 \le e^+ \le 60R$ $f = 1.325e^{-0.0078}(W/H)^{-0.4}(P/e)^{0.2695}\exp[-0.762\ln(P/e)^2(e^+)^{-0.075}]$
Bhagoria et al. [130]	Wedge shaped ribs	$60.17\,\Phi^{-1.0264} < P/e < 12.12$ $\Phi = 8° - 15°$ $e/D_h = 0.015 - 0.033$ $\mathrm{Re} = 3000 - 18000$	$\mathrm{Nu} = 1.89 \times 10^{-4}\mathrm{Re}^{1.21}(e/D_h)^{0.426}(P/e)^{2.94}(\phi/10)^{-0.018}$ $\times \exp\{-0.71[\ln(P/e)]^2\}\exp\{-1.50[\ln(\phi/10)]^2\}$ $f = 12.44\mathrm{Re}^{-0.18}(e/D_h)^{0.99}(P/e)^{-0.52}(\phi/10)^{0.49}$
Kumar et al. [100]	Forward facing chamfered rectangular ribs	$e/D = 0.018 - 0.043$ $P/e = 12$ $e/w = 1.5$ $e'/e = 0.75$ $\mathrm{Re} = 4000 - 17\,000$	$\mathrm{Nu} = 0.066\mathrm{Re}^{0.858}(e'/e)^{0.022}(e/w)^{0.12}(e/D)^{0.241}\exp\{0.039[\ln(e'/e)]^2\}$ $f = 11.79\mathrm{Re}^{-0.58}(e'/e)^{0.169}(e/w)^{0.131}(e/D)^{0.318}\exp\{0.203[\ln(e'/e)]^2\}$
Inclined baffles			
Kumar et al. [137]	Angled perforated baffles	$W/H = 10$ $H_B/H = 0.50$ $P_B/H_B = 10$ $O_B/H_B = 0.266$ $\alpha = 35° - 65°$ $\beta_0 = 12\%$ $\mathrm{Re} = 5000 - 17\,000$	$\mathrm{Nu} = 1.0826 \times 10^{-18}\mathrm{Re}^{1.5805}15.694\alpha_a\exp[-1.9599(\ln\alpha_a)^2]$ $f = 2.48 \times 10^{-6}\mathrm{Re}^{-0.137}5.6517\alpha_a\exp[-0.7113(\ln\alpha_a)^2]$
S-shaped ribs			
Kumar et al. [12]	S-shaped wire ribs	$P/e = 4 - 16$ $e/D_h = 0.022 - 0.054$ $\alpha = 30° - 75°$ $W/w = 1 - 4$ $\mathrm{Re} = 2400 - 20\,000$	$\mathrm{Nu} = 1.4332 \times 10^{-4}\mathrm{Re}^{1.2764}(W/w)^{0.2748}$ $\times \exp\{-0.1084[\ln(W/w)]^2\}(P/e)^{0.4876}\exp\{-0.1107[\ln(P/e)]^{2^2}\}(\alpha/90°)^{-0.0468}$ $\times \exp\{-0.0642[\ln(P/e)]^2\}(e/D_h)^{-0.7653}\exp\{-0.1257[\ln(e/D_h)]^2\}$ $f = 1.430 \times 10^{-1}\mathrm{Re}^{-0.224}(W/w)^{0.1424}(P/e)^{0.7657}$ $\times \exp\{-0.187[\ln(P/e)]^2\}(\alpha/90°)^{0.2129}(e/D_h)^{0.2159}$
Other roughness geometries			
Saini and Verma [120]	Dimple protrusions	$e/D_h = 0.018 - 0.037$ $\mathrm{Re} = 2000 - 12000$ $P/e = 8 - 12$	$\mathrm{Nu} = 5.2 \times 10^{-4}\mathrm{Re}^{1.27}(e/D)^{0.33}(P/e)^{3.15}$ $\times \exp\{-2.2[\log(P/e)]^2\}\exp\{-1.30[\log(\mathrm{e}/D)]^2\}$ $f = 0.0642\mathrm{Re}^{-0.423}(e/D)^{-0.0214}(P/e)^{-0.465}$ $\times \exp\{0.054[\log(P/e)]^2\}\exp\{-0.840[\log(e/D)]^2\}$
Bhusan and Singh [122]	Dimple shaped roughness	$L/e = 25 - 37.5$ $S/e = 18.75 - 37.5$ $e/D = 0.03$ $d/D = 0.147 - 0.367$ $\mathrm{Re} = 4000 - 20000$	$\mathrm{Nu} = 2.1 \times 10^{-88}\mathrm{Re}^{1.452}(S/e)^{12.94}(L/e)^{992}(d/D)^{-3.9}$ $\times \exp\{-10.4[\log(S/e)]^2\}\exp\{-77.2[\log(L/e)]^2\}\exp\{-7.83[\log(d/D)]^2\}$ $f = 2.32\mathrm{Re}^{-0.201}(S/e)^{-0.383}(L/e)^{-0.484}(d/D)^{0.133}$
Yadav et al. [106]	Circular protrusions	$P/e = 12 - 24$ $e/D = 0.015 - 0.03$ $W/H = 11$ $\alpha = 45° - 75°$ $\mathrm{Re} = 3600 - 18100$	$\mathrm{Nu} = 0.154\mathrm{Re}^{1.017}(P/e)^{-0.38}(e/D)^{0.521}(\alpha/60°)^{-0.213}$ $\times \exp\{-2.0233[\ln(\alpha/60°)]^2\}$ $f = 7.207\mathrm{Re}^{-0.56}(P/e)^{-0.18}(e/D)^{0.176}(\alpha/60°)^{0.038}$ $\times \exp\{-1.412[\ln(\alpha/60°)]^2\}$
Saravanan at al. [146]	Staggered C-shape finned	$V = 0.57 - 4.4$ m/s $P/g = 3.2 - 3.8$ $h/H = 0.3 - 0.7$ $h/d_p = 1.5 - 3$ $\mathrm{Re} = 3000 - 24000$	$\mathrm{Nu}_p = 0.527\mathrm{Re}^{0.85}(P/g)^{1.009}(h/H)^{1.076}(h/d_p)^{-2.484}$ $f_p = 0.21\mathrm{Re}^{-0.21}(P/g)^{-0.782}(h/H)^{-0.502}(h/d_p)^{1.084}$ $\mathrm{Nu}_{np} = 0.009\mathrm{Re}^{0.861}(P/g)^{1.009}(h/H)^{0.482}$ $f_{np} = 1.126\mathrm{Re}^{-0.194}(P/g)^{-0.757}(h/H)^{0.593}$
Bezbaruah et al. [147]	Staggered conical vortex generators	$\mathrm{Re} = 3500 - 16\,000$ $e = 0.0075$ m $d = 0.015$ m $P = 0.020$ m $W = 0.08$ m $H = 0.03$ m $L_1 = 0.15$ m (inlet lenght) $L_2 = 1.1$ m (test section lenght) $L_3 = 0.2$ m (outlet lenght) $D = 0.044$ m	$\mathrm{Nu} = C_0\mathrm{Re}^{0.7209}(e/D)^{0.1718}(P/e)^{-0.127}\exp\{-0.0225[\ln(P/e)]^2\}$ $f = C_1\mathrm{Re}^{-0.4091}(e/D)^{0.4665}(P/e)^{-0.6123}$ C_0= 0.22805, C_1=24.5497

Table 7. Details of enhancement of heat transfer and fluid friction with optimum parameters used in the literature.

Author(s)	Geometry configuration	Reynolds number	Optimum value	Enhancement	
				Nu/Nu_s	f/f_s
Transverse ribs					
Prasad and Saini [86]	Small diameter protrusion wire	1500–24 000	$P/e = 10$ e/D_h or $e/D = 0.027$	2.38	4.25
Karwa et al. [158]	Transverse ribs	2800–15 000	$P/e = 5.5$ e/D_h or $e/D = 0.0143$ $W/H = 7.75$ $\Phi = 15°$	2.30	3.42
	Inclined ribs			2.12	3.92
	V continuous ribs			2.37	3.65
	V discrete ribs			2.47	2.47
Singh et al. [93]	Uniform/non-uniform square-wave profile transverse roughness rib	3000–15 000	$W_c/w = 85$	2.22	2.44
Sharma et al. [94]	Transverse, inclined transverse, dimple, inclined dimple, arc and sine wave	3000–18 000	For sine wave Re = 15000	3.60	–
Mahanand and Senapati [95]	Transverse inverted T-shaped ribs	3800–18 000	$e/D_h = 0.042$ $P/e = 7.14$ Re = 15 000	2.747	3.263
Gawande et al. [96]	Combined square and equilateral triangular ribs	3800–18 000	$e = 1.4$ $e/D = 0.042$ $P = 10$ $P/e = 7.14$ Re = 18 000	2.877	3.661
Kumar and Layek [98]	Circular ribs	8551–11 149	$P/e = 10$ $e = 1.2$	1.97	–
Kumar et al. [99]	Square ribs	4000–18 000	$P/e = 10$ $e/D = 0.05$ Re = 17 900	1.97	2.53
Kumar et al. [117]	Rectangular ribs roughened	4000–18 000	$P/e = 10$ $e/D = 0.04$ $e/w = 4.0$ Re = 15 000	2.70	4.93
Kumar et al. [152]	Semicircular ribs	4000–24 000	$e = 0.067$ $P/e = 25$ $P = 100$ Re = 24 000	2.20	2.50
Arc-shaped roughness					
Saini and Saini [102]	Arc-shaped wire ribs	2000–17 000	$P/e = 10$ e/D_h or $e/D = 0.0422$ $\alpha/90° = 0.3333$	3.80	1.75
Kumar et al. [105]	Discrete multiple-arc ribs	3000–19 000	$W/W_{AC} = 5.0$ $D_d/L_v = 0.67$ $g_w/H_r = 0.87$ $H_r/H = 0.047$ $P_r/H = 1.7$ $\alpha = 60°$ $X/D_h = 1.72$ $Y/D_h = 0.82$	7.61	6.48
Yadav et al. [106]	Circular protrusions in arc shape	3600–18 100	$P/e = 12$ e/D_h or $e/D = 0.03$ $\alpha = 60°$	2.89	2.93
Ghritlahre [107]	Arc-shaped wire ribs with apex upstream	No data*	$P/e = 10$ $e/D = 0.0395$ $e = 2.5$ $\alpha = 60°$	2.56	–
	Arc-shaped wire ribs with apex downstream			1.81	–
Srivastava et al. [108]	Arc-shaped ribs with gap	3000–15 000	$P/e = 10$ $e/D = 0.043$ $g/e = 1$ $d/W = 0.67$ $\alpha = 60°$ Re = 3000	2.40	3.94
	V-shaped ribs with gap		$P/e = 10$ $e/D = 0.043$ $g/e = 1$ $d/W = 0.67$ $\alpha = 60°$ Re = 15 000	3.40	4.05

Table 7. Details of enhancement of heat transfer and fluid friction with optimum parameters used in the literature (*continued*).

Author(s)	Geometry configuration	Reynolds number	Optimum value	Enhancement	
				Nu/Nu_s	f/f_s
V-shaped ribs					
Singh et al. [113]	Discrete V down ribs	3000–15 000	$P/e = 10$ e/D_h or $e/D = 0.033$ $\alpha = 60°$	3.04	3.11
Momin et al. [114]	V-shaped continuous wire ribs	17 034	$P/e = 10$ e/D_h or $e/D = 0.034$ $\alpha = 60°$	2.30	2.83
Hans et al. [167]	Multiple V-shaped ribs	2000–20 000	$P/e = 8$ e/D_h or $e/D = 0.03$ $\alpha = 60°$ $W/w = 10$	6.00	5.00
Singh et al. [168]	Discrete V-shaped ribs with gap	3000–15 000	$P/e = 8$ $e/D = 0.043$ $\alpha = 60°$ $W/w = 12$	–	–
Kumar et al. [117]	Multiple V-shaped ribs with gap	2000–20 000	$P/e = 10$ $e/D = 0.043$ $\alpha = 60°$ $G_d/L_v = 0.69$ $g/e = 1$	6.32	6.12
Kumar et al. [169]	Multiple V-shaped ribs with gap	2000–20 000	$P/e = 10$ $e/D = 0.043$ $\alpha = 60°$ $G_d/L_v = 0.69$ $g/e = 1$ $W/w = 6$	6.74	6.37
Dimple or protrusion ribs					
Saini and Verma [120]	Dimple shape	2000–12 000	$P/e = 10$ e/D_h or $e/D = 0.0379$	7.58	4.68
Kumar and Verma [145]	Sinusoidal ribs	4000–15 000	$D_h = 33.33$ mm $P = 10, 14, 18$ mm $e = 1$ mm $W/H = 5$ $q = 1000\ W/m^2$ $Re = 4000 - 15\,000$	2.48	1.76
Bhushan and Singh [170]	Protrusion	1900–13 000	$S/e = 31.25$ $L/e = 31.25$ $d/D = 0.294$	3.80	2.20
Hassan et al. [123]	Dimple	2000–18 000		5.56	1.62
Vikash Kumar [119]	Concave dimple	2000–13 500	$P/e = 8 - 15$ $e/D_h = 0.018 - 0.045$ $e/d = 1 - 2$	3.94	2.56
Tabish and Kim [124]	Conical protrusion rib over spherical ribs	4000–16 000	$P/e = 10$ $e/D = 0.044$	2.49	7.29
W-shaped ribs					
Kumar et al. [126]	Discritised W-shaped ribs	3000–15 000	$P/e = 10$ e/D_h or $e/D = 0.038$ $\alpha = 60°$	2.16	2.75
Lanjewar et al. [171]	W-shaped ribs	2300–14 000	$P/e = 10$ $e/D = 0.0375$ $\alpha = 60°$ $W/H = 8$	2.36	2.01
Thakur and Thakur [128]	Multi-staggered rib parameters of the W-rib roughness	4000–14 000	$P/e = 12$ $e/D_h = 0.0423$ $\alpha = 60°$ $g/e = 1$ $n = 2$ $p/P = 0.65$ $w/e = 4.5$	4.10	2.50
Spherical ball roughness					
Murmu et al. [156]	Inclined spherical ball	2500–18 500	$p/e = 15$ $e/D_h = 0.036$ $e/d_b = 1$ $\alpha = 55°$	3.56	2.34

Table 7. Details of enhancement of heat transfer and fluid friction with optimum parameters used in the literature (*continued*).

Author(s)	Geometry configuration	Reynolds number	Optimum value	Enhancement	
				Nu/Nu$_s$	f/f_s
Non-uniform ribs					
Layek et al. [89]	Chamfered compound rib	3000–21 000	$P/e = 10$ e/D_h or $e/D = 0.03$ $\Phi = 18°$	2.60	3.35
Kumar et al. [100]	Forward facing chamfered rectangular ribs	4000–17 000	$e/D = 0.043$ $P/e = 12$ $e/w = 1.5$ $e'/e = 0.75$ $\mathrm{Re} = 17000$	2.88	3.52
Bhagoria et al. [130]	Wedge shaped ribs	3000–18 000	$P/e = 7.57$ e/D_h or $e/D = 0.033$ $\Phi = 10°$	2.40	5.30
Barik et al. [131]	T-rib, left arm inclined T-rib, right arm inclined T-rib, Y-rib, concave and convex T-ribs	5000–20 000	$P = 80$ mm $\mathrm{Re} = 20000$	1.91	–
Kumar and Goel [132]	Semi-circular, circular, triangular, square, rectangular	3700–18 700	For a forward-chamfered rectangular rib: $e/D = 0.0433$ $e/w = 1.67, 2$ $e'/e = 0.75$ $P/e = 11$ $\mathrm{Re} = 3700 - 18700$	3.82	–
Zina et al. [133]	Triangular ribs with semi-circular nooks	3800–18 000	$\mathrm{Re} = 5000$ $P = 10$ mm $e = 2.2, 1.8, 1.4$ mm	2.55	2.42
Inclined baffles					
Aharwal et al. [135]	Inclined continuous with gap ribs	3000–18 000	$P/e = 10$ e/D_h or $e/D = 0.0377$ $\alpha = 60°$ $W/H = 5.84$ $g/e = 1$ $d/W = 0.25$	2.95	2.87
Aharwal et al. [136]	Integral inclined discrete rib	3000–18 000	$P/e = 8$ e/D_h or $e/D = 0.037$ $\alpha = 60°$ $d/W = 0.25$ $g/e = 1$	2.83	3.60
Kumar et al. [137]	Angled perforated baffles	5000–17 000	$\alpha = 55°$ $\mathrm{Re} = 9000$	3.82	7.14
Kumar and Layek [138]	Winglet shaped ribs	No data**	$P/e = 8$ $\alpha = 60°$ $W/w = 5$ $\mathrm{Re} = 22\,000$	2.83	3.63
Other roughness geometries					
Saini and Saini [142]	Expanded metal mesh	1900–13 000	e/D_h or $e/D = 0.037$ $\alpha = 60°$ $L/e = 46.87$ $S/e = 25$ $W/H = 11$	4.00	5.00
Chandra et al. [172]	One ribbed wall	10 000–80 000	$P/e = 8$ e/D_h or $e/D = 0.0625$ $L/D_h = 20$	2.43	3.14
	Two ribbed walls			2.64	5.39
	Three ribbed walls			2.81	3.14
	Four ribbed walls			2.99	9.50
Jaurker et al. [141]	Rib grooved combination	3000–21 000	$P/e = 6$ e/D_h or $e/D = 0.0363$ $g/p = 0.4$	2.75	3.61
Bopche and Tandale [144]	U-shaped ribs	3800–18 000	$P/e = 6.67$ $e/D = 0.03986$ $\alpha = 90°$	2.82	3.72
Saravanan at al. [146]	Staggered C-shape finned	3000–24 000	$V = 0.57 - 4.4$ m/s $P/g = 3.2 - 3.8$ $h/H = 0.3 - 0.7$ $h/d_p = 1.5 - 3$ $\mathrm{Re} = 3000 - 24\,000$	2.67	5.34
Bezbaruah et al. [147]	Staggered conical vortex generators	3500–16 000	$P/e = 2.67$ $e/D = 0.34$ $\mathrm{Re} = 16\,000$	2.57	–

Table 7. Details of enhancement of heat transfer and fluid friction with optimum parameters used in the literature (*continued*).

Author(s)	Geometry configuration	Reynolds number	Optimum value	Enhancement	
				Nu/Nu_s	f/f_s
Goel et al. [148]	Hemispherical cavities	2100–18 500	$x/r_d = 11$ $y/r_d = 11$ $r_d/D_h = 0.039$ $Re = 2160$	5.33	3.60
Yadav and Saini [149]	Impinging jet	3500–17 500	$D_j/D_h = 0.065 - 0.195$ $H_j/D_h = 0 - 0.433$ $Re = 3500 - 17\,500$	7.18	8.48
Wang et al. [150]	S-shaped ribs with gap	2300–23 000	$Re = 19258$ $P/e = 20$ $W/w = 4$ $e/D = 0.023 - 0.036$ $g/e = 1.5$ $q = 450 - 650\ W/m^2$	5.42	5.87
Gawande et al. [134]	20° chamfered ribs	3800–18 000	$P/e = 7.14$ $e/D = 0.042$ $\alpha = 0° - 40°$ $W/H = 5$ $Re = 15\,000$	3.218	4.04
	Right-angle triangular ribs			3.100	3.80
	Reverse L-shaped ribs			2.827	3.42

*Mass flow rate $\dot{m} = 0.007 - 0.022$ kg/s.
**Mass flow rate $\dot{m} = 0.00531 - 0.04041$ kg/s.

10. Thermo-hydraulic performance

The performance of a solar air heater can be evaluated using artificial roughness on the underside of the absorber plate surface. The use of artificial roughness increases heat transfer, as well as causes a pressure drop due to friction. The performance of SAH can be enhanced when heat transfer increases simultaneously, allowing a minimum possible friction factor.

The overall performance of SAH is judged by thermo-hydraulic performance as $THP = (Nu/Nu_s)/(f/f_s)^{1/3}$. The term 'thermo-hydraulic performance' was first used by Webb and Eckert [173], who considered parameters, such as heat transfer and the friction factor caused by fluid pressure drop.

In this paper, various research works are referred to in order to get an overview of the THP value determined based on experimental studies conducted by researchers. It is found that the value of THP ranges from 1.38 to 4.73 under various arrangements utilised over the absorber plate and environmental conditions, as enlisted in Table 8.

11. Discussion

11.1. Correlations

In the field of correlation development, Prasad and Saini [86] used *P*/*e*, *e*/*D* and Re as influencing parameters to modify conventional SAH, and they developed correlations for Nu and *f*. Similarly, Hong and Hsieh [162], Verma and Prasad [91], Kumar et al. [99] and Varun et al. [165] developed correlations for Nu and *f* for the performance prediction of SAH. There are many other authors who have been associated in the same field of interest and developed correlations for Nu and *f*. The parameters considered were: *e*/*D*, *w*/*H* and Re used by Gupta et al. [151], *w*/*H*, *P*/*e*, e^+ and *e* used by Karwa [88], *P*/*e*, *e*/*D*, *g*/*P* and Re adopted by Layek et al. [89], *P*/*e* and Re taken by Varun et al. [165], Mahanand and Senapati [95] and Gawande et al. [134], *d*/*H* and D_h utilised by Kumar et al. [152], *P*/*e*, *e*/*w*, *e*/*D* and Re used by Kumar et al.[153], *e*/*D*, *d*/*w*, *g*/*e* and Re adopted by Aharwal et al. [136] for developing correlation and modification of conventional SAH.

The correlations for Nu and *f* using arc-shaped rib roughness were first developed by Saini and Saini [102] with *e*/*D*, *α*, Re as variable parameters in a modified SAH. Bhuvad et al. [110] used *f*, *e*/*D* and Re for apex-up discrete arc rib roughness; Kumar et al. [105] used Re, D_d/L_v, g_w/H_r, H_r/H, R_r/H, α, X/D_h and Y/D_h parameters for discrete multiple-arc rib roughness; Kumar et al. [112] used *g*/*e*, *d*/*x*, Re and N_g parameters for correlation development of Nu and *f* for discrete multiple arc-shaped ribs. Kumar et al. [161] arranged arcs in forward and backwards facing, using parameters such as Re, *g*/*e*, *d*/*x*, *W*/*w*, *P*/*e*, *e*/*D* and *g*/*e* for correlation development, whereas Korpale et al. [111] developed correlations using Re, *P*/*e*, *e*/*D* and *w*/*e* as roughness factors for a rectangular-section rib configuration.

Gupta et al. [163] firstly reported correlations for Nu and *f* based on V-shaped wire ribs with and without inclination angle through *e*/*D*, *W*/*H*, *α* and *K*/*D* parameters. Muluwork et al. [166] additionally used the *B*/*S* ratio to develop the correlation. Momin et al. [114] arranged wire ribs in a continuous manner to develop correlations by using *e*/*D*, *α* and Re as governing parameters. Hans et al [167] used multiple V-shaped ribs to modify the correlation with parameters such as *e*/*D*, *W*/*w*, Re, *P*/*e* and *α*. Singh et al. [116] used discrete V-shaped ribs with parameters such as Re, *P*/*e*, *α*, *g*/*e*, *e*/*D*, *d*/*w* to develop correlations for Nu and *f*. Kumar et al. [169] developed correlations for Nu and *f* using Re, *e*/*D*, *W*/*w*, G_d/L_v, *g*/*e*, *α*, *P*/*e* for multiple V-shaped ribs with a gap.

Table 8. Details of thermo-hydraulic performance of solar air heaters reported to date.

Authors	Roughness type	Roughness parameters	$THP = \frac{Nu/Nu_s}{(f/f_s)^{1/3}}$
Tranverse ribs			
Prasad and Saini [86]	Transverse wire	$e/D_h = 0.020 - 0.033$ $P/e = 10 - 20$ $Re = 500 - 50\,000$	1.78
Bhagoria et al. [130]	Transverse wedge shaped ribs	$60.17\Phi^{-1.0264} < P/e < 12.12$ $\Phi = 8° - 15°$ $e/D = 0.015 - 0.033$ $Re = 3000 - 18000$	1.38
Karwa et al. [88]	Transverse ribs	$P/e = 5.5$ e/D_h or $e/D = 0.0143$ $W/H = 7.75$ $\alpha = 15°$	1.53
	Inclined ribs		1.34
	V continuous ribs		1.54
	V discrete ribs		1.83
Singh et al. [93]	Uniform/non-uniform square-wave profile transverse roughness ribs	$Re = 3000 - 15\,000$	1.49
Sharma et al. [94]	Transverse, inclined transverse, dimple, inclined dimple, arc and sine wave	Sine wave $e/D_h = 0.271$ $P/e = 10$ $Re = 15\,000$ $\alpha = 45°$	2.05
Mahanand and Senapati [95]	Transverse inverted T-shaped ribs	$e/D_h = 0.042$ $P/e = 7.14$ $Re = 15\,000$	1.86
Gawande et al. [96]	Combined square and equilateral triangular ribs	$e = 1.4$ mm $e/D = 0.042$ $P = 10$ mm $P/e = 7.14$ $Re = 18\,000$	1.86
Korpale et al. [111]	Rectangular section ribs	$P/e = 17.22$ $e/D = 0.044$ $w/e = 0.5$ $Re = 20\,000$	2.77
Kumar et al. [99]	Square ribs	$P/e = 10$ $e/D = 0.05$ $Re = 17\,900$	1.44
Kumar et al. [153]	Rectangular ribs roughened	$P/e = 10$ $e/D = 0.04$ $e/w = 4.0$ $Re = 15\,000$	1.89
Kumar et al. [152]	Semicircular ribs	$e = 0.067$ mm $P/e = 25$ $P = 100$ mm $Re = 24\,000$	1.7
Arc-shaped roughness			
Bhuvad et al. [110]	Apex-up discrete arc ribs	$W = 200$ mm $W/H = 8$ $\alpha = 30°,\ 45°,\ 60°$ $e/D_h = 0.045$ $P/e = 10$ $N_g = 3$ $g/e = 3$	2.01
Kumar et al. [105]	Discrete multiple-arc ribs	$D_d/L_v = 0.27 - 0.86$ $g/H_r = 0.32 - 1.72$ $H_r/H = 0.025 - 0.047$ $P_r/H = 0.58 - 3.1$ $\alpha = 35° - 65°$ $X/D_h = 0.47 - 1.72$ $Y/D_h = 0.46 - 0.82$ $D_j/D_h = 0.065$ $W/W_{AC} = 5$ $Re = 3000 - 19\,000$	4.1
Ghritlahre [107]	Arc-shaped wire ribs with apex upstream	$\dot{m} = 0.007 - 0.022$ kg/s	2.09
	Arc-shaped wire ribs with apex downstream		1.59

Table 8. Details of thermo-hydraulic performance of solar air heaters reported to date (*continued*).

Authors	Roughness type	Roughness parameters	$THP = \frac{Nu/Nu_s}{(f/f_s)^{1/3}}$
Kumar et al. [161]	Innovatively arranged arc (combination of alternatively arranged forward and backward facing arced ribs)	$e/D = 0.045$ $\alpha = 60°$ $d/x = 0.65$ $g/e = 1.0$ $W/w = 3$ $P/e = 8$	3.61
Kumar et al. [112]	Discrete multiple arc-shaped ribs	$g/e = 1$ $N_g = 3$ $d/x = 0.6$ $Re = 19000$	3.85
Srivastava et al. [174]	Arc-shaped rib with gap	$P/e = 10$ $e/D = 0.043$ $g/e = 1$ $d/W = 0.67$ $\alpha = 60°$ $Re = 3000$	1.5
	V-shaped rib with gap		2.21
V-shaped ribs			
Singh et al. [113]	V down ribs	$P/e = 10$ e/D_h or $e/D = 0.033$ $\alpha = 61.9°$	2.03
Momin et al. [114]	V-shaped continuous wire rib	$P/e = 10$ e/D_h or $e/D = 0.034$ $\alpha = 60°$	1.63
Hans et al. [167]	Multiple V-shaped ribs	$P/e = 8$ e/D_h or $e/D = 0.03$ $W/w = 10$ $\alpha = 60°$	3.51
Singh et al. [115]	Discrete V-shaped ribs with gap	$P/e = 8$ $e/D = 0.043$ $\alpha = 60°$ $W/H = 12$	2.06
Kumar et al. [175]	Multiple V-shaped ribs with gap	$P/e = 10$ $e/D = 0.043$ $G_d/L_v = 0.69$ $g/e = 1.0$ $\alpha = 60°$	3.46
Kumar et al. [117]	Multiple V-shaped ribs with gap	$P/e = 10$ e/D_h or $e/D = 0.043$ $g/e = 1$ $G_d/L_v = 0.69$ $W/w = 6$ $\alpha = 60°$	3.64
Dimple or protrusion ribs			
Saini and Verma [120]	Dimple shape	$P/e = 10$ e/D_h or $e/D = 0.0379$	4.53
Kumar and Verma [145]	Sinusoidal rib	$D_h = 33.33$ mm $P = 10,\ 14,\ 18$ mm $e = 1$ mm $W/H = 5$ $q = 1000\ W/m^2$ $Re = 4000 - 15\,000$	2.05
Bhushan and Singh [170]	Protrusion	$S/e = 31.25$ $L/e = 31.25$ $d/D = 0.294$	2.92
Hassan et al. [123]	Dimple	$P/e = 4 - 16$ $e/D_h = 0.018 - 0.045$ $W/w = 1 - 5$ $\alpha = 30° - 75°$	4.73
Kumar and Prasad [119]	Concave dimple	$P/e = 4 - 15$ $e/D_h = 0.018 - 0.045$ $e/d_d = 1 - 2$	2.88
Alam and Kim [176]	Conical protrusion rib over spherical ribs	$P/e = 10$ $e/D = 0.044$	1.28
W-shaped ribs			
Kumar et al. [126]	Discritised W-shaped ribs	$P/e = 10$ e/D_h or $e/D = 0.0338$ $\alpha = 60°$	1.54

Table 8. Details of thermo-hydraulic performance of solar air heaters reported to date (*continued*).

Authors	Roughness type	Roughness parameters	$\text{THP} = \frac{\text{Nu}/\text{Nu}_s}{(f/f_s)^{1/3}}$
Lanjewar et al. [171]	W-down ribs	$e/D_h = 0.03375$ $P/e = 10$ $e = 1.5$ mm $\alpha = 30°, 45°, 60°, 75°$ $W/H = 8$ $e^+ = 8 - 44$ $\text{Re} = 2300 - 14\,000$	1.98
	W-up ribs		1.81
Thakur and Thakur [127]	W-shaped ribs with symmetrical gaps along with staggered ribs	$P/e = 12$ $g/e = 1$ $w/e = 4.5$ $p/P = 0.65$ $N_g = 2$ $\text{Re} = 12\,000$	3.24
Thakur and Thakur [128]	Multiple-staggered rib parameters of the W'-shaped roughness	$P/e = 12$ $e/D_h = 0.0423$ $\alpha = 60°$ $g/e = 1$ $w/e = 4.5$ $p/P = 0.65$ $N_g = 2$	3.02
Spherical ball roughness			
Murmu et al. [156]	Inclined spherical ball	$P/e = 15$ $e/D_h = 0.036$ $e/d_b = 1$ $\alpha = 55°$	2.68
Non-uniform ribs			
Layek et al. [89]	Chamfered compound rib	$P/e = 10$ e/D_h or $e/D = 0.03$ $\Phi = 18°$	1.74
Kumar et al. [100]	Forward-facing chamfered rectangular ribs	$e/D = 0.043$ $P/e = 12$ $e/w = 1.5$ $e'/e = 0.75$ $\text{Re} = 17\,000$	1.89
Bhagoria et al. [130]	Wedge shaped ribs	$P/e = 7.57$ e/D_h or $e/D = 0.033$ $\Phi = 10°$	1.38
Barik et al. [131]	T-shaped rib, left arm inclined T-shaped rib, right arm inclined T-shaped rib, Y-shaped rib, concave and convex T-shaped ribs	For T-shaped rib $P = 80$ mm $\text{Re} = 18\,000$	1.7
Kumar and Goel [132]	Semi-circular, circular, triangular, square, rectangular	For forward-chamfered rectangular rib $e/D = 0.0433$ $e/w = 0.67, 2.0$ $P/e = 11$ $e'/e = 0.75$ $\text{Re} = 3700 - 18\,700$	2.66
Zina et al. [133]	Triangular ribs with semi-circular nooks	$P = 10$ $e = 2.2, 1.8, 1.4$ mm $\text{Re} = 5000$	1.93
Gawande et al. [134]	20° chamfered rib	$P/e = 7.14$ $e/D = 0.042$ $W/H = 5$ $\text{Re} = 15\,000$	2.05
	Right-angle triangular rib		2.04
	Reverse L-shaped rib		1.90
Inclined baffles			
Kumar et al. [137]	Angled perforated baffles	$W/H = 10$ $H_B/H = 0.50$ $P_B/H_B = 10$ $O_B/H_B = 0.266$ $\alpha = 35° - 65°$ $\beta_0 = 12\%$ $\text{Re} = 5000 - 17\,000$	1.94
Kottayat et al. [139]	Discrete multiple inclined baffle	$\text{Re} = 6000 - 14000$	2.69

Table 8. Details of thermo-hydraulic performance of solar air heaters reported to date (*continued*).

Authors	Roughness type	Roughness parameters	$\mathrm{THP} = \frac{\mathrm{Nu}/\mathrm{Nu}_s}{(f/f_s)^{1/3}}$
Parsa et al. [140]	Staggered cuboid baffles	$a/H = 2.5$ (relative length) $b/H = 0.8$ (relative width) $c/H = 0.7$ (relative height) $s/H = 1.5$ (relative pitch) $\alpha = 22.5°$ $\mathrm{Re} = 5080$	3.28
Aharwal et al. [135]	Inclined and continuous rib with gap	$P/e = 10$ e/D_h or $e/D = 0.0377$ $\alpha = 60°$ $W/H = 5.84$ $g/e = 1$ $d/W = 0.25$	2.08
Aharwal et al. [136]	Integral inclined discrete ribs	$P/e = 8$ e/D_h or $e/D = 0.037$ $\alpha = 60°$ $d/W = 0.25$ $g/e = 1$	1.85
Kumar and Layek [138]	Winglet shaped ribs	$P/e = 8$ $W/w = 5$ $\alpha = 60°$ $\mathrm{Re} = 22\,000$	1.84
Other roughness geometries			
Jaurker et al. [141]	Rib groove	$P/e = 4.5 - 10.0$ $g/p = 0.3 - 0.7$ $e/D = 0.0181 - 0.0363$ $\mathrm{Re} = 3000 - 21000$	1.76
Saini and Saini [90]	Expanded metal mesh	$l/e = 25 - 71.87$ $s/e = 15.62 - 46.87$ $e/D_h = 0.012 - 0.0390$ $\mathrm{Re} = 1900 - 13\,000$	2.34
Karmare and Tikekar [143]	Metal grit ribs	$e/D_h = 0.035 - 0.044$ $P/e = 12.5 - 36$ $l/s = 1.72 - 1$ $\mathrm{Re} = 4000 - 17000$	2.39
Bopche and Tandale [144]	Inverted U-shaped ribs	$e/D_h = 0.0186 - 0.03986$ $p/e = 6.667 - 57.14$ $\alpha = 90°$ $W/H = 6$ $\mathrm{Re} = 3800 - 18\,000$	1.82
Kumar and Verma [145]	Sinusoidal protrusion ribs	$P_T = 10,\ 14,\ 18$ mm (transverse) $P_L = 10, 14,\ 18$ mm (longitudinal) $e = 1$ mm $W/H = 5$ $D_h = 33.33$ mm $\mathrm{Re} = 4000 - 15\,000$	2.02
Saravanan et al. [146]	Staggered C-shape finned absorber plate	$P/g = 3.8$ $h/H = 0.6$ $\mathrm{Re} = 24\,000$	1.64
Bezbaruah et al. [147]	Staggered conical vortex generators	$P/e = 2.67$ $e/D = 0.17$ $\mathrm{Re} = 16\,000$	2.04
Goel et al. [148]	Hemispherical cavities	$x/r_d = 11$ $y/r_d = 11$ $r_d/D = 0.039$ $\mathrm{Re} = 2160$	3.48
Yadav and Saini [149]	Impinging jet	$D_j/D_h = 0.065 - 0.195$ $H_j/D_h = 0 - 0.433$ $\mathrm{Re} = 3500 - 17\,500$	3.66

Table 8. Details of thermo-hydraulic performance of solar air heaters reported to date *(continued)*.

Authors	Roughness type	Roughness parameters	$THP = \frac{Nu/Nu_s}{(f/f_s)^{1/3}}$
Kumar and Verma [121]	Sinusoidal ribs	$D_h = 33.33$ mm $P = 10, 14, 18$ mm $e = 1$ mm $W/H = 5$ $q = 1000$ W/m^2 Re = 4000 – 15 000	2.05
Wang et al. [150]	S-shaped ribs with gap	$p/e = 20$ $W/w = 4$ $e/D = 0.023 - 0.036$ $g/e = 1.5$ $q = 450 - 650$ W/m^2 Re = 19 258	3.00

Karmare and Tikekar [143] modified SAH using wire ribs grid shape roughness, considering parameters such as *e*/*D*, *L/S*, Re and *P*/*e* for determining Nu and *f*. Saini and Saini [142] used expanded metal mesh with the following parameters: Re, *e*/*D*, *S*/*e* and *L*/*e*. Karwa et al. [158] adopted *w*/*H*, *P*/*e* and e^+ parameters for machined ribs for modification of a SAH. Bhagoria et al. [130] modified SAH using wedge shaped ribs for parameters such as Re, *e*/*D*, *P*/*e* and ϕ. Kumar et al. [100] developed correlations of Nu and *f* for forward-facing chamfered rectangular ribs through *e'*/*e*, *e*/*w*, *e*/*D* and Re as parameters.

Kumar et al. [137] used angled perforated baffles for modification of SAH through Re and α as parameters.

Saini and Verma [119] used dimple protrusions using parameters such as Re, *e*/*D* and *P*/*e*. Bhushan and Singh [170] used dimple-shaped roughness with Re, *S*/*e*, *L*/*e* and *d*/*D* as governing parameters. Yadav et al. [106] used circular protrusions and adopted Re, *P*/*e*, *e*/*D* and α as influencing parameters for modification of SAH. Saravaran et al. [146] utilised staggered C-shape finned absorber plate with factors affecting the performance of a SAH, such as *P*/*g*, *h*/*H* and h/d_p as parameters.

Murmu et al. [156] modified the conventional SAH using spherical ball-shaped ribs over the absorber plate and successfully developed strong predictive correlations for Nu and *f*. They used Re, *e*/*D*, *P*/*e*, *e*/*d* and α as control variables.

No reports on the development of correlations for W-shaped ribs to date have been reported by any author.

11.2. Maximum enhancement of Nusselt number and friction factor

This section is dedicated to disseminating the maximum values of Nu and *f* for roughness geometries considered in the present review work.

Gawande et al. [96] investigated transverse ribs in the form of combined square and equilateral triangular ribs as roughness elements to modify conventional SAH. They found the maximum enhancement in the Nusselt number as 2.877 and the friction factor as 3.661 compared to a smooth duct of SAH. They achieved maximum Nu and *f* at the optimum control parameters of *P*/*e* = 7.14 (fixed), *e*/*D* = 0.042 (fixed) and Re = 18 000, resulting from combining square and equilateral triangular shapes that enhanced the heat transfer.

Kumar et al. [105] modified conventional SAH with novel roughness elements in the form of discrete multiple arc-shaped ribs in the view of enhancing heat transfer. They reported the highest increment in Nu and *f* of 7.61 and 6.48, respectively, in a modified SAH with the optimum parameters of $W/W_{AC} = 5.0$, $D_d/L_v = 0.67$, $g_w/H_r = 0.87$, $H_r/H = 0.047$, $P_r/H = 1.7$, $\alpha = 60°$, $X/D_h = 1.72$ and $Y/D_h = 0.82$. The maximum enhancement was ensured due to gaps in the multi-arc shaped ribs, which ensured the frontal discharge of flowing fluid through both primary flow and secondary flow. This further contributes to better mixing, i.e. limited surface side growth of the boundary layer, which leads to an enhancement of heat transfer.

Kumar et al. [117] used multi V-shaped ribs with a gap as roughness elements to extend the absorber plate in the expectation of improved SAH with higher heat transfer rates. They found maximum augmentation in Nu and *f* of 6.74 and 6.37, respectively, at the optimum variables of *P*/*e* = 10, e/D_h or *e*/*D* = 0.043, $\alpha = 60°$, *g*/*e* = 1, G_d/L_v =0.69, *W*/*w* = 6 and Re of 20 000. The gap distance used in the roughness geometry provided passage for secondary flow, which enhanced the heat transfer between the fluid and the surface.

Saini and Verma [120] employed a novel artificial roughness element in the form of dimple-shaped rib over the absorber plate in a SAH. They achieved maximum enhancement in Nu and *f* of 7.58 and 4.68, respectively, at the optimum influencing parameters, such as *P*/*e* of 10, *e*/*D* of 0.0379 and Re of 12 000. The dimple shape of roughness elements led to the reattachment of the free shear layer after the flow separation in the fluid domain.

This enhances the heat transfer rate between the fluid and the surface by virtue of the vicinity of the reattachment region.

Thakur and Thakur [128] proposed a modified SAH featuring a novel roughness geometry based on multi-staggered W-shaped ribs. They conducted experiments by varying different operating and geometric parameters, and reported the results at the optimum conditions of P/e = 12, e/D_h = 0.0423, α = 60°, g/e = 1, N_g = 2, p/P = 0.65, w/e = 4.5 and Re = 12 000. They reported an enhancement in Nu and f of 4.1 and 2.5, respectively. It was observed that W-shaped staggered ribs further energise the flow within the gaps, promoting enhanced flow development and vortex formation, which in turn significantly improves the Nusselt number.

Murmu et al. [156] experimentally investigated SAH modified using inclined spherical balls as roughness elements. They reported an enhancement in Nu and f by 3.56 and 2.34, respectively, compared to a smooth duct SAH at the optimum parameters of P/e = 15, e/D_h = 0.036, e/d_b = 1 and α = 55°. They concluded that due to the spherical ball shape roughness, the secondary flow stream rejoins the primary flow, which accelerates the rate of heat transfer.

Kumar and Goel [132] used a non-uniform type of rib roughness specifically in the form of forward-chamfered rectangular rib to the developed modified SAH. They achieved maximum increases in Nu and f as 3.82 and 2.68, respectively, at the optimum parameters such as the e/D ratio of 0.0433, e/w ratio of 0.67 and 2.0, P/e ratio of 11, e'/e ratio of 0.75 and Re of 3700 to 18 700. The authors observed that the main reason for heat transfer increment is that the chamfered elements guide the fluid flow in the centre of SAH, which leads to better mixing of a broken laminar sublayer over the absorber plate to the mainstream flow.

Kumar et al. [137] investigated experimentally the modified SAH using angled perforated baffles as novel baffle roughness in the view of heat transfer enhancement and controlled fluid flow. They optimised the system and operating parameters to α = 55° and Re = 9000. The reported maximum enhancement in Nu and f was 3.82 and 7.14, respectively.

Wang et al. [150] modified conventional SAH using S-shaped ribs with a gap as artificial roughness over the absorber plate, focusing on the heat transfer enhancement. The maximum obtained enhancement in Nu and f was, respectively, 5.42 and 5.87 times the smooth duct SAH at the optimum variables, such as Re of 19 258, P/e ratio of 20, W/w ratio of 4, e/D ratio of 0.023 to 0.036 and g/e ratio of 1.5. Due to S-shaped ribs over the absorber plate, the incoming fluid stream underwent the flow separation, causing vortices to form downstream of the flow. These vortices improved air mixing, thereby enhancing the heat transfer and increasing pressure drop.

11.3. Thermo-hydraulic performance

As regards the thermo-hydraulic performance of the solar air heater geometries based on various transverse rectangular sectioned ribs, the maximum value obtained was 2.77, as shown in the comparison presented in Fig. 70. This SAH model was developed by Korpale et al. [111], who incorporated transverse rectangular finned types of ribs to roughen the solar air heaters. The rectangular sectioned fins installed on the absorber surface

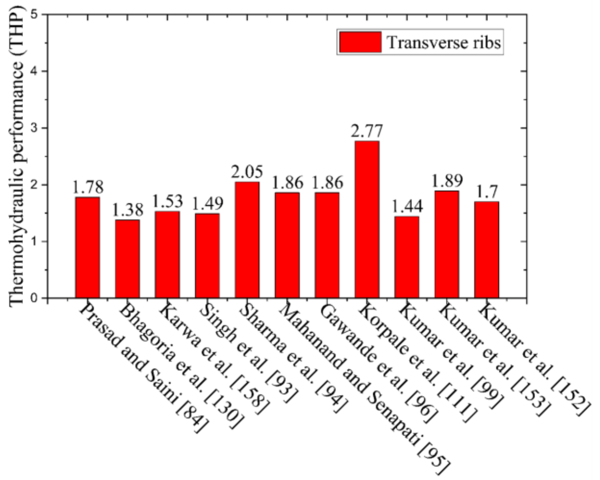

Fig. 70. Variation in THP of SAH based on various transverse ribs.

helped in creating wall-induced turbulence affecting the temperature of the air, as well as the local temperature of walls in contact with hot air. The THP value obtained from the CFD approach was 2.37, showing minor error for Nu and f calculations. The validation experiment was also performed to confirm the accuracy of optimisation and CFD results. The authors obtained a THP value of 2.55 for the same case, which was a maximum value among all other models achieved in the transverse rib SAH type.

There have been various investigations carried out on SAHs based on the arc-shaped roughness. The maximum value of THP was found to be 4.1. It was obtained by Kumar et al. [105], who developed an impingement jet SAH with discrete multiple arc-shaped ribs as roughness elements. The gaps in the multiple arc-shaped ribs permit the discharge of fluid from the secondary and mainstream. The mainstream flowing through the gap is a stable stream with a denser boundary layer containing the viscous sublayer. The occurrence of a gap results in the mixing of a secondary stream with the mainstream. This mixing facilitates and strengthens the limited boundary layer stream beside the surface, resulting in increased heat transfer. This leads to an improved heat transfer rate. However, it is accompanied by a simultaneous enhancement in Reynolds number and a relatively small increase in the friction factor for the augmented SAH. Therefore, the thermal hydraulic performance (THP) was found to be superior compared to other available models, as shown in Fig. 71.

The maximum THP value of 4.73 was obtained in the group of SAHs utilising dimple or protrusion ribs, as depicted in Fig. 72. The SAH setup, which produced the maximum THP, was built by Hassan et al. [123], who utilised multiple arc arrangements using dimple or protrusion ribs to develop an efficient SAH setup. Due to the presence of multiple arc arrangements, the highest number of flow reattachment points was formed. Two phenomena worked here to enhance the heat transfer. Firstly, the destruction of the laminar sublayer due to the flow stream and secondly, the generation, propagation and mixing of accelerating secondary flow with the primary flow. The

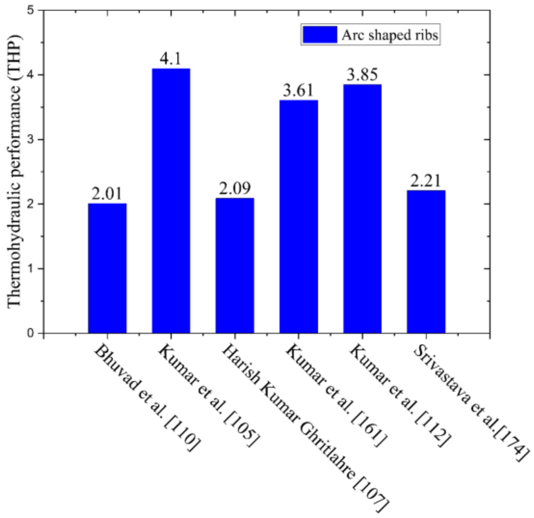

Fig. 71. Variation in THP of SAH based on various arc-shaped roughness.

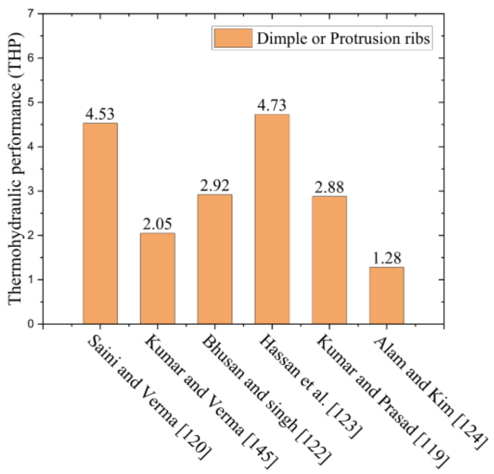

Fig. 72. Variation in THP of SAH based on various dimple or protrusion roughness.

secondary flow generated due to the dimple shape of ribs compels the less heated portion of air to get mixed with the primary highly heated air under the absorber plate, and then propagates to the trailing edge with much higher temperature. These two streams enhanced the destruction of the laminar sublayer, ultimately promoting higher heat transfer between air and the absorber.

Figure 73 shows the comparison among all reported V-shaped ribs roughened SAHs, in which Kumar et al. [117] obtained the maximum THP value of 3.64. They developed an experimental setup of SAH using multiple V-shaped ribs with gaps. The absorber plate was single-sided roughened with varying pitch that played a vital role in enhancing heat transfer, ensuring availability of lesser or greater number of reattachment points. The optimum pitch obtained was 10, at which the highest number of available reattachment points was observed, and fewer reattachment points were observed below and above this value, yielding the highest heat transfer and the lowest heat transfer, respectively.

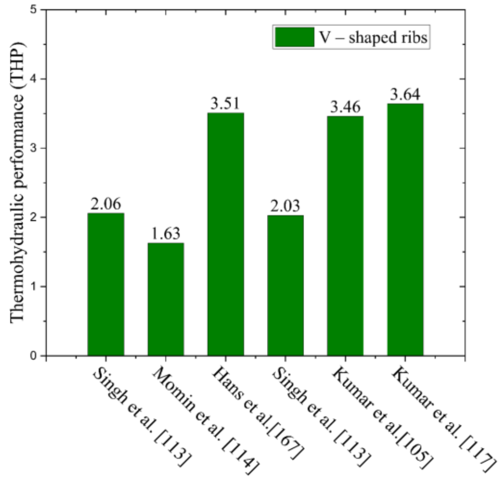

Fig. 73. Variation in THP of SAH based on various V-shaped rib roughness.

Figure 74 illustrates the THP results from various investigations on SAHs with W-shaped roughness. Thakur and Thakur [127] developed the SAH model using roughness elements in the form of W-shaped ribs with symmetrical gaps along with the staggered ribs, and found that the maximum value of THP was 3.24. The plot shows that as the Reynolds number increases, larger gaps lead to a reduction in heat transfer, possibly because more extensive gaps allow a larger part of the flow to pass without going over the ribs. Moreover, the friction factor decreases for the full arrangement values due to the weakening of the laminar sublayer. The quality of secondary stream vortices close to the shorter W-shaped rib sections of roughness design is influenced by increasing the number of gaps on every appendage of the rib geometry. As the number of gaps increases, the friction factor values decrease, which might be due to the overwhelming effect of debilitating secondary flow vortices. The Nusselt number values go on increasing due to the interaction of incoming flow from gaps to cause interruption to the flow between the two adjacent ribs. The greatest improvement in Nusselt number was

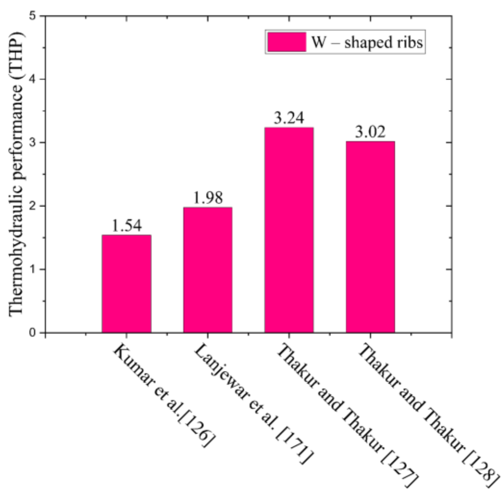

Fig. 74. Variation in THP of SAH based on various W-shaped rib roughness.

at the relative staggered pitch (p/P) equal to 0.65, which corresponds to the situation of a redevelopment of the boundary layer following the reattachment of the stream. The plot also shows a variety of friction variables with Reynolds number for relative staggered pitch. The most extreme estimate of friction was found at p/P = 0.75, and the least at p/P = 0.65. A staggered rib enables the stream to mix with the incoming flow from gaps to create more disturbances in the flow between two adjacent ribs, which leads to an increase in friction. In the case of low friction values, the cause was attributed to the flow separation and reattachment. The most extreme heat exchange credited to w/e = 4.5 might be the result of reattachment of the primary stream and breaking of the redeveloping boundary layer. The low value of the friction factor at w/e = 4.5 might be credited to the dissipation of the approaching stream from gaps, while in the case of w/e = 6, redirections of the primary stream happen towards the trailing edge of the multigap staggered W-shaped rib roughness.

Among all reported inclined baffles roughened SAHs, Parsa et al. [140] obtained the maximum THP factor of 3.28, as depicted in Fig. 75. They used novel staggered cuboid baffles as roughness elements for the development of the SAH setup. The cuboid baffles under the absorber plate increase the heat transfer. They also increase the frictional resistance to the flow, which increases the requirement of pumping power. The cuboid baffles are more effective at lower Reynolds numbers compared to higher Reynolds numbers due to the nature of heat transfer that decreases with an increase in Reynolds number. Various cuboid baffle arrangements were employed under that study, but the most effective were ‘I’, ‘T’ and ‘L’ shaped configurations, which yielded the highest THP. The rise in THP indicated higher heat transfer and nominal increment in friction factor, due to the additional secondary flow generation by baffles and thereby, better mixing and turbulence created under the absorber plate.

The maximum THP obtained amongst the SAHs modified with non-uniform ribs, as reported under this review work, was 2.66. The model, which exhibited the maximum THP, was built

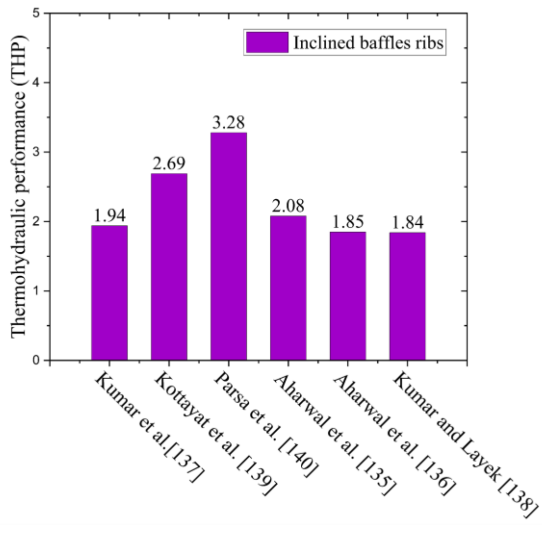

Fig. 75. Variation in THP of SAH based on various inclined baffles.

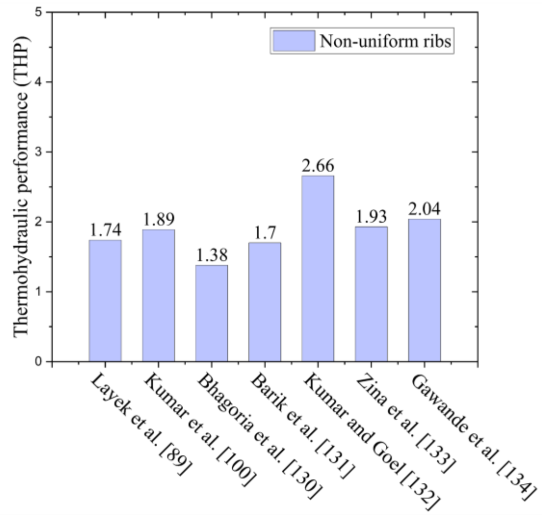

Fig. 76. Variation in THP of SAH based on various non-uniform rib roughness.

by Kumar and Goel [132], as shown in Fig. 76. The experimental setup developed by them had five types of rib roughness, such as circular, semi-circular, square, triangular and rectangular, in a triangular fluid passage as the test section. These ribs were employed to break the laminar sublayer to yield more mixing of fluid near the absorber wall, thereby advancing heat transfer. These ribs generated primary, as well as secondary flow due to their geometrical shape. The microlevel view indicated that ribs created various reattachment points between two successive ribs. The multiple reattachments of the fluid stream cause flow separation and attachment of the flow at the upstream and downstream sides. These phenomena introduce local turbulence under the absorber plate, which ensures THP as high as 2.66, as was demonstrated by the authors in this experimental study.

Within the group of other rib geometries reported here in this review work, the maximum THP was 3.66, which was obtained by Yadav and Saini [149]. They developed SAH based on impinging jet to numerically investigate heat transfer behaviour of a solar air heater. Nusselt number was increased initially with an increase in the jet height, and it started to decline beyond jet height ratio (H_j/D_h) of 0.216. It was due to crossflow of air to the upward direction through the jet height that causes back pressure with the increasing height of jet and velocity inside the jets. The maximum TPH found with these ribs was because of the interference between jet was minimised with an increment in the jet height. The detailed comparison of THP values for other roughness geometries reported is presented in Fig. 77.

According to the comprehensive comparison of optimum SAH in every type of SAH considered in the present review paper (Table 9), the maximum THP was reported by Hassan et al. [123], who used dimples or protrusions as roughness elements for roughened SAH (Fig. 78). The authors introduced modified SAH using dimple ribs of multiple arc arrangements. They led to the highest heat transfer due to availability of maximum reattachments point, destruction of laminar sublayer because of the presence of arc array and two-way flow pattern, such as primary – secondary flow stream.

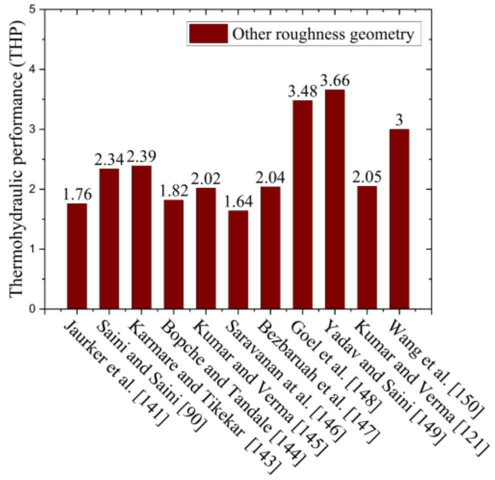

Fig. 77. Variation in THP of SAH based on various other roughness geometries.

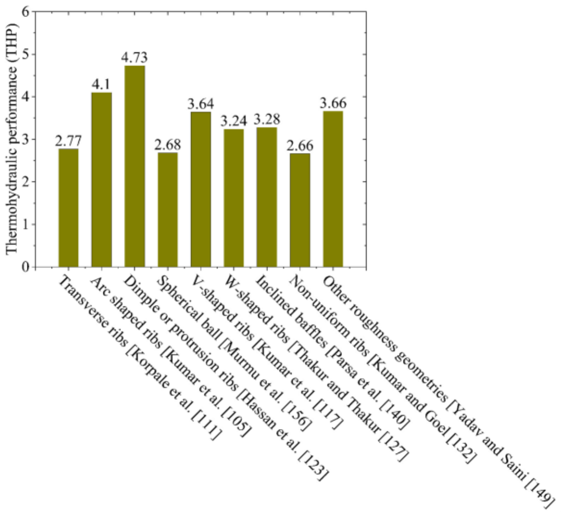

Fig. 78. Optimal THP of SAH based on various rib roughness.

12. Research gaps for future works

Based on the extensive literature review, the following observations were found for future work. These recommendations would be very beneficial for those who are working in the field of solar air heater performance improvements, especially on roughened solar air heaters:

- Very limited work involving gap and multiple gaps of roughness geometry over the absorber plate of SAH has been reported to date. There is a very significant scope to study various thermal performance enhancements in transverse wire ribs with a gap and with multiple gaps.
- Numerous studies have been conducted on plate roughness (absorber plate) to improve the thermal and thermo-hydraulic performance of solar air heaters and heat exchangers. However, there is room for and a need for research on the effect of roughness geometry on flat plates with and without reflectors (on the left and right sides of the duct walls).
- There have been numerical studies conducted separately, such as CFD and ANN techniques, but no combined comparative studies containing various well-established numerical approaches or open source-based tools, such as CFD, ANN, Taguchi method, surface volume methods, or OpenFOAM, on the specific new novel roughness geometry over the flat surface of the absorber in solar air heaters have been reported yet.
- So far, only a few studies been undertaken to investigate the effect of spherical ball-based artificial roughness in SAH. Various setup configurations, such as transverse shape, W-shape, V-shape, with and without gaps, can be used using this type of artificial roughness in SAH.
- There is also the possibility of observing the effect of coating and nanocoating, since nanoparticle change the roughness over the flat plate (absorber plate). Nanocoating may be applied on many types of roughness to improve the thermal performance of SAHs.
- There have been relatively few works documented on three-sided roughness for effective SAH. There is scope and potential to expand the work done on one-side roughness (bottom plate/absorber plate) geometry to three-side roughness geometry in the SAH duct for improved thermal and thermo-hydraulic performance.
- Various studies on SAH have been conducted utilising various duct shapes, but no study has been reported on comparative studies on duct shapes of SAH for the optimum configuration to improve overall performance of SAH.
- A lot of studies have been done on the dimple shape, and dimples with gap has also been examined for effective efficiency of SAH; however, there is no report by any author on continuous dimple roughness geometry. There are other patterns that may be used, including a transverse shape, an S-shape, a C-shape, and so on.
- The angle of attack has a substantial impact on the performance evaluation of SAH. This may be adjusted by switching the absorber plate’s side (upstream/downstream). Various studies have been published in this respect for the performance assessment of SAH, especially as an arc with gap, i.e. apex-down roughness geometry, but there is potential to employ apex-up with gap and multiple gaps for an optimum thermal performance of SAH.
- There have been very few works done employing a combination of different roughness geometries. Mixed roughness geometries can be applied here, such as dimple continuous and discontinuous, transverse wire ribs and arc-shaped ribs, apex up and apex down arrangement in W-shaped, C-shaped and S-shaped roughness geometries.

Table 9. Optimal thermo-hydraulic performance of solar air heaters based on different artificial roughness.

Authors	Type of artificial roughness utilised	Thermo-hydraulic performance
Hassan et al. [123]	Dimple or protrusion ribs	4.73
Kumar et al. [105]	Discrete multi arc-shaped ribs	4.10
Kumar et al. [112]	Discrete multiple arc-shaped ribs	3.85
Yadav and Saini [149]	Impinging jet	3.66
Kumar et al. [161]	Innovatively arranged arcs (combination of alternatively arranged forward and backward facing arced-ribs)	3.61
Goel et al. [148]	Hemispherical cavities	3.48
Parsa et al. [140]	Staggered cuboid baffles	3.28
Korpale et al. [111]	Rectangular section ribs	2.77
Kottayat et al. [139]	Discrete multiple inclined baffle	2.69
Kumar and Goel [132]	Semi-circular, circular, triangular, square, rectangular ribs	2.66
Karmare and Tikekar [143]	Metal grit ribs	2.39
Saini and Saini [90]	Expanded metal mesh	2.34
Srivastava et al. [174]	V-shaped ribs with gap	2.21
Ghritlahre [107]	Arc-shaped wire ribs with apex upstream	2.09
Sharma et al. [94]	Transverse, inclined transverse, dimple, inclined dimple, arc and sine wave ribs	2.05
Kumar and Verma [145]	Sinusoidal rib	2.05
Gawande et al. [134]	20° chamfered rib	2.05
Bezbaruah et al. [147]	Staggered conical vortex generators	2.04
Gawande et al. [134]	Right-angle triangular rib	2.04
Kumar and Verma [145]	Sinusoidal protrusion rib	2.02
Bhuvad, Azad and Lanjewar [110]	Apex-up discrete arc ribs	2.01
Lanjewar et al. [171]	W-shaped ribs of different orientations	1.98
Kumar et al. [137]	Angled perforated baffles	1.94
Zina et al. [133]	Triangular ribs with semi-circular nooks	1.93
Gawande et al. [134]	Reverse l-shaped rib	1.90
Kumar et al. [153]	Rectangular rib roughened	1.89
Mahanand and Senapati [95]	Transverse inverted-t shaped rib	1.86
Gawande et al. [96]	Combined square and equilateral triangular ribs as	1.86
Bopche and Tandale [144]	Inverted u shape rib	1.82
Prasad and Saini [86]	Transverse wire	1.78
Jaurker et al. [141]	Rib groove	1.76
Barik et al. [131]	T-rib, left arm inclined T-rib, right arm inclined T-rib, Y-rib, concave and convex T-ribs	1.70
Kumar et al. [152]	Semicircular rib	1.70
Saravanan at al. [146]	Staggered C-shape finned absorber plate	1.64
Ghritlahre [107]	Apex downstream	1.59
Srivastava et al. [108]	Arc-shaped ribs with gap	1.50
Singh et al. [93]	Uniform/non-uniform square-wave profile transverse roughness rib	1.49
Kumar et al. [99]	Square rib	1.44
Bhagoria et al. [130]	Transverse wedge-shaped ribs	1.38

13. Conclusions

This paper aims to analyse the diverse experimental studies conducted on ducts and solar air heaters incorporating artificial roughness rib elements, focusing on their impact on heat transfer and friction factor characteristics. Various elements, materials, and geometric parameters have been employed to assess the thermo-hydraulic performance of the ducts and solar air heaters. Drawing from a thorough literature review, the following conclusions can be derived:

1) An evident enhancement in heat transfer is observed in solar air heaters when the flow is subjected to surface roughening, leading to increased friction. Nevertheless, it is important to note that various researchers have reported varying increments in heat transfer and friction factor values for each specific rib geometry employed.
2) A comparison of the investigations conducted by different researchers, in terms of the Nusselt number and friction factor increments compared to a smooth duct, showed that the highest values, of 7.61 for the Nusselt number and 6.48 for the friction factor, were obtained utilising artificial roughness elements in the form of discrete multi-arc ribs. It also indicated that an increase in heat transfer is accompanied by a simultaneous increase in the friction factor.
3) Among the various rib geometries studied in experiments thus far, it has been observed that protrusions or dimple-shaped elements tend to exhibit the lowest friction factor values compared to other rib elements. Simultaneously, these protrusions or dimple-shaped elements also contribute to an increase in the Nusselt number at the optimum parameter settings. Therefore, in terms of achieving a balance between heat transfer enhancement and minimising friction, protrusions or dimple-shaped rib elements appear to be more favourable compared to other alternatives.
4) The experiments conducted on solar air heaters with various rib geometries and the set of corresponding parameter values identified the specific parameter values for each rib element that yield the best overall performance.
5) The developed correlations for the Nusselt number and friction factor based on the range of parameters considered in the experiments provide valuable insights for designers and researchers. These correlations, along with the heat transfer values, can assist beginners in this field by providing an understanding of the different geometries used and the impact of each parameter on heat transfer and flow characteristics. This knowledge enables designers and investigators to work towards identifying the optimum values for enhanced performance in their respective applications.
6) Dimple protrusion ribs have proven to be the most suitable rib elements in terms of thermo-hydraulic performance parameters. Extensive research and experimentation have demonstrated their effectiveness in enhancing heat transfer, while simultaneously minimising friction. The unique characteristics of dimple protrusion ribs, such as their roughness profile and surface texture, contribute to improved heat transfer coefficients and efficient fluid flow. Thus, in terms of overall thermo-hydraulic performance, dimple protrusion ribs have emerged as a favourable choice among rib elements.
7) In the study conducted, it has been observed that the friction factor decreases as the Reynolds number increases for all roughness geometries considered. Among the different roughness geometries, the one of four ribbed walls resulted in the highest frictional losses. This can be attributed to their large frontal area, which contributes to increased form drag. On the other hand, circular protrusions arranged in an arc fashion exhibit the lowest values of the friction factor. This may be due to the discrete arrangement of the circular protrusions, which results in relatively lower form drag, as well as skin drag. In fact, the skin drag for circular protrusions can be even lower than that of rib roughness, leading to their favourable performance in terms of frictional losses.

Acknowledgements

The authors would like to thank Chhattisgarh Swami Vivekanand Technical University, Bhilai, Chhattisgarh, 491107, India, and Chhattisgarh Institute of Technology (CGIT) Jagdalpur, Bastar, Chhattisgarh, India, as well as the University Teaching Department of Engineering for their continuous support and encouragement in preparing this research article.

References

[1] Kumar, A., Saini, R.P., & Saini, J S. (2014). A review of thermo-hydraulic performance of artificially roughened solar air heaters. *Renewable and Sustainable Energy Reviews*, 37, 100–122. doi: 10.1016/j.rser.2014.04.063

[2] Prakash, C., & Saini, R.P. (2019). Use of artificial roughness for performance enhancement of solar air heaters—a review. *International Journal of Green Energy*, 16(7), 549–569. doi: 10.1080/ 15435075.2019.1598418

[3] Mohammadi, K., & Sabzpooshani, M. (2013). Comprehensive performance evaluation and parametric studies of single pass solar air heater with fins and baffles attached over the absorber plate. *Energy*, 57, 741–750. doi: 10.1016/j.energy.2013.05.016

[4] Chamoli, S., Chauhan, R., Thakur, N.S., & Saini, J.S. (2012). A review of the performance of double pass solar air heater. *Renewable and Sustainable Energy Reviews*, 16(1), 481–492. doi: 10.1016/j.rser.2011.08.012

[5] Khanlari, A., Sözen, A., Afshari, F., Tuncer, A.D., Ağbulut, Ü., & Aytaç Yılmaz, Z. (2022). Numerical and experimental analysis of parallel-pass forced convection solar air heating wall with different plenum and absorber configurations. *International Journal of Numerical Methods for Heat & Fluid Flow*, 32(3), 978–1001. doi: 10.1108/ HFF-03-2021-0160

[6] Sahu, M.K., Sharma, M., Matheswaran, M.M., & Maitra, K. (2019). On the Use of Longitudinal Fins to Enhance the Performance in Rectangular Duct of Solar Air Heaters – A Review. *Journal of Solar Energy Engineering*, 141(3), 030801. doi: 10.1115/1.4042827

[7] Ghritlahre, H.K. (2019). Performance evaluation of solar air heating systems using artificial neural network. PhD thesis, NIT Jamshedpur.

[8] Ghritlahre, H.K., & Prasad, R.K. (2018). Prediction of heat transfer of two different types of roughened solar air heater using Artificial Neural Network technique. *Thermal Science and Engineering Progress*, 8, 145–153. doi: 10.1016/j.tsep.2018.08.014

[9] Kumar, V. (2019). Nusselt number and friction factor correlations of three sides concave dimple roughened solar air heater. *Renewable Energy*, 135, 355–377. doi: 10.1016/j.renene.2018.12.002

[10] Kumar, R., Nadda, R., Rana, A., Chauhan, R., & Chandel, S.S. (2022). Impact of artificial roughness variation on heat transfer and friction characteristics of solar air heating system. *Alexandria Engineering Journal*, 61(1), 481–491. doi: 10.1016/j.aej.2021.06.031

[11] Kumar, R., Nadda, R., Rana, A., Chauhan, R., & Chandel, S.S. (2020). Performance investigation of a solar thermal collector provided with air jets impingement on multi V-shaped protrusion ribs absorber plate. *Heat and Mass Transfer*, 56(3), 913–930. doi: 10.1007/s00231-019-02755-2

[12] Kumar, K., Prajapati, D.R., & Samir, S. (2017). Heat transfer and friction factor correlations development for solar air heater duct artificially roughened with 'S' shape ribs. *Experimental Thermal and Fluid Science*, 82, 249–261. doi: 10.1016/j.expthermflusci.2016.11.012

[13] Abdulmejeed, A.E.A., Tuncer, A.D., Khanlari, A., & Gungor, A. (2024). Investigation of combined parallel and triple-pass v-corrugated solar air heater: A numerical and experimental study. *Process Safety and Environmental Protection*, 185, 1385–1398. doi: 10.1016/j.psep.2024.03.107

[14] Khanlari, A., Tuncer, A.D., Afshari, F., & Sözen, A. (2023). Utilization of recyclable aluminum cans as fins in a vertical solar air heating system: An experimental and numerical study. *Journal of Building Engineering*, 63, 105446. doi: 10.1016/j.jobe.2022.105446

[15] Khanlari, A., Aytaç, İ., Tuncer, A.D., Variyenli, H.İ., & Şahin, H.N. (2024). Improving the performance of a PCM integrated solar air collector by adding porous fins over the bottom side of the absorber: A transient CFD study. *Journal of Energy Storage*, 90, 111847. doi: 10.1016/j.est.2024.111847

[16] Sharma, S.P., Saini, J.S., & Varma, H.K. (1991). Thermal performance of packed-bed solar air heaters. *Solar Energy*, 47(2), 59–67. doi: 10.1016/0038-092X(91)90035-U

[17] Ghritlahre, H.K., & Prasad, R.K. (2018). Investigation of thermal performance of unidirectional flow porous bed solar air heater using MLP, GRNN, and RBF models of ANN technique. *Thermal Science and Engineering Progress*, 6, 226–235. doi: 10.1016/j.tsep.2018.04.006

[18] Varshney, L., & Saini, J.S. (1998). Heat transfer and friction factor correlations for rectangular solar air heater duct packed with wire mesh screen matrices. *Solar Energy*, 62(4), 255–262. doi: 10.1016/S0038-092X(98)00017-6

[19] Choudhury, C., & Garg, H.P. (1991). Design analysis of corrugated and flat plate solar air heaters. *Renewable Energy*, 1(5-6), 595–607. doi: 10.1016/0960-1481(91)90003-8

[20] Priyam, A., & Chand, P. (2016). Thermal and thermohydraulic performance of wavy finned absorber solar air heater. *Solar Energy*, 130, 250–259. doi: 10.1016/j.solener.2016.02.030

[21] Afshari, F., Sözen, A., Khanlari, A., Tuncer, A.D., & Şirin, C. (2020). Effect of turbulator modifications on the thermal performance of cost-effective alternative solar air heater. *Renewable Energy*, 158, 297–310. doi:10.1016/j.renene.2020.05.148

[22] Khanlari, A., Sözen, A., Tuncer, A.D., Afshari, F., Gürbüz, E.Y., & Bilge, Y. C. (2021). Numerical and experimental analysis of longitudinal tubular solar air heaters made from plastic and metal waste materials. *Heat Transfer Research*, 52(10), 19–45. doi: 10.1615/HeatTransRes.2021038204

[23] Varun, Saini, R.P., & Singal, S.K. (2007). A review on roughness geometry used in solar air heaters. *Solar Energy*, 81(11), 1340–1350. doi: 10.1016/j.solener.2007.01.017

[24] Gupta, M.K., & Kaushik, S.C. (2009). Performance evaluation of solar air heater for various artificial roughness geometries based on energy, effective and exergy efficiencies. *Renewable Energy*, 34(3), 465–476. doi: 10.1016/j.renene.2008.06.001

[25] Hans, V.S., Saini, R.P., & Saini, J.S. (2009). Performance of artificially roughened solar air heaters—A review. *Renewable and Sustainable Energy Reviews*, 13(8), 1854–1869. doi: 10.1016/j.rser.2009.01.030

[26] Chamoli, S., Thakur, N.S., & Saini, J.S. (2012). A review of turbulence promoters used in solar thermal systems. *Renewable and Sustainable Energy Reviews*, 16(5), 3154–3175. doi: 10.1016/j.rser.2012.01.021

[27] El-Sebaii, A.A., & Shalaby, S.M. (2012). Solar drying of agricultural products: A review. *Renewable and Sustainable Energy Reviews*, 16(1), 37–43. doi: 10.1016/j.rser.2011.07.134

[28] Yadav, A.S., & Bhagoria, J.L. (2013). Heat transfer and fluid flow analysis of solar air heater: A review of CFD approach. *Renewable and Sustainable Energy Reviews*, 23, 60–79. doi: 10.1016/j.rser.2013.02.035

[29] Yadav, A.S., & Thapak, M.K. (2014). Artificially roughened solar air heater: Experimental investigations. *Renewable and Sustainable Energy Reviews*, 36, 370–411. doi: 10.1016/j.rser.2014.04.077

[30] Gawande, V.B., Dhoble, A.S., & Zodpe, D.B. (2014). Effect of roughness geometries on heat transfer enhancement in solar thermal systems − A review. *Renewable and Sustainable Energy Reviews*, 32, 347–378. doi: 10.1016/j.rser.2014.01.024

[31] Alam, T., Saini, R.P., & Saini, J.S. (2014). Heat and flow characteristics of air heater ducts provided with turbulators − A review. *Renewable and Sustainable Energy Reviews*, 31, 289–304. doi: 10.1016/j.rser.2013.11.050

[32] Alam, T., Saini, R.P., & Saini, J.S. (2014). Use of turbulators for heat transfer augmentation in an air duct − A review. *Renewable Energy*, 62, 689–715. doi: 10.1016/j.renene.2013.08.024

[33] Mund, C., Rathore, S.K., & Sahoo, R.K. (2021). A review of solar air collectors about various modifications for performance enhancement. *Solar Energy*, 228, 140–167. doi: 10.1016/j.solener.2021.08.040

[34] Patil, A.K. (2015). Heat transfer mechanism and energy efficiency of artificially roughened solar air heaters − A review. *Renewable and Sustainable Energy Reviews*, 42, 681–689. doi: 10.1016/j.rser.2014.10.063

[35] Sharma, S.K., & Kalamkar, V.R. (2015). Thermo-hydraulic performance analysis of solar air heaters having artificial roughness–A review. *Renewable and Sustainable Energy Reviews*, 41, 413–435. doi: 10.1016/j.rser.2014.08.051

[36] Kumar, A., & Kim, M.H. (2015). Convective heat transfer enhancement in solar air channels. *Applied Thermal Engineering*, 89, 239–261. doi: 10.1016/j.applthermaleng.2015.06.015

[37] Lanjewar, A.M., Bhagoria, J.L., & Agrawal, M.K. (2015). Review of development of artificial roughness in solar air heater and performance evaluation of different orientations for double arc rib roughness. *Renewable and Sustainable Energy Reviews*, 43, 1214–1223. doi: 10.1016/j.rser.2014.11.081

[38] Sheikholeslami, M., Gorji-Bandpy, M., & Ganji, D.D. (2015). Review of heat transfer enhancement methods: Focus on passive methods using swirl flow devices. *Renewable and Sustainable Energy Reviews*, 49, 444–469. doi: 10.1016/j.rser.2015.04.113

[39] Singh, S., Chander, S., & Saini, J.S. (2015). Thermo-hydraulic performance due to relative roughness pitch in V-down rib with

gap in solar air heater duct – Comparison with similar rib roughness geometries. *Renewable and Sustainable Energy Reviews*, 43, 1159–1166. doi: 10.1016/j.rser.2014.11.087

[40] Saxena, A., Varun, & El-Sebaii, A.A. (2015). A thermodynamic review of solar air heaters. *Renewable and Sustainable Energy Reviews*, 43, 863–890. doi: 10.1016/j.rser.2014.11.059

[41] Kumar, R., Varun, & Kumar, A. (2016). Thermal and fluid dynamic characteristics of flow through triangular cross-sectional duct: A review. *Renewable and Sustainable Energy Reviews*, 61, 123–140. doi: 10.1016/j.rser.2016.03.011

[42] Aravindh, M.A., & Sreekumar, A. (2016). Efficiency enhancement in solar air heaters by modification of absorber plate-a review. *International Journal of Green Energy*, 13(12), 1209–1223. doi: 10.1080/15435075.2016.1183207

[43] Sharma, S.K., & Kalamkar, V.R. (2016). Computational Fluid Dynamics approach in thermo-hydraulic analysis of flow in ducts with rib roughened walls – A review. *Renewable and Sustainable Energy Reviews*, 55, 756–788. doi: 10.1016/j.rser.2015.10.160

[44] Kumar, A., & Kim, M.H. (2016). Thermohydraulic performance of rectangular ducts with different multiple V-rib roughness shapes: A comprehensive review and comparative study. *Renewable and Sustainable Energy Reviews*, 54, 635–652. doi: 10.1016/j.rser.2015.10.030

[45] Ravi, R.K., & Saini, R.P. (2016). A review on different techniques used for performance enhancement of double pass solar air heaters. *Renewable and Sustainable Energy Reviews*, 56, 941–952. doi: 10.1016/j.rser.2015.12.004

[46] Gawande, V.B., Dhoble, A.S., Zodpe, D.B., & Chamoli, S. (2016). A review of CFD methodology used in literature for predicting thermo-hydraulic performance of a roughened solar air heater. *Renewable and Sustainable Energy Reviews*, 54, 550–605. doi: 10.1016/j.rser.2015.10.025

[47] Yadav, A.S., & Thapak, M.K. (2016). Artificially roughened solar air heater: A comparative study. *International Journal of Green Energy*, 13(2), 143–172. doi: 10.1080/15435075.2014.917419

[48] Kabeel, A.E., Hamed, M.H., Omara, Z.M., & Kandeal, A.W. (2017). Solar air heaters: Design configurations, improvement methods and applications – A detailed review. *Renewable and Sustainable Energy Reviews*, 70, 1189–1206. doi: 10.1016/j.rser.2016.12.021

[49] Alam, T., & Kim, M.H. (2017). A critical review on artificial roughness provided in rectangular solar air heater duct. *Renewable and Sustainable Energy Reviews*, 69, 387–400. doi: 10.1016/j.rser.2016.11.192

[50] Singh, I., & Singh, S. (2018). A review of artificial roughness geometries employed in solar air heaters. *Renewable and Sustainable Energy Reviews*, 92, 405–425. doi: 10.1016/j.rser.2018.04.108

[51] Singh Bisht, V., Patil, A.K., & Gupta, A. (2018). Review and performance evaluation of roughened solar air heaters. *Renewable and Sustainable Energy Reviews*, 81, 954–977. doi: 10.1016/j.rser.2017.08.036

[52] Kumar, R., Kumar, A., Chauhan, R., & Maithani, R. (2018). Comparative study of effect of various blockage arrangements on thermal hydraulic performance in a roughened air passage. *Renewable and Sustainable Energy Reviews*, 81, 447–463. doi: 10.1016/j.rser.2017.08.023

[53] Chauhan, R., Singh, T., Thakur, N.S., Kumar, N., Kumar, R., & Kumar, A. (2018). Heat transfer augmentation in solar thermal collectors using impinging air jets: A comprehensive review. *Renewable and Sustainable Energy Reviews*, 82, 3179–3190. doi: 10.1016/j.rser.2017.10.025

[54] Elsheikh, A.H., Sharshir, S.W., Abd Elaziz, M., Kabeel, A.E., Guilan, W., & Haiou, Z. (2019). Modeling of solar energy systems using artificial neural network: A comprehensive review. *Solar Energy*, 180, 622–639. doi: 10.1016/j.solener.2019.01.037

[55] Hu, J., & Zhang, G. (2019). Performance improvement of solar air collector based on airflow reorganization: A review. *Applied Thermal Engineering*, 155, 592–611. doi: 10.1016/j.applthermaleng.2019.04.021

[56] Chhaparwal, G.K., Srivastava, A., & Dayal, R. (2019). Artificial repeated-rib roughness in a solar air heater – A review. *Solar Energy*, 193, 329–359. doi: 10.1016/j.solener.2019.10.011

[57] Ghritlahre, H.K., & Sahu, P.K. (2020). A comprehensive review on energy and exergy analysis of solar air heaters. *Archives of Thermodynamics*, 41(3), 183–222. doi: 10.24425/ather.2020.134577

[58] Vengadesan, E., & Senthil, R. (2020). A review on recent developments in thermal performance enhancement methods of flat plate solar air collector. *Renewable and Sustainable Energy Reviews*, 134, 110315. doi: 10.1016/j.rser.2020.110315

[59] Yadav, K.D., & Prasad, R.K. (2020). Performance analysis of parallel flow flat plate solar air heater having arc shaped wire roughened absorber plate. *Renewable Energy Focus*, 32, 23–44. doi: 10.1016/j.ref.2019.10.002

[60] Arunkumar, H.S., Karanth, K.V., & Kumar, S. (2020). Review on the design modifications of a solar air heater for improvement in the thermal performance. *Sustainable Energy Technologies and Assessments*, 39, 100685. doi: 10.1016/j.seta.2020.100685

[61] Nidhul, K., Yadav, A.K., Anish, S., & Kumar, S. (2021). Critical review of ribbed solar air heater and performance evaluation of various V-rib configuration. *Renewable and Sustainable Energy Reviews*, 142, 110871. doi: 10.1016/j.rser.2021.110871

[62] Chamarthi, S., & Singh, S. (2021). A comprehensive review of experimental investigation procedures and thermal performance enhancement techniques of solar air heaters. *International Journal of Energy Research*, 45(4), 5098–5164. doi: 10.1002/er.6255

[63] Ghritlahre, H.K., Chandrakar, P., & Ahmad, A. (2021). A Comprehensive Review on Performance Prediction of Solar Air Heaters Using Artificial Neural Network. *Annals of Data Science*, 8(3), 547–570. doi: 10.1007/s40745-019-00236-1

[64] Ghritlahre, H.K., Verma, M., Parihar, J.S., Mondloe, D.S., & Agrawal, S. (2022). A detailed review of various types of solar air heaters performance. *Solar Energy*, 237, 173–195. doi: 10.1016/j.solener.2022.03.042

[65] Rice, D. (1867). *Quoted in Solar Energy Research by Daniels and Duffie*. US Patent No. 68 459.

[66] Morse, E.S. (1881). *Warming and ventilating apartments by Sun's rays*. US Patent No. 246 626.

[67] Cabot, G.L. (1938). *Solar 1: The MIT Solar House*.

[68] Telkes, M., & Raymond, E. (1949). Storing solar heat in chemicals. *Heating and Ventilating*, 46, 79–86.

[69] Bliss Jr, R.W. (1955). Design and performance of nation's only fully solar-heated house. *Air Conditioning, Heating, Ventilating*, 52(10), 68–73.

[70] Löf, G.O.G. (1954). *Solar heating apparatus and method*. US Patent No. 2 680 565.

[71] Doherty, P. (2007). *Solar air heater*. US Patent No. US2007/0199562A1.

[72] Vachon, C. (2010). *Perforated transparent glazing for heat recovery and solar air heating*. US Patent No. US2010/0000520A1.

[73] MacKay, K.H. (2011). *Solar air heating device*. US Patent No. US2011/0180058A1.

[74] Ryan, T.D. (2011). *Curved transpired solar air heater and conduit*. US Patent No. US2011/0120449A1.

[75] Wu, H. (2013). *Solar energy air heater*. Chinese Patent No. CN202973585U.

[76] Goldstein, L., & Sparrow, E.M. (1976). Experiments on the Transfer Characteristics of a Corrugated Fin and Tube Heat Exchanger Configuration. *Journal of Heat Transfer*, 98(1), 26–34. doi: 10.1115/1.3450464

[77] Okamoto, S., Seo, S., Nakaso, K., & Kawai, I. (1993). Turbulent shear flow and heat transfer over the repeated two-dimensional square ribs on ground plane. *ASME Journal of Fluids Engineering*, 115(4), 631–637. doi: 10.1115/1.2910191

[78] Nikuradse, J. (1950). Laws of flow in rough pipes. *VDI-Forschungsheft*, 361.

[79] Nunner, W. (1958). *Heat transfer and pressure drop in rough tubes*. Atomic Energy Research Establishment, AERE Lib/Trans 786.

[80] Dipprey, D.F., & Sabersky, R.H. (1963). Heat and momentum transfer in smooth and rough tubes at various Prandtl numbers. *International Journal of Heat and Mass Transfer*, 6(5), 329–353. doi: 10.1016/0017-9310(63)90120-2

[81] Lewis, M.J. (1975). Optimising the thermohydraulic performance of rough surfaces. *International Journal of Heat and Mass Transfer*, 18(11), 1243–1248. doi: 10.1016/0017-9310(75)90232-X

[82] Han, J.C. (1984). Heat Transfer and Friction in Channels With Two Opposite Rib-Roughened Walls. *Journal of Heat Transfer*, 106(4), 774–781. doi: 10.1115/1.3246751

[83] Prasad, B.N., & Saini, J.S. (1991). Optimal thermohydraulic performance of artificially roughened solar air heaters. *Solar Energy*, 47(2), 91–96. doi: 10.1016/0038-092X(91)90039-Y

[84] Prasad, B.N., & Saini, J.S. (1988). Effect of artificial roughness on heat transfer and friction factor in a solar air heater. *Solar Energy*, 41(6), 555–560. doi: 10.1016/0038-092X(88)90058-8

[85] Sethi, M., Varun, & Thakur, N.S. (2012). Correlations for solar air heater duct with dimpled shape roughness elements on absorber plate. *Solar Energy*, 86(9), 2852–2861. doi: 10.1016/j.solener.2012.06.024

[86] Prasad, B.N., & Saini, J.S. (1990). Enhancement of solar air heater performance using artificial roughness. In *Proceedings of the 1st World Renewable Energy Congress* (pp. 1067–1071), 23–28 September, Reading, UK.

[87] Gupta, D. (1993). *Investigations on fluid flow and heat transfer in solar air heaters with roughened absorbers*. PhD thesis, University of Roorkee, India.

[88] Karwa, R. (2003). Experimental studies of augmented heat transfer and friction in asymmetrically heated rectangular ducts with ribs on the heated wall in transverse, inclined, v-continuous and v-discrete pattern. *International Communications in Heat and Mass Transfer*, 30(2), 241–250. doi: 10.1016/S0735-1933(03)00035-6

[89] Layek, A., Saini, J.S., & Solanki, S.C. (2009). Effect of chamfering on heat transfer and friction characteristics of solar air heater having absorber plate roughened with compound turbulators. *Renewable Energy*, 34(5), 1292–1298. doi: 10.1016/j.renene.2008.09.016

[90] Saini, R.P., & Saini, J.S. (1997). Heat transfer and friction factor correlations for artificially roughened ducts with expanded metal mesh as roughness element. *International Journal of Heat and Mass Transfer*, 40(4), 973–986. doi: 10.1016/0017-9310(96)00019-1

[91] Verma, S., & Prasad, B. (2000). Investigation for the optimal thermohydraulic performance of artificially roughened solar air heaters. *Renewable Energy*, 20(1), 19–36. doi: 10.1016/S0960-1481(99)00081-6

[92] Singh, I., Vardhan, S., Singh, S., & Singh, A. (2019). Experimental and CFD analysis of solar air heater duct roughened with multiple broken transverse ribs: A comparative study. *Solar Energy*, 188, 519–532. doi: 10.1016/j.solener.2019.06.022

[93] Singh, I., Singh, S., & Vardhan, S. (2021). Heat transfer and fluid flow characteristics of solar air heater duct with non-uniform ribs. *Journal of Mechanical Science and Technology*, 35(1), 343–350. doi: 10.1007/s12206-020-1234-9

[94] Sharma, S., Das, R.K., & Kulkarni, K. (2021). Computational and experimental assessment of solar air heater roughened with six different baffles. *Case Studies in Thermal Engineering*, 27, 101350. doi: 10.1016/j.csite.2021.101350

[95] Mahanand, Y., & Senapati, J.R. (2020). Thermal enhancement study of a transverse inverted-T shaped ribbed solar air heater. *International Communications in Heat and Mass Transfer*, 119, 104922. doi: 10.1016/j.icheatmasstransfer.2020.104922

[96] Gawande, V.B., Dhoble, A.S., Zodpe, D.B., & Fale, S.G. (2020). Thermal performance evaluation of solar air heater using combined square and equilateral triangular rib roughness. *Australian Journal of Mechanical Engineering*, 18(2), 234–244. doi: 10.1080/14484846.2018.1519986

[97] Kumar, A., Akshayveer, Singh, A.P., & Singh, O.P. (2020). Efficient designs of double-pass curved solar air heaters. *Renewable Energy*, 160, 1105–1118. doi: 10.1016/j.renene.2020.06.115

[98] Kumar, A., & Layek, A. (2019). Nusselt number and fluid flow analysis of solar air heater having transverse circular rib roughness on absorber plate using LCT and computational technique. *Thermal Science and Engineering Progress*, 14, 100398. doi: 10.1016/j.tsep.2019.100398

[99] Kumar, R., Kumar, A., & Goel, V. (2019). Performance improvement and development of correlation for friction factor and heat transfer using computational fluid dynamics for ribbed triangular duct solar air heater. *Renewable Energy*, 131, 788–799. doi: 10.1016/j.renene.2018.07.078

[100] Kumar, R., Goel, V., & Kumar, A. (2018). Investigation of heat transfer augmentation and friction factor in triangular duct solar air heater due to forward facing chamfered rectangular ribs: A CFD based analysis. *Renewable Energy*, 115, 824–835. doi: 10.1016/j.renene.2017.09.010

[101] Kumar, R., Varun, & Kumar, A. (2017). Experimental and Computational Fluid Dynamics Study on Fluid Flow and Heat Transfer in Triangular Passage Solar Air Heater of Different Configurations. *Journal of Solar Energy Engineering*, 139(4), 041003. doi: 10.1115/1.4036775

[102] Saini, S.K., & Saini, R.P. (2008). Development of correlations for Nusselt number and friction factor for solar air heater with roughened duct having arc-shaped wire as artificial roughness. *Solar Energy*, 82(12), 1118–1130. doi: 10.1016/j.solener.2008.05.010

[103] Singh, A.P., Varun, & Siddhartha. (2014). Effect of artificial roughness on heat transfer and friction characteristics having multiple arc shaped roughness element on the absorber plate. *Solar Energy*, 105, 479–493. doi: 10.1016/j.solener.2014.04.007

[104] Sahu, M.K., & Prasad, R.K. (2016). Exergy based performance evaluation of solar air heater with arc-shaped wire roughened absorber plate. *Renewable Energy*, 96, 233–243. doi: 10.1016/j.renene.2016.04.083

[105] Kumar, R., Kumar, S., Nadda, R., Kumar, K., & Goel, V. (2022). Thermo-hydraulic efficiency and correlation development of an indoor designed jet impingement solar thermal collector roughened with discrete multi-arc ribs. *Renewable Energy*, 189, 1259–1277. doi: 10.1016/j.renene.2022.03.037

[106] Yadav, S., Kaushal, M., Varun, & Siddhartha. (2013). Nusselt number and friction factor correlations for solar air heater duct having protrusions as roughness elements on absorber plate. *Ex-*

perimental Thermal and Fluid Science, 44, 34–41. doi: 10.1016/j.expthermflusci.2012.05.011

[107] Ghritlahre, H.K. (2021). Heat transfer and friction factor characteristic investigation of roughened solar air heater using arc-shaped wire rib roughness. *International Journal of Ambient Energy*, 43(1), 1866–1877. doi: 10.1080/01430750.2021.1934115

[108] Srivastava, A., Chhaparwal, G.K., & Sharma, R.K. (2020). Numerical and experimental investigation of different rib roughness in a solar air heater. *Thermal Science and Engineering Progress*, 19, 100576. doi: 10.1016/j.tsep.2020.100576

[109] Gill, R.S., Hans, V.S., Saini, J.S., & Singh, S. (2017). Investigation on performance enhancement due to staggered piece in a broken arc rib roughened solar air heater duct. *Renewable Energy*, 104, 148–162. doi: 10.1016/j.renene.2016.12.002

[110] Bhuvad, S.S., Azad, R., & Lanjewar, A. (2022). Thermal performance analysis of apex-up discrete arc ribs solar air heater-an experimental study. *Renewable Energy*, 185, 403–415. doi: 10.1016/j.renene.2021.12.037

[111] Korpale, V.S., Deshmukh, S.P., Mathpati, C.S., & Dalvi, V.H. (2020). Numerical simulations and optimization of solar air heaters. *Applied Thermal Engineering*, 180, 115744. doi: j.applthermaleng.2020.115744

[112] Kumar, R., Goel, V., Singh, P., Saxena, A., Kashyap, A.S., & Rai, A. (2019). Performance evaluation and optimization of solar assisted air heater with discrete multiple arc shaped ribs. *Journal of Energy Storage*, 26, 100978. doi: 10.1016/j.est.2019.100978

[113] Singh, S., Chander, S., & Saini, J.S. (2011). Heat transfer and friction factor of discrete V-down rib roughened solar air heater ducts. *Journal of Renewable and Sustainable Energy*, 3(1), 013108. doi: 10.1063/1.3558865

[114] Ebrahim Momin, A.-M., Saini, J.S., & Solanki, S.C. (2002). Heat transfer and friction in solar air heater duct with V-shaped rib roughness on absorber plate. International *Journal of Heat and Mass Transfer*, 45(16), 3383–3396. doi: 10.1016/S0017-9310(02)00046-7

[115] Deo, N.S., Chander, S., & Saini, J.S. (2016). Performance analysis of solar air heater duct roughened with multigap V-down ribs combined with staggered ribs. *Renewable Energy*, 91, 484–500. doi: 10.1016/j.renene.2016.01.067

[116] Singh, S., Chander, S., & Saini, J.S. (2011). Heat transfer and friction factor correlations of solar air heater ducts artificially roughened with discrete V-down ribs. *Energy*, 36(8), 5053–5064. doi: 10.1016/j.energy.2011.05.052

[117] Kumar, A., Saini, R.P., & Saini, J.S. (2012). Experimental investigation on heat transfer and fluid flow characteristics of air flow in a rectangular duct with Multi v-shaped rib with gap roughness on the heated plate. *Solar Energy*, 86(6), 1733–1749. doi: 10.1016/j.solener.2012.03.014

[118] Patel, S.S., & Lanjewar, A. (2021). Heat transfer enhancement using additional gap in symmetrical element of V-geometry roughened solar air heater. *Journal of Energy Storage*, 38, 102545. doi: 10.1016/j.est.2021.102545

[119] Kumar, V., & Prasad, L. (2019). Thermal performance investigation of three sides concave dimple roughened solar air heaters. *Solar Energy*, 188, 361–379. doi: 10.1016/j.solener.2019.06.008

[120] Saini, R.P., & Verma, J. (2008). Heat transfer and friction factor correlations for a duct having dimple-shape artificial roughness for solar air heaters. *Energy*, 33(8), 1277–1287. doi: 10.1016/j.energy.2008.02.017

[121] Kumar, S., & Verma, S.K. (2020). Three-dimensional simulation and experimental validation of solar air heater having sinusoidal rib. *Energy Sources, Part A: Recovery, Utilization, and Environmental Effects*, 43(24), 3170–3188. doi: 10.1080/15567036.2020.1818007

[122] Bhushan, B., & Singh, R. (2011). Nusselt number and friction factor correlations for solar air heater duct having artificially roughened absorber plate. *Solar Energy*, 85(5), 1109–1118. doi: 10.1016/j.solener.2011.03.007

[123] Hassan, A.K., Hasan, M.M., & Khan, M.E. (2022). Heat transfer and fluid flow investigation in dimple roughened solar duct arranged in multiple arc pattern. *International Journal of Ambient Energy*, 43(1), 1866–1877. doi: 10.1080/01430750.2020.1722742

[124] Alam, T., & Kim, M.H. (2017). Heat transfer enhancement in solar air heater duct with conical protrusion roughness ribs. *Applied Thermal Engineering*, 126, 458–469. doi: 10.1016/j.applthermaleng.2017.07.181

[125] Lanjewar, A., Bhagoria, J.L., & Sarviya, R.M. (2011). Heat transfer and friction in solar air heater duct with W-shaped rib roughness on absorber plate. *Energy*, 36(7), 4531–4541. doi: 10.1016/j.energy.2011.03.054

[126] Kumar, A., Bhagoria, J.L., & Sarviya, R. M. (2009). Heat transfer and friction correlations for artificially roughened solar air heater duct with discrete W-shaped ribs. *Energy Conversion and Management*, 50(8), 2106–2117. doi: 10.1016/j.enconman.2009.01.025

[127] Thakur, S., & Thakur, N.S. (2019). Investigational analysis of roughened solar air heater channel having W-shaped ribs with symmetrical gaps along with staggered ribs. *Energy Sources, Part A: Recovery, Utilization, and Environmental Effects*, 42(7), 886–901. doi: 10.1080/15567036.2019.1675815

[128] Thakur, S., & Thakur, N.S. (2020). Impact of multi-staggered rib parameters of the 'W' shaped roughness on the performance of a solar air heater channel. *Energy Sources, Part A: Recovery, Utilization, and Environmental Effects*, 43(8), 960–979. doi: 10.1080/15567036.2020.1764672

[129] Murmu, R., Kumar, P., & Singh, H. (2018). Experimental investigation on heat transfer and friction factor for an inclined spherical ball roughened solar air heater. *Instrumentation Mesure Métrologie*, 18(1), 7–36. doi: 10.3166/i2m.17.7-36

[130] Bhagoria, J.L., Saini, J.S., & Solanki, S.C. (2002). Heat transfer coefficient and friction factor correlations for rectangular solar air heater duct having transverse wedge shaped rib roughness on the absorber plate. *Renewable Energy*, 25(3), 341–369. doi: 10.1016/S0960-1481(01)00057-X

[131] Barik, A.K., Mohanty, A., Senapati, J.R., & Awad, M.M. (2021). Constructal design of different ribs for thermo-fluid performance enhancement of a solar air heater (SAH). *International Journal of Thermal Sciences*, 160, 106655. doi: 10.1016/j.ijthermalsci.2020.106655

[132] Kumar, R., & Goel, V. (2021). Unconventional solar air heater with triangular flow-passage: A CFD based comparative performance assessment of different cross-sectional rib-roughnesses. *Renewable Energy*, 172, 1267–1278. doi: 10.1016/j.renene.2021.03.068

[133] Zina, B., Filali, A., Benamara, N., Laouedj, S., & Ahmed, H. (2020). Numerical simulation of heat transfer improvement of a new designed artificially roughened solar air heater using triangular ribs with semi-circular nooks. *Energy Sources, Part A: Recovery, Utilization, and Environmental Effects*, 43(22), 2820–2838. doi: 10.1080/15567036.2020.1825564

[134] Gawande, V.B., Dhoble, A.S., Zodpe, D.B., & Mangrulkar, C. (2020). A comparative analysis of thermo-hydraulic performance of a roughened solar air heater using various rib shapes. *Australian Journal of Mechanical Engineering*, 18(3), 331–350. doi: 10.1080/14484846.2018.1525171

[135] Aharwal, K.R., Gandhi, B.K., & Saini, J.S. (2008). Experimental investigation on heat-transfer enhancement due to a gap in an inclined continuous rib arrangement in a rectangular duct of solar air heater. *Renewable Energy*, 33(4), 585–596. doi: 10.1016/j.renene.2007.03.023

[136] Aharwal, K.R., Gandhi, B.K., & Saini, J.S. (2009). Heat transfer and friction characteristics of solar air heater ducts having integral inclined discrete ribs on absorber plate. *International Journal of Heat and Mass Transfer*, 52(25-26), 5970–5977. doi: 10.1016/j.ijheatmasstransfer.2009.05.032

[137] Kumar, R., Nadda, R., Kumar, S., Razak, A., Sharifpur, M., Aybar, H.S., Saleel, C.A., & Afzal, A. (2022). Influence of artificial roughness parametric variation on thermal performance of solar thermal collector: An experimental study, response surface analysis and ANN modelling. *Sustainable Energy Technologies and Assessments*, 52(A), 102047. doi: 10.1016/j.seta.2022.102047

[138] Kumar, A., & Layek, A. (2020). Evaluation of the performance analysis of an improved solar air heater with Winglet shaped ribs. *Experimental Heat Transfer*, 34(4), 358–377. doi: 10.1080/08916152.2020.1838670

[139] Nidhul, K., Yadav, A.K., Anish, S., & Arunachala, U.C. (2022). Thermo-hydraulic and exergetic performance of a cost-effective solar air heater: CFD and experimental study. *Renewable Energy*, 184, 627–641. doi: 10.1016/j.renene.2021.11.111

[140] Parsa, H., Saffar-Avval, M., & Hajmohammadi, M.R. (2021). 3D simulation and parametric optimization of a solar air heater with novel staggered cuboid baffles. *International Journal of Mechanical Sciences*, 205, 106607. doi: 10.1016/j.ijmecsci.2021.106607

[141] Jaurker, A.R., Saini, J.S., & Gandhi, B.K. (2006). Heat transfer and friction characteristics of rectangular solar air heater duct using rib-grooved artificial roughness. *Solar Energy*, 80(8), 895–907. https://doi.org/10.1016/j.solener.2005.08.006

[142] Karmare, S.V., & Tikekar, A.N. (2009). Experimental investigation of optimum thermohydraulic performance of solar air heaters with metal rib grits roughness. *Solar Energy*, 83(1), 6–13. doi: 10.1016/j.solener.2008.05.017

[143] Karmare, S.V., & Tikekar, A.N. (2007). Heat transfer and friction factor correlation for artificially roughened duct with metal grit ribs. *International Journal of Heat and Mass Transfer*, 50(21–22), 4342–4351. doi: 10.1016/j.ijheatmasstransfer.2007.01.065

[144] Bopche, S.B., & Tandale, M.S. (2009). Experimental investigations on heat transfer and frictional characteristics of a turbulator roughened solar air heater duct. *International Journal of Heat and Mass Transfer*, 52(11–12), 2834–2848. doi: 10.1016/j.ijheatmasstransfer.2008.09.039

[145] Kumar, S., & Verma, S.K. (2022). Heat transfer and fluid flow analysis of sinusoidal protrusion rib in solar air heater. *International Journal of Thermal Sciences*, 172, 107323. doi: 10.1016/j.ijthermalsci.2021.107323

[146] Saravanan, A., Murugan, M., Sreenivasa Reddy, M., Ranjit, P.S., Elumalai, P.V., Kumar, P., & Rama Sree, S. (2021). Thermo-hydraulic performance of a solar air heater with staggered C-shape finned absorber plate. *International Journal of Thermal Sciences*, 168, 107068. doi: 10.1016/j.ijthermalsci.2021.107068

[147] Bezbaruah, P.J., Das, R.S., & Sarkar, B.K. (2021). Experimental and numerical analysis of solar air heater accoutered with modified conical vortex generators in a staggered fashion. *Renewable Energy*, 180, 109–131. doi: 10.1016/j.renene.2021.08.046

[148] Goel, V., Kumar, R., Bhattacharyya, S., Tyagi, V.V., & Abusorrah, A.M. (2021). A comprehensive parametric investigation of hemispherical cavities on thermal performance and flow-dynamics in the triangular-duct solar-assisted air-heater. *Renewable Energy*, 173, 896–912. doi: 10.1016/j.renene.2021.04.006

[149] Yadav, S., & Saini, R.P. (2020). Numerical investigation on the performance of a solar air heater using jet impingement with absorber plate. *Solar Energy*, 208, 236–248. doi: 10.1016/j.solener.2020.07.088

[150] Wang, D., Liu, J., Liu, Y., Wang, Y., Li, B., & Liu, J. (2020). Evaluation of the performance of an improved solar air heater with 'S' shaped ribs with gap. *Solar Energy*, 195, 89–101. doi: 10.1016/j.solener.2019.11.034

[151] Gupta, D., Solanki, S.C., & Saini, J.S. (1993). Heat and fluid flow in rectangular solar air heater ducts having transverse rib roughness on absorber plates. *Solar Energy*, 51(1), 31–37. doi: 10.1016/0038-092X(93)90039-Q

[152] Kumar, R., Kumar, A., & Varun. (2017). Computational fluid dynamics based study for analyzing heat transfer and friction factor in semi-circular rib-roughened equilateral triangular duct. *International Journal of Numerical Methods for Heat & Fluid Flow*, 27(4), 941–957. doi: 10.1108/HFF-10-2015-0438

[153] Kumar, R., Kumar, A., & Goel, V. (2017). A parametric analysis of rectangular rib roughened triangular duct solar air heater using computational fluid dynamics. *Solar Energy*, 157, 1095–1107. doi: 10.1016/j.solener.2017.08.071

[154] Sahu, M.K., & Prasad, R.K. (2017). Thermohydraulic performance analysis of an arc shape wire roughened solar air heater. *Renewable Energy*, 108, 598–614. doi: 10.1016/j.renene.2017.02.075

[155] Saravanakumar, P.T., Somasundaram, D., & Matheswaran, M.M. (2019). Thermal and thermo-hydraulic analysis of arc shaped rib roughened solar air heater integrated with fins and baffles. *Solar Energy*, 180, 360–371. doi: 10.1016/j.solener.2019.01.036

[156] Murmu, R., Kumar, P., & Singh, H.N. (2019). Effects of roughness parameters on the heat transfer and friction of an inclined spherical ball roughened flat plate solar collector. *International Journal of Ambient Energy*, 42(15), 1781–1797. doi: 10.1080/01430750.2019.1693426

[157] Kumar, V., & Murmu, R. (2021). Experimental investigation for thermal performance of inclined spherical ball roughened solar air duct. *Renewable Energy*, 172, 1365–1392. doi: 10.1016/j.renene.2020.11.150

[158] Karwa, R., Solanki, S.C., & Saini, J.S. (1999). Heat transfer coefficient and friction factor correlations for the transitional flow regime in rib-roughened rectangular ducts. *International Journal of Heat and Mass Transfer*, 42(9), 1597–1615. doi: 10.1016/S0017-9310(98)00252-X

[159] Patel, Y.M., Jain, S.V., & Lakhera, V.J. (2021). Thermo-hydraulic performance analysis of a solar air heater roughened with discrete reverse NACA profile ribs. *International Journal of Thermal Sciences*, 167, 107026. doi: 10.1016/j.ijthermalsci.2021.107026

[160] Arunkumar, H.S., Kumar, S., & Karanth, K.V. (2021). Experimental study on thermo-hydraulic performance of a solar air heater with rectangular perforated duct inserts. *Solar Energy*, 227, 179–189. doi: 10.1016/j.solener.2021.09.005

[161] Kumar, R., Kashyap, A.S., Singh, P., Goel, V., & Kumar, K. (2020). Innovatively arranged curved-ribbed solar-assisted air heater: Performance and correlation development for heat and flow characteristics. *Journal of Solar Energy Engineering*, 142(3), 031008. doi: 10.1115/1.4045827

[162] Hong, Y.J., & Hsieh, S.S. (1991). An experimental investigation of heat transfer characteristics for turbulent flow over staggered ribs in a square duct. *Experimental Thermal and Fluid Science*, 4(6), 714–722. doi: 10.1016/0894-1777(91)90078-6

[163] Gupta, D., Solanki, S.C., & Saini, J.S. (1997). Thermohydraulic performance of solar air heaters with roughened absorber plates.

Solar Energy, 61(1), 33–42. doi: 10.1016/S0038-092X(97)00005-4

[164] Layek, A., Saini, J.S., & Solanki, S.C. (2007). Second law optimization of a solar air heater having chamfered rib-groove roughness on absorber plate. *Renewable Energy*, 32(12), 1967–1980. doi: 10.1016/j.renene.2006.11.005

[165] Varun, Saini, R.P., & Singal, S.K. (2008). Investigation of thermal performance of solar air heater having roughness elements as a combination of inclined and transverse ribs on the absorber plate. *Renewable Energy*, 33(6), 1398–1405. doi: 10.1016/j.renene.2007.07.013

[166] Muluwork, K.B., Saini, J.S., & Solanki, S.C. (1998). Studies on discrete rib roughened solar air heaters. In *Proceedings of National Solar Energy Convention* (pp. 75–84), 30 Nov. – 2 Dec., Roorkee, USA.

[167] Hans, V.S., Saini, R.P., & Saini, J.S. (2010). Heat transfer and friction factor correlations for a solar air heater duct roughened artificially with multiple v-ribs. *Solar Energy*, 84(6), 898–911. doi: 10.1016/j.solener.2010.02.004

[168] Singh, S., Chander, S., & Saini, J.S. (2012). Investigations on thermo-hydraulic performance due to flow-attack-angle in V-down rib with gap in a rectangular duct of solar air heater. *Applied Energy*, 97, 907–912. doi: 10.1016/j.apenergy.2011.11.090

[169] Kumar, A., Saini, R.P., & Saini, J.S. (2013). Development of correlations for Nusselt number and friction factor for solar air heater with roughened duct having multi v-shaped with gap rib as artificial roughness. *Renewable Energy*, 58, 151–163. doi: 10.1016/j.renene.2013.03.013

[170] Bhushan, B., & Singh, R. (2012). Thermal and thermohydraulic performance of roughened solar air heater having protruded absorber plate. *Solar Energy*, 86(11), 3388–3396. doi: 10.1016/j.solener.2012.09.004

[171] Lanjewar, A., Bhagoria, J.L., & Sarviya, R.M. (2011). Experimental study of augmented heat transfer and friction in solar air heater with different orientations of W-Rib roughness. *Experimental Thermal and Fluid Science*, 35(6), 986–995. doi: 10.1016/j.expthermflusci.2011.01.019

[172] Chandra, P.R., Alexander, C.R., & Han, J.C. (2003). Heat transfer and friction behaviors in rectangular channels with varying number of ribbed walls. *International Journal of Heat and Mass Transfer*, 46(3), 481–495. doi: 10.1016/S0017-9310(02)00297-1

[173] Webb, R.L., Eckert, E.R.G., & Goldstein, R.J. (1971). Heat transfer and friction in tubes with repeated-rib roughness. *International Journal of Heat and Mass Transfer*, 14(4), 601–617. doi: 10.1016/0017-9310(71)90009-3

[174] Srivastava, A., Chhaparwal, G.K., & Sharma, R.K. (2020). Numerical and experimental investigation of different rib roughness in a solar air heater. *Thermal Science and Engineering Progress*, 19, 100576. doi: 10.1016/j.tsep.2020.100576

[175] Kumar, R., Goel, V., & Kumar, M. (2020). Effect of providing gap in multiple-arc rib-roughened solar air heater – Part 1. *Journal of Mechanical Science and Technology*, 34(6), 2619–2625. doi: 10.1007/s12206-020-0535-3

[176] Alam, T., & Kim, M.H. (2018). A comprehensive review on single phase heat transfer enhancement techniques in heat exchanger applications. *Renewable and Sustainable Energy Reviews*, 81, 813–839. doi: 10.1016/j.rser.2017.08.060